

mgr inż. Patryk Michał Ślusarczyk

**Badanie zależności pomiędzy akumulacją żelaza w starzeniu
a zdolnością do recyklingu żelaza w makrofagach czerwonej
miazgi śledziony**

**Rozprawa na stopień doktora nauk medycznych i nauk o zdrowiu
w dyscyplinie nauki medyczne**

Promotor:

dr hab. Wojciech Pokrzywa

Promotor pomocniczy:

dr Katarzyna Mleczko-Sanecka

Międzynarodowy Instytut Biologii Molekularnej i Komórkowej
w Warszawie

Laboratorium Homeostazy Żelaza



Obrona rozprawy doktorskiej przed Radą Dyscypliny Nauk Medycznych
Warszawskiego Uniwersytetu Medycznego

Warszawa 2023 r.

Słowa kluczowe: żelazo, makrofagi, śledziona, starzenie, fagocytoza

Key words: iron, macrophages, spleen, aging, phagocytosis



Fundusze Europejskie



NARODOWE CENTRUM NAUKI



**Rzeczpospolita
Polska**

Unia Europejska
Europejskie Fundusze
Strukturalne i Inwestycyjne



Wykaz publikacji stanowiących prace doktorską

1. „**The Multiple Facets of Iron Recycling**”

Patryk Ślusarczyk, Katarzyna Mleczko-Sanecka

Genes, 2021, 12(9):1-22

IF: 4,141 MEiN: 100

2. „**Impaired iron recycling from erythrocytes is an early hallmark of aging**”

Patryk Ślusarczyk, Pratik Kumar Mandal, Gabriela Żurawska, Marta Niklewicz, Komal Chouhan, Raghunandan Mahadeva, Aneta Jończy, Matylda Macias, Aleksandra Szybińska, Magdalena Cybulska, Olga Krawczyk, Sylwia Herman, Michał Mikula, Remigiusz Serwa, Małgorzata Lenartowicz, Wojciech Pokrzywa, Katarzyna Mleczko-Sanecka

eLife, 2023, 12:1-39

IF: 8,713 MEiN: 200

Dziękuję mojej rodzinie i przyjaciołom, byliście moją opoką podczas drogi przez doktorat. Wasze wsparcie i miłość były źródłem mojej siły i zawsze będę za to wdzięczny.

Dziękuję moim nauczycielom, mentorom i współpracownikom. Wasza wiedza, doświadczenie i wskazówki odegrały kluczową rolę w kształtowaniu moich zainteresowań i umiejętności.

Spis treści

1. Wykaz stosowanych skrótów.....	11
2. Streszczenie	13
3. Summary	15
4. Wstęp	17
4.1 Funkcje żelaza w organizmie	17
4.2 Wchłanianie żelaza w jelitach	17
4.3 Recykling żelaza przez makrofagi	18
4.4 Oś ferroportyna-hepcydyna.....	19
4.5 Homeostaza żelaza w komórkach	20
4.6 Wpływ starzenia się na ogólnoustrojowy i komórkowy metabolizm żelaza ...	21
4.7 Omówienie osiągnięcia naukowego.....	23
5. Założenia i cele pracy	25
6. Publikacje stanowiące prace doktorską	27
6.1 The Multiple Facets of Iron Recycling	29
6.2 Impaired iron recycling from erythrocytes is an early hallmark of aging	51
7. Podsumowanie i wnioski	91
8. Bibliografia	93
9. Opinia komisji bioetycznej	99
10. Oświadczenia współautorów publikacji	101

1. Wykaz stosowanych skrótów

BMP (ang. Bone Morphogenetic Protein) - białko morfogenetyczne kości

Dcytb (ang. duodenal cytochrome B) – dwunastniczy cytochrom b

DMT1 (ang. Divalent Metal Transporter 1) – transporter metali dwuwartościowych 1

DNA (ang. deoxyribonucleic acid) – kwas deoksyrybonukleinowy

FPN (ang. ferroportin) – ferroportyna

HCP1 - transporter kwasu foliowego sprzężony z białkiem nośnikowym hemu-1

HIF1 α (ang. Hypoxia-Inducible Factor 1-alpha) - czynnik indukowany hipoksją 1-alfa

HO1 (ang. Heme Oxygenase 1) – oksigenaza hemowa 1

HRG1 (ang. Heme-Responsive Gene 1) – gen reagujący na hem 1

IL-6 (ang. interleukin 6) – interleukina 6

KC (ang. Kupffer Cells) – komórki Kupffera

LIP (ang. Labile Iron Pool) – labilna pula żelaza

NTBI (ang. Non-Transferrin Bound Iron) – żelazo niezwiązane z transferyną

RBC (ang. Red Blood Cell) – czerwona krwinka; erytrocyt

ROS (ang. Reactive Oxygen Species) – reaktywne formy tlenu

RPMs (ang. Red Pulp Macrophages) – makrofagi czerwonej miazgi śledziony

Sec15l1 (ang. exocyst complex component 6) - składnik kompleksu egzocyst 6

TBI (ang. Transferrin Bound Iron) – żelazo związane z transferyną

Tf (ang. transferrin) – transferyna

TfR1 (ang. Transferrin Receptor 1) – receptor transferyny 1

2. Streszczenie

Żelazo jest metalem niezbędnym do życia ze względu na jego zdolność do wymiany elektronów z różnymi biomolekułami. W organizmie ssaków większość żelaza zawarta jest w hemie stanowiącym prostetyczną grupę hemoglobiny, która wiąże tlen w erytrocytach. Makrofagi czerwonej miazgi śledziony (red pulp macrophages; RPMs) reprezentują główny typ komórek, który zapewnia obieg wewnętrznej puli żelaza. Poprzez fagocytozę starzejących się erytrocytów w procesie zwanym erytrofagocytozą, a następnie ich degradację, żelazo uwalniane jest do krwioobiegu, umożliwiając jego ponowne wykorzystanie w procesie krwiotwórczym. Wskazuje to na istotność RPMs w utrzymaniu homeostazy krwi oraz recyklingu żelaza w organizmie. Ze względu na swoje funkcje, komórki te specjalizują się w rozkładzie hemoglobiny, katabolizmie hemu i eksporcie żelaza, przez co przystosowały się do dużego przepływu tego pierwiastka. Natomiast nadal nie wiadomo, czy ciągła ekspozycja na wysoki poziom żelaza może upośledzać zdolność tych komórek do erytrofagocytozy oraz czy proces ten może być regulowany przez ogólnoustrojowy lub komórkowy poziom żelaza. Odkładanie się żelaza w śledzionie występuje fizjologicznie podczas wczesnego starzenia. Postawiono zatem hipotezę, że zwiększona ekspozycja na żelazo może sprzyjać starzeniu RPMs i tym samym wpływać na parametry żelaza w organizmie oraz homeostazę erytrocytów. Niniejsze badanie miało zatem na celu lepsze zrozumienie związku pomiędzy zdolnościami komórek RPM do recyklingu żelaza a akumulacją żelaza w śledzionie podczas starzenia.

W celu zbadania wpływu starzenia na RPMs, wykorzystano samice myszy w wieku 10-11 miesięcy, które wykazują podwyższony poziom żelaza w śledzionie i wątrobie oraz mniejszą biodostępność żelaza w surowicy w porównaniu z 2-miesięcznymi myszami kontrolnymi. Zaobserwowano, że bardzo znacząca akumulacja żelaza u myszy starszych następuje w RPMs, co spowodowane jest redukcją poziomu białka odpowiedzialnego za eksport żelaza, ferroportyny. Wykazano, że przeładownie żelazem w RPMs prowadzi do zwiększonego stresu oksydacyjnego, zmniejszonej aktywności lizosomalnej i mitochondrialną a, co najważniejsze, upośledzonej zdolności erytrofagocytozy. Zidentyfikowano również utratę RPMs podczas starzenia, u której podstaw leży stres proteotoksyczny i zależna od żelaza śmierć komórkowa przypominająca ferroptozę. Upośledzenia te prowadzą do retencji starzejących się hemolitycznych erytrocytów w śledzionie oraz do tworzenia

nierozkładalnych pozakomórkowych agregatów białkowych bogatych w hem i żelazo, pochodzących prawdopodobnie z ferroptotycznych RPMs. Następnie odkryto, że redukcja zawartości żelaza w diecie łagodzi gromadzenie się żelaza w RPMs, zmniejsza ich stres oksydacyjny, usprawnia funkcję mitochondriów i lizosomów, oraz skutkuje poprawą zdolności usuwania starych erytrocytów. W konsekwencji dieta ta poprawia kondycję samych erytrocytów w śledzionie, ograniczając ich hemolizę oraz hamuje tworzenie się agregatów żelazowych. Dodatkowo, normalizuje poziom żelaza w wątrobie i śledzionie oraz zwiększa biodostępność żelaza w surowicy. Dzięki badaniu RPMs *in vivo* oraz stworzeniu protokołu pozwalającego na różnicowanie monocytów szpiku kostnego do komórek przypominających RPMs *in vitro* (induced-RPMs), pokazano, że mechanizm obniżonej erytrofagocytozy wynika przede wszystkim z akumulacji żelaza, obniżonej aktywności oksygenazy hemowej (HO1) oraz w mniejszym stopniu ze stresu pojawiającego się w retikulum endoplazmatycznym.

Podsumowując, praca ta pozwoliła na zidentyfikowanie dysfunkcji RPMs jako wczesnej oznaki starzenia. Wykazano również, że redukcja żelaza w diecie poprawia wydajność obrotu żelazem w organizmie.

3. Summary

Title: Dissecting the relationship between iron accumulation in aging and iron recycling capacity of splenic red pulp macrophages.

Iron is an essential metal for life due to its ability to exchange electrons with various biomolecules. In mammals, most of the iron is incorporated in heme, the prosthetic group of hemoglobin that binds oxygen in red blood cells. Red pulp macrophages (RPMs) are the main type of cells that ensure the internal iron pool circulation by phagocytosing aging red blood cells in a process called erythrophagocytosis, and then degrading them, releasing iron into the bloodstream for reuse in erythropoiesis. This highlights the importance of RPMs in maintaining blood homeostasis and iron recycling in the body. However, it is not known whether continuous exposure to high levels of iron can impair the ability of these cells to perform erythrophagocytosis and whether red blood cell clearance can be regulated by systemic or cellular levels of iron. Iron accumulation in the spleen occurs physiologically during early aging. Therefore, it has been hypothesized that increased exposure to iron may accelerate RPM aging and in turn affect systemic iron parameters and red blood cell homeostasis. Thus, the purpose of this study was to better understand the relationship between RPMs' iron recycling capabilities and iron accumulation in the spleen during aging.

To investigate the effect of aging on RPMs, we used female mice aged 10-11 months, which show elevated levels of iron in the spleen and liver and lower serum iron bioavailability compared to 2-month-old control mice. It was observed that a very significant accumulation of iron in older mice occurs in the RPMs, which is caused by a reduction in the protein level of the iron exporter ferroportin. Iron overload in RPMs was shown to cause increased oxidative stress, decreased lysosomal and mitochondrial activity, and most importantly, impaired erythrophagocytosis capacity. We also identified loss of RPMs during aging, which was attributed to proteotoxic stress and iron-dependent cell death resembling ferroptosis. These impairments lead to the retention of aging hemolytic erythrocytes in the spleen and the formation of non-degradable extracellular protein aggregates rich in heme and iron, likely derived from ferroptotic RPMs. Furthermore, it was discovered that dietary iron restriction alleviates iron accumulation, reduces oxidative stress, and improves mitochondrial and lysosomal function, resulting

in enhanced old red blood cells removal by RPMs. As a result, this diet improves the condition of red blood cells in the spleen, limiting their hemolysis, and reducing the formation of protein iron-rich aggregates. It further normalizes iron levels in the liver and spleen and increases serum iron bioavailability. Combining in vivo approaches with experiments on a newly established in vitro model of RPMs (induced-RPMs) showed that erythrophagocytosis capacity is chiefly suppressed by iron accumulation and reduced heme oxygenase-1 (HO1) activity, and to a lesser extent, by stress that arises in the endoplasmic reticulum.

In summary, this study identified RPM dysfunction as an early hallmark of aging. It also demonstrated that reducing dietary iron content improves iron turnover efficiency in the body.

4. Wstęp

4.1 Funkcje żelaza w organizmie

Żelazo jest fundamentem dla przeżycia, proliferacji i metabolizmu komórek u niemal wszystkich organizmów. Jako kluczowy element wielu białek i kofaktorów, żelazo jest niezbędne do transportu tlenu, bierze udział w biosyntezie kolagenu, mieliny, neuroprzekazników i składników mitochondrialnego łańcucha transportu elektronów [1-4]. Ponadto żelazo odgrywa istotną rolę we wrodzonej odpowiedzi immunologicznej, ponieważ jednym z ważnych mechanizmów obrony gospodarza przed infekcją jest zmniejszenie dostępności żelaza dla patogenów [5]. Niskie stężenie żelaza w organizmie skutkuje ograniczeniem erytropoezy, a w konsekwencji niedokrwistością. Natomiast wysoki poziom jonów Fe^{2+} może prowadzić do wytworzenia wysoce reaktywnych wolnych rodników hydroksylowych w reakcji Fentona. W konsekwencji, dalsze powstawanie reaktywnych form tlenu (ROS) doprowadza do stresu oksydacyjnego, peroksydacji lipidów i oksydacyjnego uszkodzenia uszkodzeń DNA i białek [6].

Żelazo jest niczym obosieczny miecz, przez co jego poziom wymaga ścisłej regulacji oraz precyzyjnego zachowania równowagi pomiędzy wchłanianiem, magazynowaniem i eksportem [7]. Wchłanianie żelaza to dynamiczny proces, który zależy przede wszystkim od absorbowania tego pierwiastka z pożywienia. Jednak w przeciwieństwie do wchłaniania, usuwanie żelaza z organizmu zachodzi w nieznacznym stopniu i nie podlega mechanizmom regulacyjnym zależnym od jego fizjologicznego stężenia [8]. W związku z tym żelazo może akumulować się w nadmiarze, prowadząc do jego przeładowania w tkankach.

4.2 Wchłanianie żelaza w jelitach

Żelazo do organizmu dostaje się poprzez jelita, gdzie wchłaniane jest z pożywienia w dwóch formach – hemowej i niehemowej. Komórkami wyspecjalizowanymi do wchłaniania żelaza w dwunastnicy są enterocyty [9]. Na błonie powierzchniowej, zwróconej w stronę światła jelita posiadają one maszynię pozwalającą na skuteczne pozyskiwanie żelaza. Metaloreduktaza dwunastniczego cytochromu B (Dcytb) przekształca żelazo Fe^{3+} w rozpuszczalną postać Fe^{2+} [10], która jest następnie transportowana do komórek przez transporter metali dwuwartościowych 1 (DMT1) [11].

Uwalnianie żelaza do krwioobiegu odbywa się następnie za pośrednictwem ferroportyny (FPN) [12, 13], związanej z hefaestyną, która utlenia Fe^{2+} do Fe^{3+} umożliwiając jego wiązanie przez transferynę, białko transportujące żelazo w osoczu [14].

Wchłanianie żelaza z hemu oraz ferrytyny zostało mniej poznane. Istnieją dowody, że hem wychwytywany jest na drodze endocytozy za pośrednictwem receptora [15], ale jak dotąd receptor o wysokim powinowactwie do hemu w enterocytach nie został jeszcze zidentyfikowany. HCP1 został zidentyfikowany jako powierzchniowy transporter hemu [16], jednak wydaje się, że białko to odgrywa ważniejszą rolę w absorpcji kwasu foliowego i ma znacznie mniejsze powinowactwo do samego hemu. W przypadku ferrytyny również istnieją dowody, że z pożywienia pobierana jest do enterocytów na drodze endocytozy [17]

4.3 Recykling żelaza przez makrofagi

Wchłanianie żelaza w jelitach stanowi około 10% dziennego zapotrzebowania na ten pierwiastek. Reszta żelaza odzyskiwana jest z hemu pochodzącego ze starych lub uszkodzonych erytrocytów. Makrofagi czerwonej miazgi śledziony (RPMs) oraz w mniejszym ilościowo stopniu komórki Kupffera (KCs) wątroby pobierają żelazo na drodze fagocytozy erytrocytów zawierających bogatą w hem hemoglobinę. Z hemoglobiny zawartej w jednym erytrocycie, makrofagi są w stanie odzyskać aż miliard atomów żelaza [18]. Tak więc, prawie wszystkie atomy żelaza, które wykorzystywane są w organizmie „przechodzą” przez makrofagi. Pierwszym etapem, który doprowadza do odzyskania żelaza przez makrofagi, jest rozpoznanie starzejących się erytrocytów, a później ich pochłanianie (w procesie nazywanym erytrofagocytozą) i degradacja. Po internalizacji erytrocytów, fagosomy zawierające erytrocyty łączą się z pęcherzykami lizosomalnymi, tworząc fagolizosomy, w których trawione są erytrocyty. Co istotne, ostatnie odkrycia rzucają nowe światło na przebieg procesu erytrofagocytozy, pokazując, że starzejące się czerwone krwinki wykazują ekspresję cząsteczek adhezyjnych. Umożliwiają im one wiązanie się z macierzą zewnątrzkomórkową w architekturze śledziony, sprzyjając ich zatrzymywaniu w narządzie. Skutkuje to miejscową hemolizą i wiązaniem hemoglobiny z haptoglobina, a następnie jej wychwytem przy pomocy CD163 na powierzchni RPMs. Powstające w ten sposób „duchy” erytrocytów, czyli ich membrany, są rozpoznawane i fagocytowane przez RPMs zamiast całych nienaruszonych erytrocytów [19]. Praca ta nie scharakteryzowała

jednak ilościowo, w jakim stopniu erytrocyty lizują i są usuwane jako „duchy” a jaki ich procent ulega fagocytozie, będącej dotychczas głównym znanym procesem usuwania starych erytrocytów [20]. Nie udowodniono również, czy RPMs rzeczywiście pobierają kompleks hemoglobiny z haptoglobina.

Następnie, na drodze hydrolitycznego rozkładu hemoglobiny uwalniany jest hem, który następnie jest transportowany z erytrofagolizosomów do cytozolu [21, 22]. Za transport hemu z erytrofagolizosomu odpowiedzialny jest transporter HRG1, którego ekspresja regulowana jest potranskrypcyjnie przez hem i żelazo [23]. Ekspresja HRG1 jest najwyższa w RPMs, KCs a także w makrofagach szpiku kostnego. W cytozolu makrofagów, żelazo jest natychmiast odzyskiwane z hemu dzięki enzymatycznej aktywności oksygenazy hemowej 1 (HO-1) [24]. Degradacja hemu przez ten enzym generuje równoważne ilości tlenku węgla, biliwerdyny oraz żelaza [25]. Kluczową rolę w detoksykacji hemu przez HO1 potwierdza jej wzrost zaraz po erytrofagocytozie lub po hemolizie [26, 27]. Co ważne, wyłączenie genu kodującego HO-1 (*Hmox1*) sprawia, że RPMs umierają, sugerując, że prawidłowa degradacja hemu przez makrofagi odpowiedzialne za recykling żelaza jest niezbędna dla ich funkcjonowania [26, 27].

4.4 Oś ferroportyna-hepcydyna

Warto zauważyć, że nie istnieją znane nam kontrolowane mechanizmy wydalania żelaza z organizmu, a zatem wydajna kontrola stopnia wchłaniania żelaza oraz jego uwalniania z makrofagów ma kluczowe znaczenie dla utrzymania homeostazy tego pierwiastka. Systemowo osiągnane jest to głównie przez niewielki hormon peptydowy hepcydynę, która jest syntetyzowana i wydzielana przez hepatocyty [28]. Ekspresji hepcydyny regulowana jest zarówno przez ilość żelaza w komórkach, jak i poziom krążącego żelaza związanego z transferyną [29]. Wzrost poziomu żelaza w osoczu i tkankach stymuluje produkcję tego peptydu poprzez aktywację kaskady sygnałowej BMP-SMAD w hepatocytach [30]. Na poziomie komórkowym hepcydyna wiąże się z ferroportyną powodując jej ubikwitynację, internalizację a następnie degradację [31]. Spadek poziomu FPN w enterocytach dwunastnicy zmniejsza uwalnianie żelaza do krwioobiegu i prowadzi do zmniejszenia wchłaniania żelaza [32]. Tak samo jak w enterocytach, degradacja FPN w wyniku wiązania hepcydyny następuje również w makrofagach odpowiedzialnych za odzyskiwanie żelaza z erytrocytów co ostatecznie prowadzi do zahamowania wypływu żelaza z komórek eksportujących żelazo i jego

obniżenia poziomu żelaza w osoczu. Co ciekawe, wzrost prozapalnej interleukiny-6 (IL-6) stymuluje produkcję hepcydyny i prowadzi do dyshomeostazy żelaza [33]. W takim przypadku poziom żelaza w surowicy spada, podczas gdy poziom ferrytyny wzrasta [31], co jest powszechnym zjawiskiem obserwowanym podczas stanu zapalnego i związanej z nim niedokrwistości [34].

4.5 Homeostaza żelaza w komórkach

Komórkowe mechanizmy wychwytu żelaza różnią się w zależności od typu komórki i samej postaci żelaza. Jak wspomniano, żelazo w diecie występuje w dwóch postaciach: hemowej i niehemowej. Żelazo niehemowe może być związane z transferyną (TBI) lub niezwiązane z transferyną (NTBI). Większość żelaza w organizmie występuje w krążeniu w formie związanej z transferyną [35]. Transferyna bez związanego żelaza Fe^{3+} nazywana jest apo-transferyną a po związaniu jonów żelaza nosi nazwę holo-transferyny.

Holo-transferyna (TBI) wiązana jest na powierzchni komórki z receptorem TfR1. Kompleks holo-transferyna-TfR1 jest internalizowany do komórki poprzez endocytozę zależną od klatryny [36] a następnie transportowany jest do wczesnego endosomu [37, 38]. Endocytarny szlak pobierania TBI wymaga wielu białek uczestniczących w transporcie pęcherzykowym takich jak Sec1511, Vps35, Snx3 [39], jak również CCDC115 [40]. W endosomach, żelazo redukowane jest do Fe^{2+} i uwalniane do cytozolu przez DMT1. Jak wspomniano, żelazo może być toksyczne i prowadzić do powstawania ROS. W związku z tym większość labilnej puli żelaza (LIP) jest dostarczana do mitochondriów, gdzie wykorzystywana jest do kluczowych etapów tworzenia klastrów żelazowo-siarkowych (Fe-S) i syntezy hemu [41, 42]. Reszta żelaza Fe^{2+} może być eksportowana poza komórkę przez FPN lub gromadzona w ferrytynie, heteropolimerze podobnym do nanoklatki, składającym się z 24 podjednostek L-ferrytyny i H-ferrytyny. Ta ostatnia charakteryzuje się aktywnością ferroksozydazy, niezbędnej do bezpiecznego osadzenia żelaza w jego redoksowo nieaktywnej postaci Fe^{3+} [36]. Cytozolowe żelazo dostarczane jest do ferrytyny dzięki poli-wiązującemu białku 1 i 2 (PCBP1 i PCBP2) [43]. Funkcja opiekuńcza tych białek jest ważna nie tylko dla transportu żelaza do ferrytyny, ale także dla innych enzymów cytozolowych takich jak hydrolazy prolinowe zaangażowane w degradację czynnika indukowanego

niedotlenieniem 1α (HIF 1α). Żelazo znajdujące się w ferrytynie stanowi magazyn, który może ulec mobilizacji do użytku poprzez degradację ferrytyny.

4.6 Wpływ starzenia się na ogólnoustrojowy i komórkowy metabolizm żelaza

W ciągu ostatnich dwóch dekad zdobyliśmy dużą wiedzę na temat mechanizmów leżących u podstaw homeostazy żelaza. Pojawiające się w literaturze doniesienia sugerują, że homeostaza żelaza jest ściśle związana ze starzeniem. W śledzionie, wątrobie, nerkach i mózgu dochodzi do związanej z wiekiem akumulacji żelaza, co przyczynia się do patogenezы chorób wieku starczego [44–47].

Niedobór żelaza można podzielić na dwa główne rodzaje, funkcjonalny i bezwzględny. Funkcjonalny niedobór żelaza spowodowany jest retencją żelaza w makrofagach, przez co zmniejszona jest jego biodostępność dla procesu erytropoezy [29]. Główną przyczyną funkcjonalnego niedoboru żelaza, który często nazywany jest niedokrwistością zapalną lub niedokrwistością chorób przewlekłych, jest aktywacja immunologiczna i powiązany z nią wzrost poziomu hepcydyny [48]. Za to bezwzględny niedobór żelaza polega na zmniejszeniu całkowitej zawartości żelaza w organizmie i zazwyczaj spowodowany jest ubogą zawartością żelaza w diecie lub/i upośledzeniem wchłaniania żelaza w jelitach. Wraz z wiekiem następuje obniżenie zdolności wchłaniania żelaza oraz wywołuje się łagodny stan zapalny, przez co osoby starsze są bardziej narażone na niedokrwistość wynikającą zarówno z funkcjonalnego jak i bezwzględnego niedoboru żelaza [49]. Chociaż niedobór żelaza wiąże się z osłabieniem odporności, spadkiem siły fizycznej lub pogorszeniem zdolności umysłowych, diety bogate w żelazo przyspieszają starzenie, co związane jest z indukcją stresu oksydacyjnego oraz stanu zapalnego [50].

Odkładające się w tkankach i komórkach żelazo może występować pod różnymi postaciami, do których należy wolne żelazo, ferrytyna lub częściowo zdenaturowana forma ferrytyny zwana historycznie hemosyderyną [51]. Poziom żelaza w surowicy oraz ekspresja TfR1 zmniejszają się z wiekiem a ilość ferrytyny w osoczu wzrasta [52]. Zwiększone poziomy hepcydyny hamują recykling żelaza w makrofagach, powodując jego akumulację i ogólnoustrojowy niedobór żelaza oraz podwyższone poziomy ferrytyny w osoczu [53]. Wzrost poziomu ferrytyny wraz z wiekiem [54] może również wyjaśniać zjawisko wewnątrzkomórkowej sekwestracji żelaza oraz stanowić biomarker starzenia się komórek [55]. Sama ferrytyna może gromadzić się w cytozolu oraz mitochondriach [56]. Cytozolowa ferrytyna rozkładana jest na drodze ferrytynofagii

w celu uwolnienia żelaza redokso-aktywnego i zwiększenia stężenia LIP [57]. Starzejące się komórki często wykazują upośledzoną ferrytynofagię. Zatem duża ilość nagromadzonego żelaza w starych komórkach uwięziona jest w ferrytynie, a sama komórka postrzega to jako niedobór żelaza [58]. W badaniach wykazano, że LIP w komórkach jest głównym powodem zarówno starzenia się jak i ferroptozy, będącej śmiercią komórki, która różni się od apoptozy, martwicy, autofagii i innych form śmierci komórki. Proces ferroptotycznej śmierci komórki definiowany jest przez gromadzenie się toksycznych form lipidów będących efektem peroksydacji lipidów [59]. Sama ferroptoza może przyczyniać się do chorób wieku starczego, na przykład do neurodegeneracji [60-64]. Dlatego ważne jest, aby rozszyfrować, czy mechanizmy i inicjatory ferroptozy różnią się pomiędzy typami komórek. Zrozumienie etiologii ferroptozy może pomóc w rozwikłaniu jej wpływu na choroby związane ze starzeniem.

4.7 Omówienie osiągnięcia naukowego

Niniejsza praca doktorska składa się z dwóch opublikowanych artykułów, które związane są tematyką recyklingu żelaza i składają się na spójny cykl publikacyjny.

Pierwsza praca z cyklu jest artykułem przeglądowym pod tytułem “**The Multiple Facets of Iron Recycling**”. Dokonano w nim przeglądu literatury dotyczącej recyklingu żelaza na poziomie ogólnoustrojowym oraz komórkowym i stanowi ona uzupełnienie powyższego wstępu. Artykuł miał na celu przedstawienie rosnącej ilości badań dotyczących nowych aspektów recyklingu żelaza. Omówiona została w nim erytrofagocytoza, będąca głównym procesem usuwania starych oraz uszkodzonych erytrocytów. Przedstawiono sygnały pojawiające się na powierzchni czerwonych krwinek podczas ich starzenia się, co prowadzi do ich fagocytozy przez wyspecjalizowane w tej funkcji makrofagi. W artykule zawarto również informacje na temat recyklingu żelaza w warunkach hemolizy oraz omówiono mechanizmy usuwania wolnej hemoglobiny oraz hemu w organizmie. Na koniec wyjaśniono w jaki sposób kontrolowane jest powstawanie i różnicowanie się makrofagów odpowiedzialnych za obrót żelaza oraz jak wyglądają wzajemne zależności pomiędzy metabolizmem żelaza w makrofagach a ich funkcją odpornościową.

Drugi artykuł “**Impaired iron recycling from erythrocytes is an early hallmark of aging**” jest artykułem oryginalnym przedstawiającym nigdy wcześniej niepublikowane dane. Przeprowadzono w nim analizę makrofagów czerwonej miazgi śledziony będących jednymi z głównych komórek odpowiedzialnych za recykling żelaza w organizmie ssaków. Porównano tkankowe oraz komórkowe poziomy żelaza oraz funkcje makrofagów śledzionowych w zależności od wieku oraz określono wpływ nisko-żelazowej diety na wydajności obrotu żelaza w starzeniu.

5. Założenia i cele pracy

Wiążąca się z wiekiem akumulacja żelaza w tkankach skutkująca toksycznością oraz powszechna niedokrwistość u osób starszych wskazują, że starzenie upośledza homeostazę żelaza. Śsaki zaspokajają około 80% dziennego zapotrzebowania na żelazo ze starzejących się lub uszkodzonych czerwonych krwinek w procesie erytrofagocytozy, przeprowadzanej głównie przez RPMs. Komórki te przez całe swoje życie nieustannie prowadzą recykling żelaza i są wyeksponowane na jego wysokie poziomy. Postawiono zatem hipotezę, że mogą one być szczególnie podatne na postępującą z wiekiem dysfunkcje, skutkując upośledzonym metabolizmem żelaza na poziomie całego organizmu.

Celem pracy było:

1. zbadanie wpływu starzenia na ogólnoustrojowe i komórkowe poziomy żelaza oraz funkcje makrofagów odpowiedzialnych za recykling żelaza,
2. określenie wpływu diety z ograniczoną ilością żelaza na metabolizm żelaza (szczególnie wydajność jego recyklingu),
3. stwierdzenie jak szybko w toku starzenia objawiają się zmiany funkcjonalne w makrofagach RPM i jaki jest ich mechanizm,
4. scharakteryzowanie jakie konsekwencje dla organizmu ma dysfunkcja makrofagów w starzeniu,
5. stworzenie modelu dysfunkcji RPMs podczas starzenia.

6. Publikacje stanowiące prace doktorską

Review

The Multiple Facets of Iron Recycling

Patryk Slusarczyk and Katarzyna Mleczko-Sanecka *

Laboratory of Iron Homeostasis, International Institute of Molecular and Cell Biology, 02-109 Warsaw, Poland; patryk.slusarczyk@iimcb.gov.pl

* Correspondence: kmsanecka@iimcb.gov.pl; Tel.: +48-22-597-07-76

Abstract: The production of around 2.5 million red blood cells (RBCs) per second in erythropoiesis is one of the most intense activities in the body. It continuously consumes large amounts of iron, approximately 80% of which is recycled from aged erythrocytes. Therefore, similar to the “making”, the “breaking” of red blood cells is also very rapid and represents one of the key processes in mammalian physiology. Under steady-state conditions, this important task is accomplished by specialized macrophages, mostly liver Kupffer cells (KCs) and splenic red pulp macrophages (RPMs). It relies to a large extent on the engulfment of red blood cells via so-called erythrophagocytosis. Surprisingly, we still understand little about the mechanistic details of the removal and processing of red blood cells by these specialized macrophages. We have only started to uncover the signaling pathways that imprint their identity, control their functions and enable their plasticity. Recent findings also identify other myeloid cell types capable of red blood cell removal and establish reciprocal cross-talk between the intensity of erythrophagocytosis and other cellular activities. Here, we aimed to review the multiple and emerging facets of iron recycling to illustrate how this exciting field of study is currently expanding.

Keywords: iron homeostasis; hemolysis; heme; hemoglobin; ferroportin; hepcidin



Citation: Slusarczyk, P.; Mleczko-Sanecka, K. The Multiple Facets of Iron Recycling. *Genes* **2021**, *12*, 1364. <https://doi.org/10.3390/genes12091364>

Academic Editor: Paweł Lipiński

Received: 31 July 2021
Accepted: 27 August 2021
Published: 30 August 2021

Publisher’s Note: MDPI stays neutral with regard to jurisdictional claims in published maps and institutional affiliations.



Copyright: © 2021 by the authors. Licensee MDPI, Basel, Switzerland. This article is an open access article distributed under the terms and conditions of the Creative Commons Attribution (CC BY) license (<https://creativecommons.org/licenses/by/4.0/>).

1. Introduction

Red blood cells (RBCs) or erythrocytes represent the most abundant cells in the human body, highly specialized for the shuffling of oxygen and carbon dioxide between the lungs and tissues. The binding of these gaseous particles is mediated by heme, an iron-containing prosthetic group that constitutes an integral part of the protein hemoglobin. The production of RBCs in a process called erythropoiesis is very rapid and yields approximately 200 billion RBCs daily, corresponding to 2.5 million every second [1] (Figure 1). This process tightly synchronizes intensive iron acquisition and the synthesis of heme with the translation of the globin polypeptides [2], which ultimately assemble stoichiometrically into hemoglobin composed of 2 α and 2 β globin chains, each binding one heme moiety. To perform their functions, mature RBCs are packed with remarkable amounts of hemoglobin that make up approximately one third of all erythrocytic proteins [3]. This is possible due to the expulsion of the nucleus and the elimination of all other key organelles, such as mitochondria, ribosomes, endoplasmic reticulum and the Golgi apparatus, throughout the erythroblast terminal differentiation [4].

The unique oxygen-carrying capacity of RBCs renders them particularly sensitive to oxidative damage. A fraction of hemoglobin-bound oxygen generates the superoxide anion that may further decompose into hydrogen peroxide and the highly reactive hydroxyl radical (OH) [5,6]. Hence, RBCs are well equipped with enzymes that protect them from reactive oxygen species (ROS), such as superoxide dismutase and catalase, but their activity decreases during the lifespan of RBCs [7]. Recent studies demonstrated that RBCs contain also significant amounts of non-heme iron that need to be exported by the sole iron transporter ferroportin (FPN) to sustain proper RBC functions [8]. Genetic abrogation of this efflux pathway provokes oxidative stress and results in enhanced hemolysis. Therefore,

the natural aging of circulating RBCs is in part underlain by progressive oxidative damage of proteins and lipids, which cannot be compensated due to the lack of organelles and cellular machinery responsible for de novo biosynthetic processes [5,6] (Figure 1). It has been estimated that the lifespan of RBCs is around 115 days [9] or 120 ± 4 days [6] in healthy humans and approximately 40 days in mice [10] (Figure 1). After reaching natural senescence or upon damage, RBCs are removed from the circulation by reticuloendothelial macrophages in a process called erythrophagocytosis. The continuous erythropoietic activity requires 2×10^{15} iron atoms every second and approximately 25 mg iron daily [11]. Since dietary iron availability is limited, mammals have evolved an efficient strategy for iron recycling, where approximately 90% of the iron demand for heme synthesis during erythropoiesis is ensured by the retrieval of iron from engulfed erythrocytes [12] (Figure 1). Hence, similarly to the production of RBCs, the rate of their sequestration is also estimated to be very high, reaching 2–3 million per second [13]. Over a human lifespan of around 60 years, it removes the mass of naturally aged RBCs that equals around 400 kg [6] and it continuously captures injured RBCs that otherwise could disrupt inside blood vessels and cause danger to surrounding tissues. Therefore, RBC clearance is a fundamental process for mammalian physiology that enables the turnover of the internal body iron pool. Nevertheless, the exact molecular mechanisms that are involved in the sequestration of senescent or damaged RBCs by distinct macrophage populations, primarily in the spleen and liver [14], are far from being fully elucidated. This is exemplified by a new provocative study that proposes a significant contribution of local hemolysis of RBCs in the spleen to their clearance. Furthermore, we have recently started to uncover signaling pathways important for the differentiation and biological roles of iron-recycling macrophages within their tissue microenvironment. Recent reports also illustrate how different pathophysiological conditions, such as recovery from acute anemia or inflammation, exploit the plasticity of iron-recycling macrophages to alter their functions or mediate the differentiation of novel subtypes of erythrophagocytic cells, distinct from those present under steady-state conditions. Lastly, new insights now emerge into the consequences of intensified RBC clearance for macrophage immune polarization. Within this review, we intend to cover all the above multiple facets of iron recycling. We will provide an update on the molecular mechanisms involved in the recognition and the removal of red blood cells, summarize insights into cues that mediate the development of iron-recycling cells and discuss reciprocal cross-talk between erythrophagocytosis intensity and other cellular functions of macrophages.

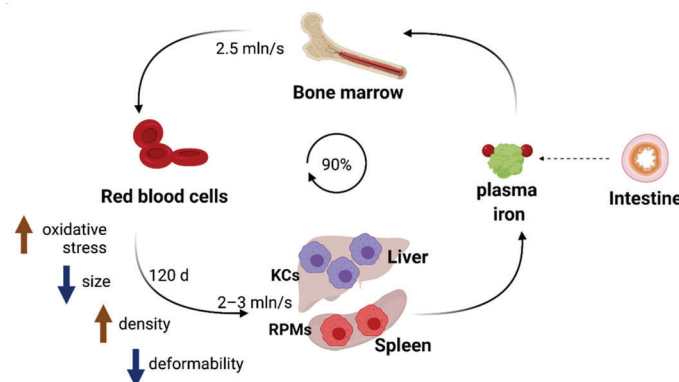


Figure 1. Iron recycling ensures the turnover of the body iron pool. Approximately 90% of iron needs for erythropoiesis are met by internal iron recycling from aged red blood cells. This task is accomplished by macrophages, predominantly Kupffer cells (KCs) in the liver and red pulp macrophages (RPMs) in the spleen. When erythrocytes age (in approximately 120 days in humans), their elasticity is reduced, which mediates their trapping in iron-recycling organs and further engulfment by KCs and RPMs.

2. Recognition of Aged or Damaged RBCs by Iron-Recycling Macrophages

Over their 120-day lifespan, human RBCs travel approximately 500 km through the blood vessels, including narrow capillaries [15]. This is possible due to the very high elasticity of these unique cells. Their deformability depends on several factors: (i) interactions between the so-called RBC cytoskeleton, composed of spectrin, actin and ankyrin, with other integral membrane proteins, such as the 4.1 and 4.2 proteins and the cytosolic domain of the highly abundant Band 3 protein, (ii) proper ion and water homeostasis, (iii) optimal volume-to-surface ratio and (iv) membrane fluidity [16,17]. One of the major characteristic changes in aged RBCs is the loss of their elasticity, tightly linked to their dehydration, densification and shrinkage [13] (Figure 1). This is underlain by a few mechanisms. First, constant exposure of RBCs to oxidative stress leads to the oxidation and denaturation of hemoglobin, as well to the formation of lipid peroxides, which both may promote the clustering of Band 3 protein [12,18]. This, in turn, disrupts the erythrocytic membrane architecture, increasing cell rigidity. Second, the depletion of ATP levels [19] in aging RBCs and the decreased number of sodium pumps per cell [20] lead to the impairment of the active ion transport, thus causing a decline in the transmembrane Na^+ and K^+ gradient [21]. Interestingly, although these alterations would be expected to mediate cell swelling, senescent RBCs lose water, becoming smaller and denser. This phenomenon may be linked to two players, the mechanoreceptor PIEZO1, whose activating mutation causes severe RBC dehydration, which is a hallmark of dehydrated hereditary stomatocytosis [22], and the Gardos Ca^{2+} calcium channel [21]. One of the models proposes that normal circulatory shear stress activates PIEZO1 and elicits surges in cell calcium, which in turn stimulates the Gardos channel and leads to progressive losses of potassium and fluid. This model is consistent with the observation that naturally aged RBCs contain higher intracellular calcium levels [23]. Densification of naturally aging RBCs is associated with a modest depletion of hemoglobin that occurs mainly via the shedding of hemoglobin-containing vesicles that are cleared by the spleen and liver macrophages [24]. The formation of such vesicles is also responsible for a drop in RBC lipid content [5]. Importantly, the loss of RBC elasticity is not only characteristic of naturally aged RBCs but also a hallmark of defective or injured RBCs in genetic disorders including sickle cell disease, thalassemia and hereditary spherocytosis, as well as acquired pathologies such as sepsis, malaria or diabetes [25,26].

Experimental data showed that poorly deformable, aged or damaged erythrocytes are engulfed primarily in the liver and in the spleen [27] (Figure 1). The spleen is characterized by an open blood system and unique architecture that confers quality control for stiffened aged RBCs [25,28]. Within the red pulp of the spleen (which constitutes approximately 75% of the spleen mass), blood arrives into areas of reticular connective tissue that forms so-called splenic cords. To re-enter into the circulation, RBCs need to pass through narrow endothelial slits of the red pulp venous sinusoids. Those that are too rigid are retained within the spleen cords and hence can be recognized and phagocytosed by iron-recycling red pulp macrophages (RPMs), which constitute approximately 50% of the red pulp [25] (Figure 1). Quantitatively, the “open” blood flow pathway receives 10% to 20% of the splenic blood flow, and the biomechanical integrity of each RBC is thus verified by the spleen approximately every 2 h [25].

It is less clear if and how senescent and poorly deformable RBCs are trapped in the liver. One report suggested that liver sinusoidal endothelial cells (LSECs) aid in the tethering of aged RBCs within hepatic sinusoids, thus facilitating their engulfment by liver macrophages called Kupffer cells (KCs) [29] (Figure 1). Recent in-depth imaging studies of the hepatic tissue architecture also illustrate that KCs not only reside within the sinusoidal vessels, often occupying most of their lumen, but also spread into the space of Disse, a niche between LSECs and hepatocytes [30]. It is plausible that such a local microenvironment, with the narrow lumen of sinusoids lined to LSECs and packed with KCs that protrude across the endothelial wall, is involved in capturing rigid RBCs.

As illustrated by the experimental data, macrophages are the major cell type that sequesters RBCs in the steady state. The liver is characterized by the highest abundance of F4/80-positive macrophages, classified typically as KCs [31]. Consistently, the liver sequesters the largest amounts of stressed RBCs [27]. Single-cell transcriptome data of liver non-parenchymal cells enriched for F4/80-positive cells revealed that KCs show some degree of heterogeneity, comprising a few distinct clusters [32]. Indicated by the presence of RBC-derived mRNAs, only a small subset might be active in RBC engulfment in a given moment. Youssef et al. demonstrated that in the spleen, mostly RPMs, and, to a much smaller extent, Ly6C-high monocytes, can engulf senescent RBCs, but other cell types, such as granulocytes, dendritic cells or lymphocytes, exhibit very little or no erythrophagocytic capacity [33]. Bian et al. showed that RPMs are the most efficient phagocytes towards RBCs as compared with other splenic macrophage subsets, such as metallophilic or marginal zone macrophages [34]. Finally, in line with the observation that, at the systemic level, the bone marrow contributes minimally to the clearance of stressed RBCs [27], macrophages in this tissue were shown to be much less efficient in erythrophagocytosis than RPMs [33]. It is important to note that the clearance of stressed RBCs is rapid and takes 10–20 min [27] up to a few hours [33,35].

Recognition and phagocytosis of “trapped” RBCs by macrophages involve additional signals, but it is not well understood if these mechanisms fully overlap between KCs and RPMs. One of the proposed recognition modes involves the binding of phosphatidylserine (PS), a phospholipid that is typically exposed on the external leaflet of the plasma membrane of apoptotic cells [5] (Figure 2). It has been shown that forced exposure of a PS derivative at the surface of RBCs triggers their clearance, predominantly in the spleen [36]. Furthermore, aged human RBCs isolated from the blood according to their high density [37] or mouse RBCs that remained in the circulation for a prolonged time (marked by prior biotinylation) [38] exposed PS on the surface and could be efficiently cleared when transfused into mice. However, other studies reported that the PS externalization does not correlate with natural RBC aging, but rather is a hallmark of injured and stressed RBCs that need to be sequestered [39]. Consistently, RBCs isolated from sickle cell disease or thalassemia patients that are prone to premature clearance contain a higher percentage of cells positive for exoplasmic PS than RBCs from control subjects [40,41]. Moreover, others showed that the induction of oxidative stress by chemical agents that mimic ROS buildup during physiological RBC aging does not lead to PS exposure [42]. In sum, PS exposure is a hallmark of defective or injured RBCs in certain pathophysiological conditions and might contribute to the clearance of naturally senescent RBCs, but it likely does not act as the most critical signal for their removal. Nevertheless, published RNA sequencing data show that both KCs [43] and RPMs [44] express relatively high levels of scavenger receptors that recognize PS (Figure 2). These include mainly TIM4, a marker of native tissue-resident macrophages [45], and the TAM receptors AXL and MERTK, whose high levels on KCs were also detected using liver tissue immunofluorescence [46]. In the context of TAM receptors, they act via an additional ligand GAS6, but its exact cellular source for the recognition of aged or injured RBCs would need to be specified. Alternatively, PS can be also bound by another ligand, MFG-E8, and further recognized by $\alpha_V\beta_{III}$ integrin [47]. The gene *Itgav* that encodes for integrin α_V (CD51) is expressed by both KCs and RPMs, albeit in low levels. Other receptors that may recognize PS are stabilins STAB1 and STAB2. They are only mildly expressed by KCs but are abundant in the liver LSECs, and they were implicated in the aforementioned tethering of stressed RBCs within liver sinusoids [29]. In RPMs, STAB2 shows an intermediate level of expression as compared to other receptors, and STAB1 is almost absent. The extent to which stabilin-mediated sequestration may operate within the splenic sinusoids and whether it can involve endothelial cells is still unknown. Another important scavenger receptor for PS, CD36, was implicated mainly in the RBC removal in malaria, which affects both infected and non-parasitized RBCs [48,49]. This is supported by the observation that individuals carrying a CD36 nonsense mutation are protected from malaria-induced anemia that was linked to augmented erythrophagocytosis [50]. CD36

appears to be weakly expressed by RPMs, whereas in KCs, depending on the dataset, the expression is either low or high [43]. Other receptors that recognize PS and were described in the clearance of apoptotic cells, such as BAI-1, or TIM1 and 3 [51–53], show little or no expression in iron-recycling cell macrophages from the liver and spleen, whereas SR-AI (encoded by *Msr1*) has intermediate expression levels in KCs and low in RPMs.

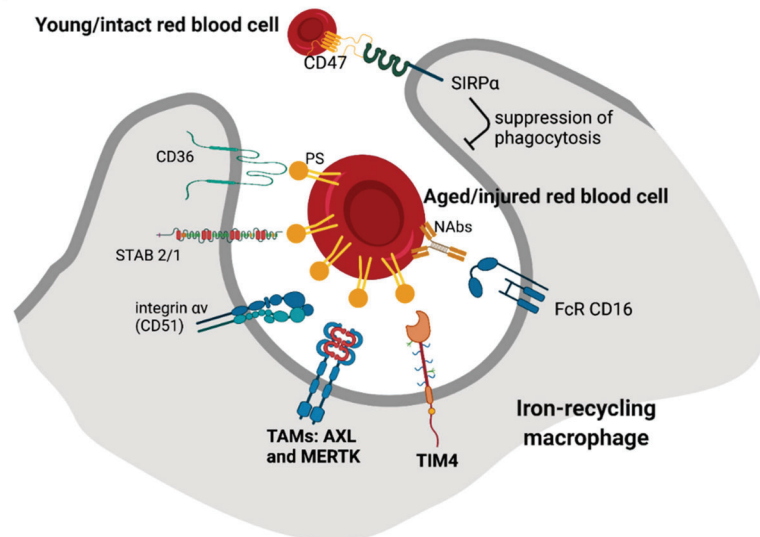


Figure 2. Recognition of red blood cells' biochemical integrity by iron-recycling macrophages. Aged/injured erythrocytes expose exoplasmic phosphatidylserine (PS) on their surface and become opsonized by naturally occurring antibodies (NAbs). Among the cognate receptors for these senescence signals that are expressed on RPMs and KCs, TAM receptors AXL and MERTK, TIM4 and Fc receptor CD16 are the most abundant. A “don't eat me” signal that prevents the clearance of young and intact erythrocytes is provided by the interaction between SIRP α at the surface of the macrophage with CD47 expressed by erythrocytes.

Another important mechanism that was proposed for the recognition of senescent RBCs is mediated by their opsonization by naturally occurring antibodies (NAbs) [6] (Figure 2). It was shown that those physiologically senescent RBCs that either constituted the densest fraction from collected human RBCs [54,55], circulated in the blood of dogs for at least 100 days [56] or were enriched in mice due to the hypertransfusion protocol [57] all showed increased binding of autologous antibodies on their surfaces. The majority of them were of the IgG isotype, but some were IgMs and IgAs [54,55]. Further studies have indicated that damaged or stressed RBCs, such as those exposed to oxidative agents or present in sickle cell patients, are also opsonized by NAbs [58,59]. The main mechanism responsible for the formation of antigens on the RBCs' surfaces is the interaction between denatured hemoglobin (termed hemichrome) with the Band 3 protein. This disrupts membrane structure and leads to Band 3 clustering and the formation of protein aggregates that also contain other RBC components [59,60]. Consistently, according to RNA sequencing data, both RPMs and KCs express high levels of the Fc receptors CD16 but very little CD32 (Figure 2). It was also shown that the binding of autologous antibodies promotes further opsonization by complement components, thus strengthening the phagocytic removal [6,61]. However, the complement receptors CR1/CR2 (CD35/CD21), CR3 (*Itgam*), CR4 (*Itgax*) or CD88 are very low or absent in RPMs and KCs, raising the question of whether physiologically complement opsonization indeed facilitates erythrophagocytosis.

Some other signals for the recognition of senescent RBC were proposed and involve the loss of sialic acid [6] and a functionally related interaction between adhesion molecules of

RBCs (Lu/BCAM) and the extracellular matrix component laminin- α 5 [62]. Nevertheless, opsonization by NAbs as well as PS exposure emerge as dominating senescence signals. Interestingly, however, the genetic loss-of-function studies of their cognate receptors in the context of erythrophagocytosis *in vivo* are still lacking. Therefore, the exact molecular nature of such “eat me” interactions between senescent or stressed RBC and endogenous RPMs and KCs, as well as their precise contribution to iron recycling both in the liver and the spleen, remain elusive. However, it should also be stated that such studies may be challenging as the iron-recycling capacity in the liver and the spleen exhibits some plasticity and may be supported by recruited monocytes, distinct from native RPMs and KCs (as described in detail below). Furthermore, one study proposed that natural aging as opposed to *in vitro* stress induces relatively moderate senescence signals that likely act additively and promote the removal of RBCs *in vivo* but not *in vitro* [38]. This raises also the possibility that the tissue microenvironment promotes RBCs’ engulfment, which will be discussed below.

In contrast to the signals that promote erythrophagocytosis, which remain not completely deciphered, it is well established that a “don’t eat me” signal is provided by an interaction between CD47 on the surface of RBCs with the SIRP α receptor on macrophages (Figure 2). It was shown that this axis prevents phagocytosis of undamaged RBCs and protects also other cell types and platelets [34]. Upon transfusion, CD47-null RBCs are rapidly sequestered from the circulation. Strikingly, this clearance is exclusively accomplished by the splenic, not liver, macrophages, and does not depend on NAbs or complement opsonization [63]. However, the binding of CD47 by its receptor is effective in suppressing antibody-mediated RBC recognition but fails to prevent the uptake of oxidatively stressed RBCs [64]. It was also demonstrated that the high degree of RBC rigidity overrides the “self” signaling conferred by CD47 [65]. It has been proposed that a drop in CD47 levels accompanies the physiological aging of murine RBCs and contributes to their natural turnover [38,66]. Decreased levels of CD47 may also represent one of the clearance signals of RBCs that are stored for a prolonged time before transfusion [67]. Mechanistically, the inhibition of phagocytosis upon CD47–SIRP α interaction depends on the binding of the phosphatases SHP-1/2 to the cytoplasmic domain of SIRP α [68]. One important study proposed that CD47 may also undergo conformational alteration during RBC aging and thus switch from an inhibitory to stimulatory signal for phagocytosis [69]. This mechanism may involve the binding of thrombospondin-1 to CD47 and other domains on the cytoplasmic part of SIRP α than those required for the inhibition of phagocytosis. Interestingly, since cancer cells often induce CD47 to evade immune eradication [70] and malaria parasites infect young CD47-high RBCs to avoid clearance, targeting of the CD47–SIRP α axis is of high therapeutic interest [71,72].

Lastly, it is worth mentioning that RPMs in the spleen may play an important role in maintaining RBCs’ fitness. It was shown that RBCs isolated from splenectomized patients contain cytoplasmic inclusion bodies (packed with chromatin, denatured hemoglobin or excessive iron), thus suggesting that the spleen facilitates their clearance [73].

3. Sequestration of Hemolytic Erythrocyte Components

Early kinetic studies implied that in the steady state in humans, slightly above 10% of RBCs may undergo intravascular hemolysis, thus releasing free hemoglobin (Hb) [74] (Figure 3). It is well established that the increased prevalence of hemolytic events is a hallmark of several hereditary anemias, including sickle cell disease, spherocytosis, autoimmune hemolytic anemia, erythropoietic protoporphyria and pyruvate kinase deficiency [75,76]. Free Hb is sequestered by haptoglobin, an acute phase plasma protein that is primarily produced in the liver [77]. The complex of Hb–haptoglobin is taken up via CD163-mediated endocytosis [78] (Figure 3). Both KCs and RPMs express high levels of CD163, as indicated by sequencing data [43,44] and immune detection in tissue sections [79,80]. Studies using radiolabeled Hb show that the clearance of injected hemoglobin is rapid [81] and mostly accomplished by the liver, spleen and kidney, with their contributions vary-

ing depending on the Hb dose [81,82]. Interestingly, pharmacokinetic experiments in non-rodent species show that the clearance rate for the Hb–haptoglobin complex is much slower than for free Hb [83] and, consistently, some reports implied that other routes for Hb sequestration exist that are independent of haptoglobin and/or CD163 [84,85]. One such mechanism involves renal glomerular filtration, as indicated by profound renal Hb uptake and iron loading in the kidney of haptoglobin-null mice [81,82]. However, it remains to be established if other means of alternative Hb clearance exist in the body. This is a particularly important question as the haptoglobin pool in the serum may become depleted during a prolonged hemolytic crisis [76].

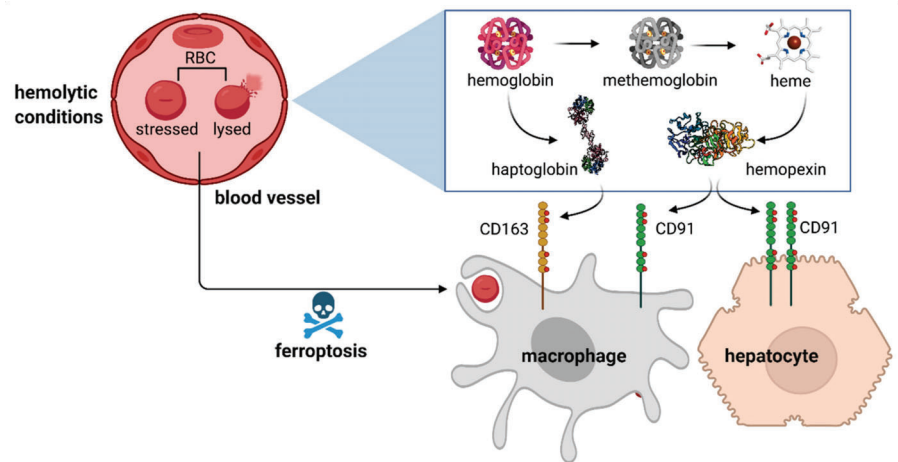


Figure 3. Sequestration of hemolytic erythrocyte components. During hemolysis, the components of RBCs, free hemoglobin and heme, are sequestered by the plasma scavenging proteins, haptoglobin and hemopexin, respectively. The removal of the formed complexes by macrophages and hepatocytes is mediated via the CD163 and CD91 receptors. Under the conditions of erythrolytic stress, macrophages are depleted by intensified erythrophagocytosis that leads to ferroptosis.

Under prooxidative conditions, ferrous iron of hemoglobin may undergo oxidation [86]. This leads to the formation of methemoglobin, which is unstable and releases free heme (Figure 3). Free heme is sequestered by another scavenging protein, hemopexin, which protects from heme-induced vascular dysfunction and heme-triggered inflammation [87,88]. The complex of heme–hemopexin is bound by the receptor CD91 (LRP-1) [89], which is expressed mainly on hepatocytes and, to a lesser extent, on iron-recycling macrophages [43,44] (Figure 3). This is also in agreement with the fact that mice deficient in heme catabolism that consequently lose macrophages due to heme-mediated toxicity show iron re-distribution to hepatocytes [90].

4. Hemolysis-Driven Iron Recycling Model

In light of the well-established view that the removal of naturally aged or stressed RBCs is accomplished predominantly via phagocytosis, a recent study by Klei et al. proposed a new mechanism mediated by local hemolysis in the spleen [80]. It was demonstrated that human spleen tissue contains a proportion of RBCs devoid of hemoglobin, so-called erythrocyte ghosts. In mice, representative flow cytometric data implied that a subset of red pulp macrophages phagocytosed preferably such ghosts upon transfusion of senescent RBCs. In support of the proposed model, *in vitro* flow assay and state-of-the-art imaging of human spleen tissue indicated that the hemolysis of aged erythrocytes is driven by the interaction between laminin- α 5 located in sinusoids with the Lu/BCAM adhesion complex at the surfaces of RBCs. The authors further propose that hemoglobin is locally sequestered by splenic haptoglobin and the complex undergoes endocytosis via CD163

expressed by RPMs. Although this novel model is highly interesting and undoubtedly contributes to the RBC turnover, it raises additional questions that may be addressed by further investigations. For example, it would be informative to quantify precisely how much hemolysis-driven vs. phagocytosis-driven RBC removal contributes to the overall turnover of RBCs and if any hemolytic events also accompany erythrocyte sequestration in the liver. Another important question would be if indeed CD163-mediated Hb uptake by macrophages represents the sole mechanism for Hb uptake, taking into account that other haptoglobin or/and CD163-independent mechanisms may exist. The authors of this novel report also used the gating strategy for RPMs, contrary to other laboratories that investigated the functions of these cells [33,91–94] (based on their autofluorescence rather than surface markers). Klei et al. did not discuss their intriguing data in relation to the work of Youssef et al., where senescent RBCs that contained GFP in their cytoplasm were employed for transfusion [33]. In their hands, approximately 40% of RPMs were GFP-positive 2 h post-injection, indicating classical phagocytic uptake, and already after 5 h, RPMs induced the heme-responsive gene *Spi-c*, suggesting that RBCs were efficiently degraded and heme was released inside the cells. Furthermore, another report by Ma et al. demonstrates that mice with a macrophage-specific activating mutation of the PIEZO1 calcium channel show increased phagocytic capacity of RPMs, thus driving intensified RBC removal. How these important data could be interpreted in light of the hemolysis-driven RBC sequestration remains to be better explained. In summary, the novel and provocative data presented by Klei et al. would benefit from further follow-up studies.

5. Erythrophagocytosis and Intracellular Iron Handling in Iron-Recycling Cells

Mechanistic details of how phagocytosis of RBCs is accomplished and regulated are still incompletely understood (Figure 4). Studies in cultured macrophages implied that this process may involve components of the autophagy machinery, hence engaging a route of so-called LC3-associated phagocytosis (LAP) [95]. LAP is known as means of the removal of apoptotic cells that triggers the anti-inflammatory and immunosuppressive responses of macrophages, a phenomenon that is of high clinical interest in the context of anti-tumor immunity [96]. However, loss-of-function studies that would address whether LAP-deficient RPMs or KCs in vivo exhibit defects in erythrophagocytosis are still lacking. As illustrated by in vitro microscopy imaging of erythrophagocytosis in primary macrophages, upon the formation of phagosomes, LAMP-1-positive lysosomes are recruited, thus maturing into phagolysosomes [97] (Figure 4A). Interestingly, this process also might be supported by the fusion with endoplasmic reticulum membranes [97,98]. Cellular components of RBCs are degraded, globins are hydrolyzed and heme is released. Both in vitro and in vivo data demonstrate that the decomposition of RBCs is a relatively rapid process, as already within the few first hours post-erythrophagocytosis, heme-responsive genes are induced [33,99–101]. Since RBCs contain both non-heme and heme iron [8], transporters for both these cargoes are recruited to phagolysosomal membranes (Figure 4A). According to in vitro data obtained in cultured primary macrophages, the former include primarily the metal transporter NRAMP1 [97]. Mice deficient for NRAMP1 show enhanced iron retention in the spleen and liver, supporting the physiological role of NRAMP1 in iron recycling from RBCs [102]. The main heme-catabolizing enzyme, heme oxygenase 1 (HO-1), was shown to reside primarily in the cytoplasm of macrophages [97]. Consistently, the heme transporter HRG1, originally identified in genetic screens in *C. elegans* [103], was shown to be recruited to erythrophagolysosomes to enable heme delivery to the cytoplasm [3,97]. Further studies using zebrafish and mouse models further corroborated the critical role of HRG1 in iron recycling, especially by demonstrating that HRG-1 deficiency is lethal in mice fed an iron-deficient diet [94,104]. Pek et al. also demonstrated that the lack of HRG1 in mice leads to the formation of hemozoin, the heme aggregate previously found only in parasites, within the enlarged lysosomes of iron-recycling macrophages [94].

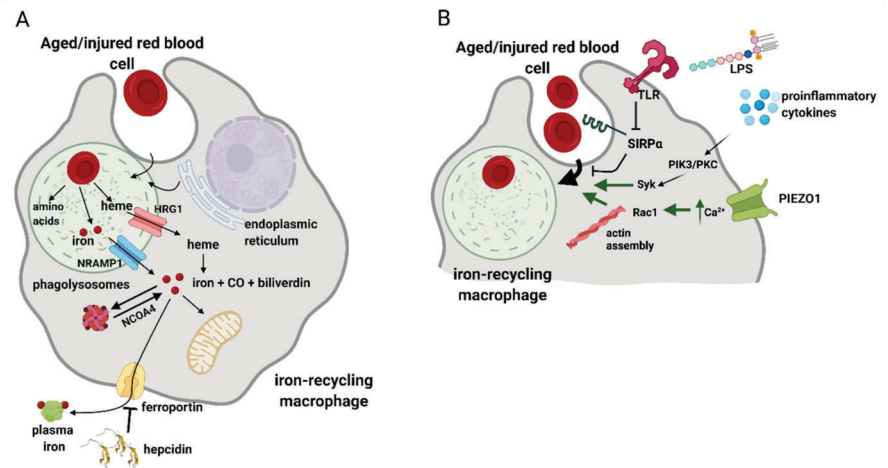


Figure 4. The process of erythrophagocytosis and the emerging mechanisms of its regulation. (A) RPMs and KCs are proficient in recognizing and engulfing aged RBCs, which, to a large extent, is mediated by the process called erythrophagocytosis. Upon the formation of phagolysosomes, cellular components of RBCs are degraded, globins are hydrolyzed to amino acids and heme is released. Non-heme iron that is present in RBCs is transported by NRAMP1. Heme is transported to the cytoplasm by HRG1 and subsequently catabolized by heme oxygenase 1 (HO-1) to carbon monoxide (CO), biliverdin and ferrous iron. Iron is sequestered by ferritin and, upon increased iron demand, can be released from ferritin via ferritinophagy in an NCOA4-dependent fashion. Iron efflux occurs via ferroportin and replenishes the pool of plasma iron. The process of iron release from macrophages is tightly regulated by hepcidin, a small liver-derived hormone that mediates ferroportin degradation and/or occlusion, hence preventing iron release from the macrophage iron reservoir. (B) Recent advances showed that the intensity of erythrophagocytosis can be enhanced by proinflammatory conditions and bacterial components, such as lipopolysaccharide (LPS). These effects are mediated by the downregulation of SIRP α and PIK3/PKC/Syk-dependent signaling. The PIEZO1 mechanoreceptor was identified as a positive regulator of erythrophagocytosis and was shown to control calcium levels and actin remodeling in iron-recycling macrophages.

In the cytoplasm, HO-1 degrades heme to carbon monoxide, biliverdin and ferrous iron (Figure 4A). Lack of HO-1 leads to a severe phenotype in mice, hallmarked by embryonic lethality of approximately 90% of homozygous knock-out mice [90,105]. Those HO-1-null mice that survive show a progressive loss of KCs and RPMs due to heme-driven toxicity and develop fibrosis in the red pulp of the spleen. Nine cases of human mutations in *HMOX-1* encoding for HO-1 were reported in the literature and the majority of these patients were characterized with chronic inflammation, hemolysis and asplenia, thus further corroborating the critical roles of HO-1 for maintaining blood homeostasis. Ferrous iron generated by HO-1 replenishes the cytoplasmic reservoir of metabolically available iron, called the labile iron pool (LIP) [11] (Figure 4A). Iron from LIP is sequestered by ferritin, a nanocage heteropolymer that oxidizes and stores iron, which is also post-transcriptionally induced upon RBC sequestration [99]. To the best of our knowledge, the characterization of iron-recycling capacity and body iron indices in macrophage-specific ferritin-null mice is still lacking. Under conditions of increased iron demand, ferritin is targeted by nuclear receptor coactivator 4 (NCOA4) for autophagic degradation, called ferritinophagy [106]. A proportion of iron from LIP is released by iron-recycling macrophages by the sole iron exporter FPN [107], which itself is induced following erythrophagocytosis [100,101] (Figure 4A). Iron efflux from macrophages is coupled with the oxidation of ferrous to ferric iron by ceruloplasmin and replenishes the pool of serum iron required for continuous erythropoiesis [11]. Hence, mice with macrophage-specific deletion of *Slc40a1* that

encodes for FPN are presented with mild anemia accompanied by splenic and hepatic iron accumulation, phenotypes that are exacerbated by hemolytic challenge or iron-deficient diet [108]. The process of iron release from RPMs is tightly regulated by hepcidin, a small liver-derived hormone that adjusts plasma iron levels to body iron needs [107,109]. Hepcidin acts by mediating FPN degradation and/or occlusion, thus causing macrophage iron retention and serum hypoferrremia [109,110]. This is characteristic of the inflammatory conditions that typically lead to high hepcidin levels [111], but hepcidin-independent and rapid FPN downregulation in response to pathogen-associated molecules was also described [112]. Conversely, low hepcidin levels, which are a hallmark of iron deficiency and other conditions characterized with high iron demand for erythropoiesis, lead to FPN stabilization and boosted iron export capacity of iron-recycling macrophages [11,113,114]. Despite the growing body of knowledge, we still do not understand completely how iron is trafficked in iron-recycling macrophages and how iron from LIP is distributed between intrinsic metabolic cellular needs and the export route.

Regarding the fate of heme iron following endocytosis of the Hb-haptoglobin complexes, another heme transporter called HCP1 was implicated in the delivery of heme to the cytoplasm from the endosomal compartment [115]. It remains to be better understood if other mechanistic details regarding heme and iron processing upon Hb uptake may reflect those associated with erythrophagocytosis.

6. Regulation of the Erythrophagocytosis Rate

The processes of RBC phagocytosis and digestion are considered largely constitutive. However, some reported data indicate that erythrophagocytosis may be subjected to different regulatory mechanisms (Figure 4B). Delaby et al. found that primary macrophages treated with proinflammatory stimuli, lipopolysaccharide (LPS) and interferon γ (INF γ) show increased phagocytic capacity towards RBCs [100]. In vivo, Bian et al. demonstrated that treatment of mice deficient for the SIRP α -CD47 inhibitory axis with interleukin 17 potentiates the erythrophagocytic activity of RPMs. In vitro follow-up studies implied that this response is mediated by protein kinase C and kinase Syk and is calcium-dependent. Another more recent study elegantly showed that the induction of a strong inflammatory response in mice leads to the downregulation of SIRP α in a toll-like receptor (TLR)-dependent fashion and, in parallel, enhances the phagocytic capacity of RPMs via PI3K- and Syk-dependent signaling [93]. Consistent with the role of calcium in controlling phagocytic activity, it was recently shown that PIEZO1, a mechanically activated nonselective cation channel, is an important regulator of erythrophagocytosis [116]. It was found that mice carrying a macrophage-specific activating mutation of PIEZO1 show enhanced phagocytic capacity of splenic RPMs. Mechanistic studies showed that this is driven by increased calcium signaling and the activation of small G protein Rac1, which controls actin cytoskeleton remodeling. In this context, it is interesting to note that heme accumulation in cultured primary macrophages was reported to inhibit phagocytosis of non-RBC-related cargoes via activation of small G protein Cdc42, which, similarly to Rac1, promotes actin polymerization. The observation that both suppression and excessive activity of small G proteins impairs phagocytosis may be explained by the fact that the complete engulfment of large cargoes relies on both actin assembly and the subsequent rapid deactivation of G proteins and actin disassembly [117]. Finally, another recent work identified transient receptor potential melastatin 7 (TRPM7), a cation channel with kinase activity, as a suppressor of RPMs' phagocytic activity through a mechanism that likely involves cytosolic alkalinization [118].

7. Development and Plasticity of Iron-Recycling Macrophages

RPMs and KCs belong to tissue-resident macrophages (ResM ϕ s), highly heterogeneous and multifunctional cells in the mammalian body that uniformly sustain homeostasis within specific microenvironments [119,120]. Genetic fate-mapping studies have shown that ResM ϕ s develop prenatally from embryonic progenitors, including yolk-sac

macrophages and fetal liver monocytes [121,122] (Figure 5). ResMφs from different organs show highly distinct transcriptional signatures and epigenetic landscapes [123–125], which reflect the niche-specific signaling programs that determine their identity. Differentiation of RPMs is governed by a few interconnected mechanisms that were discovered over the last few years (Figure 5). First, during early postnatal life, RPMs undergo rapid expansion that is accompanied by the induction of the peroxisome proliferator-activated receptor gamma (PPAR γ) transcription factor [126]. Genetic deletion of this regulator using the *Vav1*-Cre line that is specific to hematopoietic cells, including differentiating fetal monocytes, intrinsically abolished neonatal RPM development [126]. The few PPAR γ -deficient RPMs that remained showed differential transcriptomes to wild-type control cells, but the exact roles of the identified genes were not investigated in depth by the authors. One mechanistic detail provided in this work shows that PPAR γ -null RPMs fail to downregulate CD88 and integrin CD11a at the protein levels, which is characteristic of developing wild-type RPMs. Interestingly, PPAR γ -deficient RPMs, although much less in number, exhibited a similar capacity for erythrophagocytosis as wild-type cells. Finally, it was shown that the inducible deletion of PPAR γ in adult mice has no effects on RPM numbers and only mildly alters their transcriptional signature. Another important transcription factor that is dispensable for neonatal RPM expansion [126] but is critical for their survival in adulthood is SPI-C [127]. SPI-C-null mice show near-total loss of RPMs in the spleen, but a normal representation of KCs and other immune cells. Another report showed that mice lacking the VCAM-1 receptor are likewise characterized by reduced RPM numbers [128]. Similar to the *Vav1*-Cre-driven PPAR γ -null mice, SPI-C knock-out animals also surprisingly show normal hematological parameters and serum iron levels, but progressively accumulate iron in the spleen, indicative of defective iron recycling [127]. It may be speculated that the lack of iron-deficient phenotype in both models is due to the increased erythrophagocytic function of liver KCs or/and enhanced iron absorption from the diet. In line with these data, all three models (lacking PPAR γ , SPI-C or VCAM-1 in RPMs) respond also to hemolytic stress similarly to wild-type mice.

Further work identified *Spic* as the heme-responsive gene and has shown that induction of *Spic* is responsible for the differentiation of heme-loaded monocytes into RPMs under hemolytic stress [91] (Figure 5). Mechanistically, it was demonstrated that *Spic* transcription is repressed by BACH1, a factor that undergoes degradation in response to heme accumulation. This mechanism thus establishes a link between the major metabolite of RBCs' and RPMs' identity. Recent studies demonstrated that heme alone does not trigger the development of fully mature RPMs [92]. The final steps of the RPM differentiation process are dependent on the cytokine IL33, acting via its receptor IL1RL1 present on RPMs and the downstream signaling, via the ERK kinase and GATA1 transcription factor (Figure 5). Interestingly, IL-33 was shown to be derived from RBCs that recently were identified as an important source of various cytokines [129]. Finally, red pulp fibroblasts that express the WT1 transcription factor and release the CSF-1 cytokine were demonstrated to provide a meshwork that anchors and nourishes RPMs [130].

Niche-derived or cell-intrinsic signals that drive KCs' development and are required for their homeostasis are beginning to be understood (Figure 5). Sequencing data of the subsequent differentiation steps of cells during organogenesis, from myeloid progenitors through so-called pre-macrophages to specialized macrophage populations, revealed that KCs' identity is hallmarked by the induction of the *Id1*, *Id3*, *Nr1h3* and *Spic* genes [131]. Consistently, deletion of *Id3* (encoding for the transcriptional regulator inhibitor of DNA binding 3; ID3) or *Nr1h3* (encoding for the transcription factor liver X receptor- α ; LXR- α) in mice led to the loss of KCs' identity and depletion of this population [131,132]. Transcriptomic data generated by the Immgen Consortium [123] prompted studies that identified *Clec4f* as another highly KC-specific gene, although its exact role in KCs' physiology remains elusive [133]. Nevertheless, this allowed for the targeted ablation of this macrophage population from mice using a diphtheria toxin receptor-mediated strategy [133]. Scott et al. further found that the replenishment of the emptied KC niche is accomplished by the

recruitment of bone marrow monocytes. More recently, two important studies sought to decipher the mechanistic details that regulate KC niche repopulation [30,43] (Figure 5). They revealed that the recruited monocytes established close contacts with LSECs, hepatocytes and hepatic stellate cells (HSCs) in the liver sinusoids. LSECs were shown to provide Notch ligands, mainly DLL4, to induce LXR- α in monocytes, a response that was potentiated by BMP ligands released by HSCs and LSECs, with HSC-derived BMP9 playing likely a dominant role. Other factors identified as required for the imprinting of KCs' identity on replenished monocytes included transforming growth factor- β (TGF- β) released by the LSECs and endogenous hepatic LXL ligands. Furthermore, contact with hepatocytes was identified as means to induce *Id3* expression by a yet unknown mechanism. Interestingly, KCs of monocyte origin that are recruited to the emptied niche are highly similar to embryonically derived KCs [133]. Twelve genes that were >1.5-fold higher in original resident KCs compared to monocyte-derived cells included TIM4, a marker of ResM ϕ s [45], Hb-haptoglobin receptor CD163 and BMP receptor BMP9R1, which might be linked to the role of BMPs in the de novo occupancy of the KC niche, as described above [30,43].

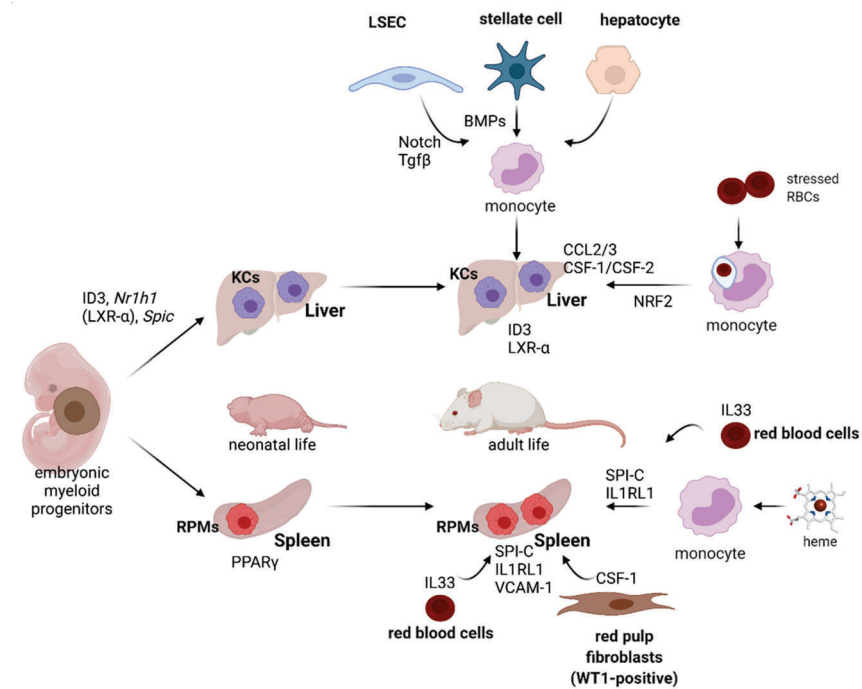


Figure 5. Pathways that imprint KCs' and RPMs' identity and enable plasticity of iron-recycling cells. RPMs' neonatal expansion depends on PPAR γ , whereas in adult life, their identity and numbers are maintained by SPI-C, VCAM-1, the IL33–IL1RL1 axis and CSF1 released by red pulp fibroblasts. Upon hemolytic stress, differentiation of monocytes into RPM-like cells is mediated by *Spi-c* induction due to heme loading and IL33 signaling. KC development is controlled mainly by ID3 and LXR- α . Differentiation of monocytes into functional KCs in emptied KC niche requires interaction with liver sinusoidal endothelial cells (LSECs), hepatic stellate cells and hepatocytes and soluble factors that are secreted by these cells, including Notch ligands, TGF- β and BMPs. Under erythrolytic stress, blood monocytes were shown to engulf stressed RBCs and differentiate into KC-like cells, which is driven by the chemotactic factors present in the liver and intrinsic NRF2 signaling in monocytes.

The ResM ϕ s of embryonic origin are proposed to maintain themselves due to their long-term self-renewal capacity, akin to that of stem cells [134]. The percentage of macrophages that are positive for Ki-67, a proliferation marker, is approximately 2% in KCs and 5–12%

in the RPM population [33,133]. Interestingly, in both these niches, partial depletion of the resident macrophages leads to enhanced proliferation of the remaining cells that contribute to de novo niche occupancy [33,133]. However, the mechanisms that regulate this increased mitotic activity are not yet elucidated.

Recent studies demonstrated that, under steady-state conditions, tissue macrophages of prenatal origin co-exist in several organs with those that are derived postnatally from monocytes [135]. By using a newly created reporter mouse model (driven by Cre recombinase under the monocyte-specific *Ms4a3* promoter) where cells of monocyte origin specifically expressed a fluorescent protein, it was revealed that in young (8-week-old) mice, approximately 20% of RPMs are already replenished from monocytes [135]. This is in agreement with the previous piece of work [133]. In contrast to RPMs, Liu et al. identified the minimal contribution of monocytes to the population of KCs in the steady state. This partially contradicts the findings of Scott et al. [133], who previously reported the replenishment rate of KCs to be approximately 30%. This discrepancy likely arises from the differential methodology, as the earlier study used an approach of adoptive transfer of congenic bone marrow cells into pups within the first few days after birth [133]. It remains an open question whether iron-recycling macrophages of monocyte vs. embryonic origin differ from each other functionally under steady-state conditions.

As exemplified above for KCs, replenishment from bone marrow-derived monocytes is particularly enhanced when the homeostasis of the resident macrophage population is disturbed. Early studies estimated that, physiologically, one KC engulfs approximately one erythrocyte per day [136]. For RPMs, around 10% of cells are actively phagocytosing in a given moment, and, typically, one erythrocyte can be detected in one red pulp macrophage [44]. KCs and RPMs are rapidly depleted by forced erythrophagocytosis [27,33], intravascular hemolysis or pharmacological inhibition of HO-1 [91]. This was proposed to occur due to heme cytotoxicity and ferroptosis, a form of cell death triggered by lipid peroxidation and promoted by the excessive cytoplasmic iron pool [137] (Figure 3). In the spleen, the differentiation of new monocyte-derived RPMs is mostly driven by the heme-mediated induction of *Spic* [91]. The extent to which the newly established RPMs resemble those originally residing in the niche, in terms of their transcriptional signature and iron-recycling functions, remains to be elucidated. Another important piece of work demonstrated that, upon exposure to an excess of stressed RBCs, and the depletion of resident iron-recycling macrophages, the liver, but not the spleen, takes over RBC clearance [27] (Figure 5). Damaged RBCs are first engulfed by circulating Ly6C-high monocytes, which migrate to the liver following chemotactic signals conferred by CCL2 and CCL3. Next, a high ratio of CSF-1/CSF-2 cytokines that is characteristic of the liver, but not the spleen, was shown to drive the further differentiation of monocytes into a myeloid population, which the authors termed transient macrophages (tMφs). These cells, characterized by high FPN levels, but negative for the ResMφs marker TIM4 [45], further acquired a transcriptional profile that resembled iron-recycling KCs, but still differed significantly from resident KCs of embryonic origin. This also implies that these KC-like cells that emerge after erythrolytic stress have a distinct identity from those that are recruited to the liver when the KC niche is depleted by the diphtheria toxin strategy [133]. The KC-like cells catabolized RBC-derived heme and delivered iron to hepatocytes. When the stress imposed by stressed RBCs declined, this population disappeared from the liver. The appearance of tMφs was dependent on the external chemotactic cues described above and intrinsic signaling via NRF2 (Figure 5). Interestingly, similar responses hallmarked by monocyte-mediated niche replenishment were absent in the spleen, a phenomenon explained by Threl et al. by the high inhibitory levels of CSF-2. These high-quality data and attractive model, however, contrast other important studies that clearly illustrated the contribution of monocytes to the renewal of the splenic iron-recycling niche after the stress imposed by damaged RBCs [33,91]. The reason for this discrepancy is not clear. Nevertheless, it may be expected that the defective iron recycling in the spleen may enhance RBCs' clearance in the liver. Indeed, this seems to be the case in IL-33- and IL1RL1-null mice, characterized by

diminished and less phagocytic RPMs and iron deposits in the liver [92]. Interestingly, liver iron levels remained unchanged in *Spic* knock-out mice, raising the question of how iron recycling is compensated in this model. It is likely that the disruption of the heme–SPI-C axis also prevents on-demand RBC clearance in the liver, as *Spic* is also induced during KC differentiation [131].

Substantial clinical interest is now focused on the correction of iron status in iron deficiency disorders of different etiologies [113]. The intravenous delivery of new-generation compounds is considered more effective and safer than the oral route. Currently, carbohydrate-coated iron cores are the formulations of choice, and several of these compounds are now FDA-approved drugs, not only to correct iron deficiency but also for diagnostic applications [138]. Interestingly, these iron nanoparticles are targeting mostly tissue and tumor-associated macrophages [138,139]. Therefore, it might be expected that, via the transient iron loading of erythrophagocytosing RPMs and KCs, such drugs may cause the depletion of these cells and hence trigger some degree of iron-recycling niche remodeling. Novel and promising formulations for oral iron delivery that are based on liposomal encapsulation [140] still need to be investigated in more detail for their biodistribution among different cell types.

Another important context for iron-recycling niche plasticity is the recovery from acute anemia. This process relies on the activation of stress erythropoiesis, which, in mice, is extramedullary and mostly takes place in the spleen. Earlier studies demonstrated that splenic macrophages nourish and support erythrocyte precursors with so-called erythroblastic islands (EBI) and thus are critical for recovery from anemic stress [141,142]. Further studies using a model of bone marrow transplantation and phenylhydrazine-induced hemolysis identified blood monocytes as the major source of early EBI during the recovery process, which next differentiate into RPM-like mature macrophages that further support erythrocyte maturation [143]. Initial monocyte recruitment was linked to the release of the CCL2 chemokine by those resident RPMs that were active in erythrophagocytosis. Follow-up work showed that signaling events in RPMs shape the maturation of the splenic stress erythropoiesis niche [144]. In the early phase, they secrete Wnt ligands to prevent differentiation of the erythroid progenitors and promote their proliferation. In the late phase, when erythropoietin (EPO) levels increase in response to tissue hypoxia, EPO receptor-dependent signaling in RPMs promotes the synthesis of active lipid mediators. Prostaglandin J2 activates intrinsically PPAR γ , which suppresses Wnt expression. This de-represses erythroid differentiation, which is additionally stimulated by RPM-derived prostaglandin E2. It remains to be elucidated whether similar PPAR γ -mediated signaling events are important for neonatal RPM development that depends on PPAR γ [126]. Another important study showed that, during recovery from inflammation-induced anemia, the increased capacity of RPMs for erythrophagocytosis (please see also the chapter devoted to the regulation of erythrophagocytosis) induces *Spic*, which, in turn, triggers the expression of *Gdf15*, one of the cytokines important for erythroid expansion. Taken together, these examples illustrate that the splenic macrophage niche is plastic, responds to external cues and communicates with other cell types to preserve homeostasis. Importantly, erythrophagocytosis intensity acts as an important signaling means to translate environmental conditions to macrophage output behaviors.

Other lines of evidence established further links between inflammatory/danger signals and iron recycling. An important work by Akilesh et al. shed light on the possible etiology of cytopenias in so-called macrophage activation syndrome (MAS), a pathological state that accompanies arthritis and other autoimmune diseases, certain viral infections and malaria [44]. The authors demonstrated that the activation of signaling from TLR receptors 7 and 9 triggers MAS-like syndrome in mice, hallmarked by anemia and thrombocytopenia. This was caused by specialized hemophagocytes that differentiate from monocytes, localized in the spleen, but show a distinct transcriptional signature from RPMs and exhibit higher erythrophagocytic capacity. Others, however, showed that the appearance of hemophagocytes in response to TLR9 ligands, and other signals such as TLR2, TLR3 or

TLR4 agonists, as well as TNF- α , IL-6 or IL-17A, is only observed in SIRP α -deficient mice, suggesting a protective role of this “don’t eat me” receptor [145]. Earlier studies demonstrated that specialized hemophagocytes may also arise in response to INF γ signaling and may sequester RBCs via macropinocytosis, a process that is a form of unspecific endocytic fluid-phase engulfment [146]. Pathological hemophagocytosis was also proposed in the etiology of Leishmania-triggered anemia and was linked to SIRP α downregulation [147]. Another report described hemophagocytosis in calcified vascular walls and implicated IL-18 as a signal that promoted this phenomenon [148].

8. Cross-Talk between Iron Recycling and Macrophage Immune Functions

Macrophages exhibit a wide spectrum of inflammatory phenotypes, ranging from ‘classically activated’ or M1 macrophages, which are pro-inflammatory, to ‘alternatively activated’ or M2 macrophages, which have immunoregulatory functions [149]. KCs provide anti-inflammatory milieu and maintain immune tolerance during homeostasis [150]. Similarly, RPMs were shown to produce immunosuppressive cytokines IL-10 and TGF- β , which promote the differentiation of regulatory T cells [151]. However, recently, RPMs were also implicated in the priming of cytotoxic T lymphocytes during an antiviral immune response [152]. Early work showed that transfusion of stored RBCs induces inflammation and favors bacteria growth, likely due to the higher iron availability for the pathogens [153]. In line with these findings, it has been reported that excessive iron loading and heme exposure polarize macrophages in the liver and spleen into a pro-inflammatory M1 phenotype [154]. Interestingly, two recent pieces of work illustrated that intensified erythrophagocytosis in the liver provokes immunosuppressive rather than immunostimulatory skewing of myeloid cells. Olonisakin et al. showed that transfusion of stressed RBCs before *Klebsiella pneumoniae* infection promotes bacteria growth and increases the risk of fatal sepsis [155]. This phenomenon was shown to be independent of the iron acquisition by bacteria but was mediated by the weakened antibacterial immune response. Whole liver transcriptional profiling indicated that the immunosuppressive effects of forced RBC degradation were mediated by the impairment of STAT1 signaling. Further in vitro studies identified the heme protoporphyrin ring but not iron as the hemoglobin-derived entity that is responsible for the compromised inflammatory response and showed that it acted via NRF1 and NRF2 signaling. Consistently, another study, which employed single-cell RNA sequencing, demonstrated clearly that an increased burden of defective RBCs leads to the appearance of strongly immunosuppressive myeloid cells in the liver [32]. Of clinical significance, their appearance was shown to be protective in two models of macrophage-driven hepatitis. Interestingly, the authors reported that, in vitro, heme-polarized macrophages exhibited a unique transcriptional signature, distinct from M1 or M2 macrophages. The enhanced rate of RBC engulfment was also recently linked to an increased risk of sepsis in another pathophysiological setting [16]. It was reported that the increased mucosal permeability of the intestine, characteristic of, e.g., inflammatory bowel disease, and the consequent transfer of bacterial components from the gut to the bloodstream impair the synthesis of unsaturated fatty acids in the liver. This, in turn, results in the decreased membrane fluidity of RBCs that triggers their premature clearance by splenic RPMs. Such an enhanced rate of erythrophagocytosis was proposed to underlie the elevation of body iron levels that promoted bacteria growth.

Investigations of tumor-associated macrophages (TAMs), cells that are known as strongly immunosuppressive, have revealed another layer of complexity regarding the cross-talk between iron recycling and immune polarization. It was demonstrated that a subset of TAMs that are located in the hemorrhagic tumor areas and become iron-loaded show a pro-inflammatory profile and enhanced anti-tumor activity [156]. Delivery of iron nanoparticles to TAMs was proven to be a promising therapeutic approach to enhance tumor immune eradication. However, interestingly, other lines of evidence showed that the deletion of HO-1 in TAMs, which is expected to decrease the iron release following the engulfment of RBC components, boosts anti-tumor immunity [157]. Likewise, genetic

depletion of a subset of CD163-positive TAMs, likely capable of Hb uptake, improves immune responses against cancer cells [158,159]. This is also consistent with the observation that anti-inflammatory agents, glucocorticoids, strongly induce CD163 expression [160].

Taken together, it becomes apparent that iron-recycling myeloid cells are highly heterogeneous and respond to disturbances of heme and iron balance, or exposure to stressed/senescent/hemolytic RBCs, in a context-dependent manner. More work is required to better understand how iron management in different subsets of macrophages may alter their immune functions.

9. Concluding Remarks

The growing body of work sheds light on new, exciting aspects of iron recycling. However, many questions remain open. The mechanistic details of RBC recognition, phagocytosis, degradation and the further processing of heme-derived iron are incompletely understood, and we lack knowledge of whether these processes are distinct between RPMs and KCs. It is not known if other cell types than those of myeloid origin contribute to RBC clearance and iron turnover in physiological or pathological conditions. Finally, we are only starting to identify how erythrophagocytosis is linked to other processes within or outside the tissue microenvironment of iron-recycling macrophages. We expect that many of these still elusive facets of iron turnover might be uncovered by future studies.

Author Contributions: Writing—original draft preparation, P.S. and K.M.-S.; writing—review & editing, K.M.-S.; funding acquisition, K.M.-S. All authors have read and agreed to the published version of the manuscript.

Funding: K.M.-S. acknowledges the support of the NCN grant (OPUS 2018/31/B/NZ4/03676).

Institutional Review Board Statement: Not applicable.

Informed Consent Statement: Not applicable.

Data Availability Statement: No new data were created or analyzed in this study. Data sharing is not applicable to this article.

Acknowledgments: Figures were created with BioRender.com.

Conflicts of Interest: The authors declare no conflict of interest.

References

- Palis, J. Primitive and definitive erythropoiesis in mammals. *Front. Physiol.* **2014**, *5*, 3. [CrossRef]
- Chen, J.-J. Regulation of protein synthesis by the heme-regulated eIF2 α kinase: Relevance to anemias. *Blood* **2006**, *109*, 2693–2699. [CrossRef]
- White, C.; Yuan, X.; Schmidt, P.J.; Bresciani, E.; Samuel, T.K.; Campagna, D.; Hall, C.; Bishop, K.; Calicchio, M.L.; Lapierre, A.; et al. HRG1 Is Essential for Heme Transport from the Phagolysosome of Macrophages during Erythrophagocytosis. *Cell Metab.* **2013**, *17*, 261–270. [CrossRef]
- Moras, M.; Lefevre, S.D.; Ostuni, M.A. From Erythroblasts to Mature Red Blood Cells: Organelle Clearance in Mammals. *Front. Physiol.* **2017**, *8*, 1076. [CrossRef]
- Bratosin, D.; Mazurier, J.; Tissier, J.; Estaquier, J.; Huart, J.; Ameisen, J.; Aminoff, D.; Montreuil, J. Cellular and molecular mechanisms of senescent erythrocyte phagocytosis by macrophages. A review. *Biochimie* **1998**, *80*, 173–195. [CrossRef]
- Lutz, H.U. Advances in Experimental Medicine and Biology. In *Naturally Occurring Antibodies (NABs)*; Springer: Berlin/Heidelberg, Germany, 2012; Volume 750, pp. 0065–2598.
- Tyan, M.L. Age-related increase in erythrocyte oxidant sensitivity. *Mech. Ageing Dev.* **1982**, *20*, 25–32. [CrossRef]
- Zhang, D.-L.; Wu, J.; Shah, B.N.; Greutelaers, K.C.; Ghosh, M.C.; Ollivierre, H.; Su, X.-Z.; Thuma, P.E.; Bedu-Addo, G.; Mockenhaupt, F.P.; et al. Erythrocytic ferroportin reduces intracellular iron accumulation, hemolysis, and malaria risk. *Science* **2018**, *359*, 1520–1523. [CrossRef] [PubMed]
- Franco, R.S. Measurement of Red Cell Lifespan and Aging. *Transfus. Med. Hemotherapy* **2012**, *39*, 302–307. [CrossRef] [PubMed]
- Dholakia, U.; Bandyopadhyay, S.; Hod, E.A.; Prestia, K. Determination of RBC Survival in C57BL/6 and C57BL/6-Tg(UBC-GFP) Mice. *Comp. Med.* **2015**, *65*, 196–201.
- Muckenthaler, M.; Rivella, S.; Hentze, M.W.; Galy, B. A Red Carpet for Iron Metabolism. *Cell* **2017**, *168*, 344–361. [CrossRef]
- Ganz, T. Macrophages and Systemic Iron Homeostasis. *J. Innate Immun.* **2012**, *4*, 446–453. [CrossRef]
- Higgins, J.M. Red Blood Cell Population Dynamics. *Clin. Lab. Med.* **2014**, *35*, 43–57. [CrossRef] [PubMed]

14. Knutson, M.; Wessling-Resnick, M. Iron Metabolism in the Reticuloendothelial System. *Crit. Rev. Biochem. Mol. Biol.* **2003**, *38*, 61–88. [[CrossRef](#)]
15. Lasch, J.; Küllertz, G.; Opalka, J.R. Separation of Erythrocytes into Age-Related Fractions by Density or Size? Counterflow Centrifugation. *Clin. Chem. Lab. Med.* **2000**, *38*, 629–632. [[CrossRef](#)]
16. Kumar, M.; Coria, A.L.; Cornick, S.; Petri, B.; Mayengbam, S.; Jijon, H.B.; Moreau, F.; Shearer, J.; Chadee, K. Increased intestinal permeability exacerbates sepsis through reduced hepatic SCD-1 activity and dysregulated iron recycling. *Nat. Commun.* **2020**, *11*, 1–15. [[CrossRef](#)]
17. Huisjes, R.; Bogdanova, A.; Van Solinge, W.; Schiffelers, R.; Kaestner, L.; Van Wijk, R. Squeezing for Life—Properties of Red Blood Cell Deformability. *Front. Physiol.* **2018**, *9*, 656. [[CrossRef](#)] [[PubMed](#)]
18. Arashiki, N.; Kimata, N.; Manno, S.; Mohandas, N.; Takakuwa, Y. Membrane Peroxidation and Methemoglobin Formation Are Both Necessary for Band 3 Clustering: Mechanistic Insights into Human Erythrocyte Senescence. *Biochemistry* **2013**, *52*, 5760–5769. [[CrossRef](#)]
19. D'Alessandro, A.; Blasi, B. Red blood cell subpopulations in freshly drawn blood: Application of proteomics and metabolomics to a decades-long biological issue. *Blood Transfus.* **2013**, *11*, 75–87. [[CrossRef](#)] [[PubMed](#)]
20. Joiner, C.H.; Lauf, P.K. Ouabain Binding and Potassium Transport in Young and Old Populations of Human Red Cells. *Membr. Biochem.* **1978**, *1*, 187–202. [[CrossRef](#)] [[PubMed](#)]
21. Lew, V.L.; Tiffert, T. On the Mechanism of Human Red Blood Cell Longevity: Roles of Calcium, the Sodium Pump, PIEZO1, and Gardos Channels. *Front. Physiol.* **2017**, *8*, 977. [[CrossRef](#)]
22. Andolfo, I.; Alper, S.L.; De Franceschi, L.; Auremma, C.; Russo, R.; De Falco, L.; Vallefucio, F.; Esposito, M.R.; Vandorpe, D.H.; Shmukler, B.E.; et al. Multiple clinical forms of dehydrated hereditary stomatocytosis arise from mutations in PIEZO1. *Blood* **2013**, *121*, 3925–3935. [[CrossRef](#)]
23. Romero, P.J.; Romero, E.A. The Role of Calcium Metabolism in Human Red Blood Cell Ageing: A Proposal. *Blood Cells Mol. Dis.* **1999**, *25*, 9–19. [[CrossRef](#)]
24. Willekens, F.L.A.; Roerdinkholder-Stoelwinder, B.; Groenen-Döpp, Y.A.M.; Bos, H.J.; Bosman, G.J.C.G.M.; Bos, A.G.V.D.; Verkleij, A.J.; Werre, J.M. Hemoglobin loss from erythrocytes in vivo results from spleen-facilitated vesiculation. *Blood* **2003**, *101*, 747–751. [[CrossRef](#)] [[PubMed](#)]
25. Duez, J.; Holleran, J.; Ndour, P.A.; Pionneau, C.; Diakite, S.A.S.; Roussel, C.; Dussiot, M.; Amireault, P.; Avery, V.; Buffet, P. Mechanical clearance of red blood cells by the human spleen: Potential therapeutic applications of a biomimetic RBC filtration method. *Transfus. Clin. Biol.* **2015**, *22*, 151–157. [[CrossRef](#)] [[PubMed](#)]
26. Klei, T.R.L.; Meinderts, S.M.; Berg, T.K.V.D.; Van Bruggen, R. From the Cradle to the Grave: The Role of Macrophages in Erythropoiesis and Erythrophagocytosis. *Front. Immunol.* **2017**, *8*, 73. [[CrossRef](#)]
27. Theurl, I.; Hilgendorf, I.; Nairz, M.; Tymoszyk, P.; Haschka, D.; Asshoff, M.; He, S.; Gerhardt, L.M.S.; Holderried, T.; Seifert, M.; et al. On-demand erythrocyte disposal and iron recycling requires transient macrophages in the liver. *Nat. Med.* **2016**, *22*, 945–951. [[CrossRef](#)] [[PubMed](#)]
28. Mebius, R.E.; Kraal, G. Structure and function of the spleen. *Nat. Rev. Immunol.* **2005**, *5*, 606–616. [[CrossRef](#)]
29. Lee, S.-J.; Park, S.-Y.; Jung, M.-Y.; Bae, S.M.; Kim, I.-S. Mechanism for phosphatidylserine-dependent erythrophagocytosis in mouse liver. *Blood* **2011**, *117*, 5215–5223. [[CrossRef](#)]
30. Bonnardel, J.; T'Jonck, W.; Gaublonne, D.; Browaeys, R.; Scott, C.L.; Martens, L.; Vanneste, B.; De Prijck, S.; Nedospasov, S.A.; Kremer, A.; et al. Stellate Cells, Hepatocytes, and Endothelial Cells Imprint the Kupffer Cell Identity on Monocytes Colonizing the Liver Macrophage Niche. *Immunity* **2019**, *51*, 638–654.e9. [[CrossRef](#)]
31. Lee, S.-H.; Starkey, P.M.; Gordon, S. Quantitative analysis of total macrophage content in adult mouse tissues. Immunochemical studies with monoclonal antibody F4/80. *J. Exp. Med.* **1985**, *161*, 475–489. [[CrossRef](#)]
32. Pfefferlé, M.; Ingoglia, G.; Schaer, C.A.; Yalamanoglu, A.; Buzzi, R.M.; Dubach, I.L.; Tan, G.; López-Cano, E.Y.; Schulthess, N.; Hansen, K.; et al. Hemolysis transforms liver macrophages into anti-inflammatory erythrophagocytes. *J. Clin. Investig.* **2020**, *130*. [[CrossRef](#)]
33. Youssef, L.A.; Rebbaa, A.; Pampou, S.; Weisberg, S.; Stockwell, B.R.; Hod, E.A.; Spitalnik, S.L. Increased erythrophagocytosis induces ferroptosis in red pulp macrophages in a mouse model of transfusion. *Blood* **2018**, *131*, 2581–2593. [[CrossRef](#)]
34. Bian, Z.; Shi, L.; Guo, Y.L.; Lv, Z.; Tang, C.; Niu, S.; Tremblay, A.; Venkataramani, M.; Culpepper, C.; Li, L.; et al. Cd47-Sirpalpa interaction and IL-10 constrain inflammation-induced macrophage phagocytosis of healthy self-cells. *Proc. Natl. Acad. Sci. USA* **2016**, *37*, E5434–E5443. [[CrossRef](#)] [[PubMed](#)]
35. Looareesuwan, S.; Ho, M.; Wattanagoon, Y.; White, N.J.; Warrell, D.A.; Bunnag, D.; Harinasuta, T.; Wyler, D.J. Dynamic Alteration in Splenic Function during Acute falciparum Malaria. *N. Engl. J. Med.* **1987**, *317*, 675–679. [[CrossRef](#)] [[PubMed](#)]
36. Schroit, A.J.; Madsen, J.W.; Tanaka, Y. In vivo recognition and clearance of red blood cells containing phosphatidylserine in their plasma membranes. *J. Biol. Chem.* **1985**, *260*. [[CrossRef](#)]
37. Connor, J.; Pak, C.C.; Schroit, A.J. Exposure of phosphatidylserine in the outer leaflet of human red blood cells. Relationship to cell density, cell age, and clearance by mononuclear cells. *J. Biol. Chem.* **1994**, *269*, 2399–2404. [[CrossRef](#)]
38. Gottlieb, Y.; Topaz, O.; Cohen, L.A.; Yakov, L.D.; Haber, T.; Morgenstern, A.; Weiss, A.; Berman, K.C.; Fibach, E.; Meyron-Holtz, E.G. Physiologically aged red blood cells undergo erythrophagocytosis in vivo but not in vitro. *Haematologica* **2012**, *97*, 994–1002. [[CrossRef](#)]

39. Khandelwal, S.; Saxena, R.K. A role of phosphatidylserine externalization in clearance of erythrocytes exposed to stress but not in eliminating aging populations of erythrocyte in mice. *Exp. Gerontol.* **2008**, *43*, 764–770. [[CrossRef](#)] [[PubMed](#)]
40. Kuypers, F.A.; Yuan, J.; Lewis, R.A.; Snyder, L.M.; Kiefer, C.R.; Bunyaratvej, A.; Fucharoen, S.; Ma, L.; Styles, L.; De Jong, K.; et al. Membrane phospholipid asymmetry in human thalassemia. *Blood* **1998**, *91*, 3044–3051. [[CrossRef](#)] [[PubMed](#)]
41. Wood, B.L.; Gibson, D.F.; Tait, J.F. Increased erythrocyte phosphatidylserine exposure in sickle cell disease: Flow-cytometric measurement and clinical associations. *Blood* **1996**, *88*, 1873–1880. [[CrossRef](#)]
42. de Jong, K.; Geldwerth, D.; Kuypers, F.A. Oxidative damage does not alter membrane phospholipid asymmetry in human erythrocytes. *Biochemistry* **1997**, *36*, 6768–6776. [[CrossRef](#)]
43. Sakai, M.; Troutman, T.D.; Seidman, J.S.; Ouyang, Z.; Spann, N.J.; Abe, Y.; Ego, K.M.; Bruni, C.M.; Deng, Z.; Schlachetzki, J.C.; et al. Liver-Derived Signals Sequentially Reprogram Myeloid Enhancers to Initiate and Maintain Kupffer Cell Identity. *Immunity* **2019**, *51*, 655–670.e8. [[CrossRef](#)]
44. Akilesh, H.M.; Buechler, M.B.; Duggan, J.M.; Hahn, W.O.; Matta, B.; Sun, X.; Gessay, G.; Whalen, E.; Mason, M.; Presnell, S.R.; et al. Chronic TLR7 and TLR9 signaling drives anemia via differentiation of specialized hemophagocytes. *Science* **2019**, *363*, eaao5213. [[CrossRef](#)]
45. Oh, M.-H.; Collins, S.L.; Sun, I.-H.; Tam, A.J.; Patel, C.H.; Arwood, M.L.; Chan-Li, Y.; Powell, J.D.; Horton, M.R. mTORC2 Signaling Selectively Regulates the Generation and Function of Tissue-Resident Peritoneal Macrophages. *Cell Rep.* **2017**, *20*, 2439–2454. [[CrossRef](#)]
46. Zagórska, A.; Través, P.G.; Jiménez-García, L.; Strickland, J.D.; Oh, J.; Tapia, F.J.; Mayoral, R.; Burrola, P.; Coppole, B.L.; Lemke, G. Differential regulation of hepatic physiology and injury by the TAM receptors Axl and Mer. *Life Sci. Alliance* **2020**, *3*, e202000694. [[CrossRef](#)] [[PubMed](#)]
47. Hanayama, R.; Tanaka, M.; Miwa, K.; Shinohara, A.; Iwamatsu, A.; Nagata, S. Identification of a factor that links apoptotic cells to phagocytes. *Nature* **2002**, *417*, 182–187. [[CrossRef](#)]
48. McGilvray, I.D.; Serghides, L.; Kapus, A.; Rotstein, O.D.; Kain, K.C. Nonopsonic monocyte/macrophage phagocytosis of *Plasmodium falciparum*-parasitized erythrocytes: A role for CD36 in malarial clearance. *Blood* **2000**, *96*, 3231–3240. [[CrossRef](#)]
49. Totino, P.R.R.; Daniel-Ribeiro, C.T.; Ferreira-Da-Cruz, M.D.F. Evidencing the Role of Erythrocytic Apoptosis in Malarial Anemia. *Front. Cell. Infect. Microbiol.* **2016**, *6*, 176. [[CrossRef](#)] [[PubMed](#)]
50. Pain, A.; Urban, B.C.; Kai, O.; Casals-Pascual, C.; Shafi, J.; Marsh, K.; Roberts, D.J. A non-sense mutation in Cd36 gene is associated with protection from severe malaria. *Lancet* **2001**, *357*, 1502–1503. [[CrossRef](#)]
51. Hochreiter-Hufford, A.E.; Lee, C.S.; Kinchen, J.; Sokolowski, J.D.; Arandjelovic, S.; Call, J.; Klibanov, A.L.; Yan, Z.; Mandell, J.W.; Ravichandran, K. Phosphatidylserine receptor BAI1 and apoptotic cells as new promoters of myoblast fusion. *Nature* **2013**, *497*, 263–267. [[CrossRef](#)]
52. Kobayashi, N.; Karisola, P.; Peña-Cruz, V.; Dorfman, D.M.; Jinushi, M.; Umetsu, S.E.; Butte, M.; Nagumo, H.; Chernova, I.; Zhu, B.; et al. TIM-1 and TIM-4 Glycoproteins Bind Phosphatidylserine and Mediate Uptake of Apoptotic Cells. *Immunity* **2007**, *27*, 927–940. [[CrossRef](#)] [[PubMed](#)]
53. Freeman, G.J.; Casasnovas, J.M.; Umetsu, D.T.; DeKruyff, R.H. TIM genes: A family of cell surface phosphatidylserine receptors that regulate innate and adaptive immunity. *Immunol. Rev.* **2010**, *235*, 172–189. [[CrossRef](#)]
54. Alderman, E.M.; Fudenberg, H.H.; Lovins, R.E. Binding of immunoglobulin classes to subpopulations of human red blood cells separated by density-gradient centrifugation. *Blood* **1980**, *55*, 817–822. [[CrossRef](#)]
55. Kay, M.M. Mechanism of removal of senescent cells by human macrophages in situ. *Proc. Natl. Acad. Sci. USA* **1975**, *72*, 3521–3525. [[CrossRef](#)]
56. Christian, J.A.; Rebar, A.H.; Boon, G.D.; Low, P. Senescence of canine biotinylated erythrocytes: Increased autologous immunoglobulin binding occurs on erythrocytes aged in vivo for 104 to 110 days. *Blood* **1993**, *82*, 3469–3473. [[CrossRef](#)]
57. Singer, J.A.; Jennings, L.K.; Jackson, C.W.; Dockter, M.E.; Morrison, M.; Walker, W.S. Erythrocyte homeostasis: Antibody-mediated recognition of the senescent state by macrophages. *Proc. Natl. Acad. Sci. USA* **1986**, *83*, 5498–5501. [[CrossRef](#)]
58. Beppu, M.; Mizukami, A.; Nagoya, M.; Kikugawa, K. Binding of anti-band 3 autoantibody to oxidatively damaged erythrocytes. Formation of senescent antigen on erythrocyte surface by an oxidative mechanism. *J. Biol. Chem.* **1990**, *265*, 3226–3233. [[CrossRef](#)]
59. Kannan, R.; Labotka, R.; Low, P.S. Isolation and characterization of the hemichrome-stabilized membrane protein aggregates from sickle erythrocytes. Major site of autologous antibody binding. *J. Biol. Chem.* **1988**, *263*, 13766–13773. [[CrossRef](#)]
60. Kannan, R.; Yuan, J.; Low, P.S. Isolation and partial characterization of antibody- and globin-enriched complexes from membranes of dense human erythrocytes. *Biochem. J.* **1991**, *278*, 57–62. [[CrossRef](#)] [[PubMed](#)]
61. Arese, P.; Turrini, F.; Schwarzer, E. Band 3/Complement-mediated Recognition and Removal of Normally Senescent and Pathological Human Erythrocytes. *Cell. Physiol. Biochem.* **2005**, *16*, 133–146. [[CrossRef](#)]
62. Klei, T.R.L.; De Back, D.Z.; Asif, P.J.; Verkuijlen, P.J.J.H.; Veldhuis, M.; Ligthart, P.C.; Berghuis, J.; Clifford, E.; Beuger, B.M.; Berg, T.K.V.D.; et al. Glycophorin-C sialylation regulates Lu/BCAM adhesive capacity during erythrocyte aging. *Blood Adv.* **2018**, *2*, 14–24. [[CrossRef](#)] [[PubMed](#)]
63. Oldenburg, P.-A.; Zheleznyak, A.; Fang, Y.-F.; Lagenaur, C.F.; Gresham, H.D.; Lindberg, F.P. Role of CD47 as a Marker of Self on Red Blood Cells. *Science* **2000**, *288*, 2051–2054. [[CrossRef](#)]
64. Olsson, M.; Oldenburg, P.A. CD47 on experimentally senescent murine RBCs inhibits phagocytosis following Fcγ receptor-mediated but not scavenger receptor-mediated recognition by macrophages. *Blood* **2008**, *112*, 4259–4267. [[CrossRef](#)]

65. Sosale, N.G.; Rouhiparkouhi, T.; Bradshaw, A.M.; Dimova, R.; Lipowsky, R.; Discher, D.E. Cell rigidity and shape override CD47's "self"-signaling in phagocytosis by hyperactivating myosin-II. *Blood* **2015**, *125*, 542–552. [[CrossRef](#)] [[PubMed](#)]
66. Khandelwal, S.; Van Rooijen, N.; Saxena, R.K. Reduced expression of CD47 during murine red blood cell (RBC) senescence and its role in RBC clearance from the circulation. *Transfusion* **2007**, *47*, 1725–1732. [[CrossRef](#)]
67. Stewart, A.; Urbaniak, S.; Turner, M.; Bessos, H. The application of a new quantitative assay for the monitoring of integrin-associated protein CD47 on red blood cells during storage and comparison with the expression of CD47 and phosphatidylserine with flow cytometry. *Transfusion* **2005**, *45*, 1496–1503. [[CrossRef](#)]
68. Kharitononkov, A.; Chen, Z.; Sures, I.; Wang, H.; Schilling, J.; Ullrich, A. A family of proteins that inhibit signalling through tyrosine kinase receptors. *Nature* **1997**, *386*, 181–186. [[CrossRef](#)]
69. Burger, P.; Hilarius-Stokman, P.; de Korte, D.; Berg, T.K.V.D.; Van Bruggen, R. CD47 functions as a molecular switch for erythrocyte phagocytosis. *Blood* **2012**, *119*, 5512–5521. [[CrossRef](#)]
70. Zhang, W.; Huang, Q.; Xiao, W.; Zhao, Y.; Pi, J.; Xu, H.; Zhao, H.; Xu, J.; Evans, C.E.; Jin, H. Advances in Anti-Tumor Treatments Targeting the CD47/SIRPalpha Axis. *Front. Immunol.* **2020**, *11*, 18. [[CrossRef](#)] [[PubMed](#)]
71. Ayi, K.; Lu, Z.; Serghides, L.; Ho, J.M.; Finney, C.; Wang, J.C.Y.; Liles, W.C.; Kain, K.C. CD47-SIRPalpha Interactions Regulate Macrophage Uptake of Plasmodium falciparum-Infected Erythrocytes and Clearance of Malaria In Vivo. *Infect. Immun.* **2016**, *84*, 2002–2011. [[CrossRef](#)]
72. Banerjee, R.; Khandelwal, S.; Kozakai, Y.; Sahu, B.; Kumar, S. CD47 regulates the phagocytic clearance and replication of the Plasmodium yoelii malaria parasite. *Proc. Natl. Acad. Sci. USA* **2015**, *112*, 3062–3067. [[CrossRef](#)] [[PubMed](#)]
73. Wright, B.S.W.D.H. *The Illustrated Pathology of the Spleen*; Cambridge University Press: Cambridge, UK, 2000.
74. Garby, L.; Noyes, W.D. Studies on hemoglobin metabolism. I. the kinetic properties of the plasma hemoglobin pool in normal man. *J. Clin. Investig.* **1959**, *38*, 1479–1483. [[CrossRef](#)]
75. Kato, G.; Steinberg, M.H.; Gladwin, M.T. Intravascular hemolysis and the pathophysiology of sickle cell disease. *J. Clin. Investig.* **2017**, *127*, 750–760. [[CrossRef](#)]
76. Schaer, D.J.; Vinchi, F.; Ingoglia, G.; Tolosano, E.; Buehler, P.W. Haptoglobin, hemopexin, and related defense pathways—basic science, clinical perspectives, and drug development. *Front. Physiol.* **2014**, *5*, 415. [[CrossRef](#)]
77. Wang, Y.; Kinzie, E.; Berger, F.G.; Lim, S.K.; Baumann, H. Haptoglobin, an inflammation-inducible plasma protein. *Redox Rep.* **2001**, *6*, 379–385. [[CrossRef](#)] [[PubMed](#)]
78. Kristiansen, M.; Graversen, J.H.; Jacobsen, C.; Sonne, O.; Hoffman, H.-J.; Law, S.A.; Moestrup, S.K. Identification of the haemoglobin scavenger receptor. *Nature* **2001**, *409*, 198–201. [[CrossRef](#)]
79. Svendsen, P.; Graversen, J.H.; Etzerodt, A.; Hager, H.; Røge, R.; Grønbaek, H.; Christensen, E.I.; Møller, H.J.; Vilstrup, H.; Moestrup, S.K. Antibody-Directed Glucocorticoid Targeting to CD163 in M2-type Macrophages Attenuates Fructose-Induced Liver Inflammatory Changes. *Mol. Ther.-Methods Clin. Dev.* **2017**, *4*, 50–61. [[CrossRef](#)]
80. Klei, T.R.L.; Dalimot, J.; Nota, B.; Veldthuis, M.; Mul, E.; Rademakers, T.; Hoogenboezem, M.; Nagelkerke, S.Q.; Van Ijcken, W.F.; Oole, E.; et al. Hemolysis in the spleen drives erythrocyte turnover. *Blood* **2020**, *136*, 1579–1589. [[CrossRef](#)] [[PubMed](#)]
81. Fagoonee, S.; Gburek, J.; Hirsch, E.; Marro, S.; Moestrup, S.K.; Laurberg, J.M.; Christensen, E.I.; Silengo, L.; Altruda, F.; Tolosano, E. Plasma Protein Haptoglobin Modulates Renal Iron Loading. *Am. J. Pathol.* **2005**, *166*, 973–983. [[CrossRef](#)]
82. Marro, S.; Barisani, D.; Chiabrando, D.; Fagoonee, S.; Muckenthaler, M.U.; Stolte, J.; Meneveri, R.; Haile, D.; Silengo, L.; Altruda, F.; et al. Lack of Haptoglobin Affects Iron Transport Across Duodenum by Modulating Ferroportin Expression. *Gastroenterology* **2007**, *133*, 1261–1271.e3. [[CrossRef](#)] [[PubMed](#)]
83. Boretti, F.S.; Baek, J.H.; Palmer, A.F.; Schaer, D.J.; Buehler, P.W. Modeling hemoglobin and hemoglobin:haptoglobin complex clearance in a non-rodent species—pharmacokinetic and therapeutic implications. *Front. Physiol.* **2014**, *5*, 385. [[CrossRef](#)]
84. Schaer, D.J.; Schaer, C.; Buehler, P.W.; Boykins, R.A.; Schoedon, G.; Alayash, A.I.; Schaffner, A. CD163 is the macrophage scavenger receptor for native and chemically modified hemoglobins in the absence of haptoglobin. *Blood* **2006**, *107*, 373–380. [[CrossRef](#)]
85. Etzerodt, A.; Kjolby, M.; Nielsen, M.J.; Maniecki, M.; Svendsen, P.; Moestrup, S.K. Plasma Clearance of Hemoglobin and Haptoglobin in Mice and Effect of CD163 Gene Targeting Disruption. *Antioxid. Redox Signal.* **2013**, *18*, 2254–2263. [[CrossRef](#)]
86. Van Avondt, K.; Nur, E.; Zeerleder, S. Mechanisms of haemolysis-induced kidney injury. *Nat. Rev. Nephrol.* **2019**, *15*, 671–692. [[CrossRef](#)]
87. Vinchi, F.; De Franceschi, L.; Ghigo, A.; Townes, T.; Cimino, J.; Silengo, L.; Hirsch, E.; Altruda, F.; Tolosano, E. Hemopexin Therapy Improves Cardiovascular Function by Preventing Heme-Induced Endothelial Toxicity in Mouse Models of Hemolytic Diseases. *Circulation* **2013**, *127*, 1317–1329. [[CrossRef](#)]
88. Belcher, J.D.; Chen, C.; Nguyen, J.; Milbauer, L.; Abdulla, F.; Alayash, A.I.; Smith, A.; Nath, K.A.; Hebbel, R.P.; Vercellotti, G.M. Heme triggers TLR4 signaling leading to endothelial cell activation and vaso-occlusion in murine sickle cell disease. *Blood* **2014**, *123*, 377–390. [[CrossRef](#)] [[PubMed](#)]
89. Hvidberg, V.; Maniecki, M.B.; Jacobsen, C.; Højrup, P.; Møller, H.J.; Moestrup, S.K. Identification of the receptor scavenging hemopexin-heme complexes. *Blood* **2005**, *106*, 2572–2579. [[CrossRef](#)]
90. Kovtunovich, G.; Eckhaus, M.A.; Ghosh, M.C.; Ollivierre-Wilson, H.; Rouault, T.A. Dysfunction of the heme recycling system in heme oxygenase 1-deficient mice: Effects on macrophage viability and tissue iron distribution. *Blood* **2010**, *116*, 6054–6062. [[CrossRef](#)] [[PubMed](#)]

91. Haldar, M.; Kohyama, M.; So, A.Y.-L.; Kc, W.; Wu, X.; Briseno, C.; Satpathy, A.; Kretzer, N.M.; Arase, H.; Rajasekaran, N.S.; et al. Heme-Mediated SPI-C Induction Promotes Monocyte Differentiation into Iron-Recycling Macrophages. *Cell* **2014**, *156*, 1223–1234. [[CrossRef](#)] [[PubMed](#)]
92. Lu, Y.; Basatemur, G.; Scott, I.C.; Chiarugi, D.; Clement, M.; Harrison, J.; Jugdaohsingh, R.; Yu, X.; Newland, S.; Jolin, H.E.; et al. Interleukin-33 Signaling Controls the Development of Iron-Recycling Macrophages. *Immunity* **2020**, *52*, 782–793.e5. [[CrossRef](#)]
93. Bennett, L.F.; Liao, C.; Quickel, M.D.; Yeoh, B.S.; Vijay-Kumar, M.; Hankey-Giblin, P.; Prabhu, K.S.; Paulson, R.F. Inflammation induces stress erythropoiesis through heme-dependent activation of SPI-C. *Sci. Signal.* **2019**, *12*, eaap7336. [[CrossRef](#)]
94. Pek, R.H.; Yuan, X.; Rietzschel, N.; Zhang, J.; Jackson, L.; Nishibori, E.; Ribeiro, A.; Simmons, W.; Jagadeesh, J.; Sugimoto, H.; et al. Hemozoin produced by mammals confers heme tolerance. *eLife* **2019**, *8*, e49503. [[CrossRef](#)]
95. Santarino, L.; Viegas, M.S.; Domingues, N.; Ribeiro, A.M.; Soares, M.P.; Vieira, O.V. Involvement of the p62/NRF2 signal transduction pathway on erythrophagocytosis. *Sci. Rep.* **2017**, *7*, 1–16. [[CrossRef](#)]
96. Asare, P.F.; Roscioli, E.; Hurtado, P.R.; Tran, H.B.; Mah, C.Y.; Hodge, S. LC3-Associated Phagocytosis (LAP): A Potentially Influential Mediator of Efferocytosis-Related Tumor Progression and Aggressiveness. *Front. Oncol.* **2020**, *10*, 1298. [[CrossRef](#)] [[PubMed](#)]
97. Delaby, C.; Rondeau, C.; Pouzet, C.; Willemetz, A.; Pilard, N.; Desjardins, M.; Canonne-Hergaux, F. Subcellular localization of iron and heme metabolism related proteins at early stages of erythrophagocytosis. *PLoS ONE* **2012**, *7*, e42199. [[CrossRef](#)]
98. Gagnon, E.; Duclos, S.; Rondeau, C.; Chevet, E.; Cameron, P.H.; Steele-Mortimer, O.; Paiement, J.; Bergeron, J.J.; Desjardins, M. Endoplasmic Reticulum-Mediated Phagocytosis Is a Mechanism of Entry into Macrophages. *Cell* **2002**, *110*, 119–131. [[CrossRef](#)]
99. Delaby, C.; Pilard, N.; Hetet, G.; Driss, F.; Grandchamp, B.; Beaumont, C.; Canonne-Hergaux, F. A physiological model to study iron recycling in macrophages. *Exp. Cell Res.* **2005**, *310*, 43–53. [[CrossRef](#)]
100. Delaby, C.; Pilard, N.; Puy, H.; Canonne-Hergaux, F. Sequential regulation of ferroportin expression after erythrophagocytosis in murine macrophages: Early mRNA induction by haem, followed by iron-dependent protein expression. *Biochem. J.* **2008**, *411*, 123–131. [[CrossRef](#)]
101. Knutson, M.D.; Vafa, M.; Haile, D.J.; Wessling-Resnick, M. Iron loading and erythrophagocytosis increase ferroportin 1 (FPN1) expression in J774 macrophages. *Blood* **2003**, *102*, 4191–4197. [[CrossRef](#)] [[PubMed](#)]
102. Soe-Lin, S.; Apte, S.S.; Andriopoulos, B.; Andrews, M.C.; Schranzhofer, M.; Kahawita, T.; Garcia-Santos, D.; Ponka, P. Nramp1 promotes efficient macrophage recycling of iron following erythrophagocytosis in vivo. *Proc. Natl. Acad. Sci. USA* **2009**, *106*, 5960–5965. [[CrossRef](#)]
103. Rajagopal, A.; Rao, A.U.; Amigo, J.; Tian, M.; Upadhyay, S.K.; Hall, C.; Uhm, S.; Mathew, M.K.; Fleming, M.; Paw, B.; et al. Haem homeostasis is regulated by the conserved and concerted functions of HRG-1 proteins. *Nature* **2008**, *453*, 1127–1131. [[CrossRef](#)]
104. Zhang, J.; Chambers, I.; Yun, S.; Phillips, J.; Krause, M.; Hamza, I. Hrg1 promotes heme-iron recycling during hemolysis in the zebrafish kidney. *PLoS Genet.* **2018**, *14*, e1007665. [[CrossRef](#)] [[PubMed](#)]
105. Poss, K.D.; Tonegawa, S. Heme oxygenase 1 is required for mammalian iron reutilization. *Proc. Natl. Acad. Sci. USA* **1997**, *94*, 10919–10924. [[CrossRef](#)]
106. Nai, A.; Lidonnicci, M.R.; Federici, G.; Pettinato, M.; Olivari, V.; Carrillo, F.; Crich, S.G.; Ferrari, G.; Camaschella, C.; Silvestri, L.; et al. NCOA4-mediated ferritinophagy in macrophages is crucial to sustain erythropoiesis in mice. *Haematologica* **2020**, *106*, 795–805. [[CrossRef](#)] [[PubMed](#)]
107. Knutson, M.D.; Oukka, M.; Koss, L.M.; Aydemir, F.; Wessling-Resnick, M. Iron release from macrophages after erythrophagocytosis is up-regulated by ferroportin 1 overexpression and down-regulated by hepcidin. *Proc. Natl. Acad. Sci. USA* **2005**, *102*, 1324–1328. [[CrossRef](#)] [[PubMed](#)]
108. Zhang, Z.; Zhang, F.; An, P.; Guo, X.; Shen, Y.; Tao, Y.; Wu, Q.; Zhang, Y.; Yu, Y.; Ning, B.; et al. Ferroportin1 deficiency in mouse macrophages impairs iron homeostasis and inflammatory responses. *Blood* **2011**, *118*, 1912–1922. [[CrossRef](#)] [[PubMed](#)]
109. Nemeth, E.; Tuttle, M.S.; Powelson, J.; Vaughn, M.B.; Donovan, A.; Ward, D.M.; Ganz, T.; Kaplan, J. Hepcidin Regulates Cellular Iron Efflux by Binding to Ferroportin and Inducing Its Internalization. *Science* **2004**, *306*, 2090–2093. [[CrossRef](#)]
110. Aschemeyer, S.; Qiao, B.; Stefanova, D.; Valore, E.V.; Sek, A.; Ruwe, T.; Vieth, K.R.; Jung, G.; Casu, C.; Rivella, S.; et al. Structure-function analysis of ferroportin defines the binding site and an alternative mechanism of action of hepcidin. *Blood* **2018**, *131*, 899–910. [[CrossRef](#)] [[PubMed](#)]
111. Kim, A.; Fung, E.; Parikh, S.G.; Valore, E.V.; Gabayan, V.; Nemeth, E.; Ganz, T. A mouse model of anemia of inflammation: Complex pathogenesis with partial dependence on hepcidin. *Blood* **2014**, *123*, 1129–1136. [[CrossRef](#)]
112. Guida, C.; Altamura, S.; Klein, F.A.; Galy, B.; Boutros, M.; Ulmer, A.J.; Hentze, M.W.; Muckenthaler, M.U. A novel inflammatory pathway mediating rapid hepcidin-independent hypoferremia. *Blood* **2015**, *125*, 2265–2275. [[CrossRef](#)]
113. Camaschella, C. Iron deficiency. *Blood* **2019**, *133*, 30–39. [[CrossRef](#)]
114. Kautz, L.; Jung, G.; Valore, E.V.; Rivella, S.; Nemeth, E.; Ganz, T. Identification of erythroferrone as an erythroid regulator of iron metabolism. *Nat. Genet.* **2014**, *46*, 678–684. [[CrossRef](#)]
115. Schaer, C.; Vallelian, F.; Imhof, A.; Schoedon, G.; Schaer, D.J. Heme carrier protein (HCP-1) spatially interacts with the CD163 hemoglobin uptake pathway and is a target of inflammatory macrophage activation. *J. Leukoc. Biol.* **2007**, *83*, 325–333. [[CrossRef](#)]
116. Ma, S.; Dubin, A.E.; Zhang, Y.; Mousavi, S.A.R.; Wang, Y.; Coombs, A.M.; Loud, M.; Andolfo, I.; Patapoutian, A. A role of PIEZO1 in iron metabolism in mice and humans. *Cell* **2021**, *184*, 969–982.e13. [[CrossRef](#)] [[PubMed](#)]

117. Schlam, D.; Bagshaw, R.D.; Freeman, S.A.; Collins, R.F.; Pawson, T.; Fairn, G.D.; Grinstein, S. Phosphoinositide 3-kinase enables phagocytosis of large particles by terminating actin assembly through Rac/Cdc42 GTPase-activating proteins. *Nat. Commun.* **2015**, *6*, 1–12. [[CrossRef](#)]
118. Beesetty, P.; Rockwood, J.; Kaitsuka, T.; Zhelay, T.; Hourani, S.; Matsushita, M.; Kozak, J.A. Phagocytic activity of splenic macrophages is enhanced and accompanied by cytosolic alkalization in TRPM7 kinase-dead mice. *FEBS J.* **2020**, *288*, 3585–3601. [[CrossRef](#)] [[PubMed](#)]
119. Gordon, S.; Martinez-Pomares, L. Physiological roles of macrophages. *Pflugers Archiv* **2017**, *469*, 365–374. [[CrossRef](#)]
120. Wynn, T.A.; Chawla, A.; Pollard, J.W. Macrophage biology in development, homeostasis and disease. *Nature* **2013**, *496*, 445–455. [[CrossRef](#)] [[PubMed](#)]
121. Epelman, S.; LaVine, K.J.; Randolph, G.J. Origin and Functions of Tissue Macrophages. *Immunity* **2014**, *41*, 21–35. [[CrossRef](#)]
122. Yona, S.; Kim, K.-W.; Wolf, Y.; Mildner, A.; Varol, D.; Breker, M.; Strauss-Ayali, D.; Viukov, S.; Guillemins, M.; Misharin, A.; et al. Fate Mapping Reveals Origins and Dynamics of Monocytes and Tissue Macrophages under Homeostasis. *Immunity* **2012**, *38*, 79–91. [[CrossRef](#)] [[PubMed](#)]
123. Gautier, E.; Shay, T.; Miller, J.; Greter, M.; Jakubzick, C.; Ivanov, S.; Helft, J.; Chow, A.; Elpek, K.G.; the Immunological Genome Consortium; et al. Gene-expression profiles and transcriptional regulatory pathways that underlie the identity and diversity of mouse tissue macrophages. *Nat. Immunol.* **2012**, *13*, 1118–1128. [[CrossRef](#)]
124. Lavin, Y.; Winter, D.; Blecher-Gonen, R.; David, E.; Keren-Shaul, H.; Merad, M.; Jung, S.; Amit, I. Tissue-Resident Macrophage Enhancer Landscapes Are Shaped by the Local Microenvironment. *Cell* **2014**, *159*, 1312–1326. [[CrossRef](#)]
125. Gosselin, D.; Link, V.M.; Romanoski, C.E.; Fonseca, G.J.; Eichenfield, D.Z.; Spann, N.J.; Stender, J.D.; Chun, H.B.; Garner, H.; Geissmann, F.; et al. Environment drives selection and function of enhancers controlling tissue-specific macrophage identities. *Cell* **2014**, *159*, 1327–1340. [[CrossRef](#)]
126. Okreglicka, K.; Iten, I.; Pohlmeier, L.; Onder, L.; Feng, Q.; Kurrer, M.; Ludewig, B.; Nielsen, N.P.; Schneider, C.; Kopf, M. PPAR γ is essential for the development of bone marrow erythroblastic island macrophages and splenic red pulp macrophages. *J. Exp. Med.* **2021**, *218*, e20191314. [[CrossRef](#)] [[PubMed](#)]
127. Kohyama, M.; Ise, W.; Edelson, B.T.; Wilker, P.R.; Hildner, K.; Mejia, C.; Frazier, W.A.; Murphy, T.L.; Murphy, K.M. Role for Spi-C in the development of red pulp macrophages and splenic iron homeostasis. *Nature* **2008**, *457*, 318–321. [[CrossRef](#)] [[PubMed](#)]
128. Ulyanova, T.; Phelps, S.R.; Papayannopoulou, T. The macrophage contribution to stress erythropoiesis: When less is enough. *Blood* **2016**, *128*, 1756–1765. [[CrossRef](#)] [[PubMed](#)]
129. Karsten, E.; Breen, E.; Herbert, B. Red blood cells are dynamic reservoirs of cytokines. *Sci. Rep.* **2018**, *8*, 1–12. [[CrossRef](#)]
130. Bellomo, A.; Mondor, I.; Spinelli, L.; Lagueyrie, M.; Stewart, B.J.; Brouilly, N.; Malissen, B.; Clatworthy, M.R.; Bajénoff, M. Reticular Fibroblasts Expressing the Transcription Factor WT1 Define a Stromal Niche that Maintains and Replenishes Splenic Red Pulp Macrophages. *Immunity* **2020**, *53*, 127–142.e7. [[CrossRef](#)] [[PubMed](#)]
131. Mass, E.; Ballesteros, I.; Farlik, M.; Halbritter, F.; Günther, P.; Crozet, L.; Jacome-Galarza, C.E.; Händler, K.; Klughammer, J.; Kobayashi, Y.; et al. Specification of tissue-resident macrophages during organogenesis. *Science* **2016**, *353*, aaf4238. [[CrossRef](#)]
132. Scott, C.L.; T’Jonck, W.; Martens, L.; Todorov, H.; Sichen, D.; Soen, B.; Bonnardel, J.; De Prijck, S.; Vandamme, N.; Cannoodt, R.; et al. The Transcription Factor ZEB2 Is Required to Maintain the Tissue-Specific Identities of Macrophages. *Immunity* **2018**, *49*, 312–325.e5. [[CrossRef](#)]
133. Scott, C.; Zheng, F.; De Baetselier, P.; Martens, L.; Saeyns, Y.; De Prijck, S.; Lippens, S.; Abels, C.; Schoonooghe, S.; Raes, G.; et al. Bone marrow-derived monocytes give rise to self-renewing and fully differentiated Kupffer cells. *Nat. Commun.* **2016**, *7*, 10321. [[CrossRef](#)]
134. Hashimoto, D.; Chow, A.; Noizat, C.; Teo, P.; Beasley, M.B.; Leboeuf, M.; Becker, C.D.; See, P.; Price, J.; Lucas, D.; et al. Tissue-Resident Macrophages Self-Maintain Locally throughout Adult Life with Minimal Contribution from Circulating Monocytes. *Immunity* **2013**, *38*, 792–804. [[CrossRef](#)]
135. Liu, Z.; Gu, Y.; Chakarov, S.; Blieriot, C.; Kwok, I.; Chen, X.; Shin, A.; Huang, W.; Dress, R.J.; Dutertre, C.-A.; et al. Fate Mapping via Ms4a3-Expression History Traces Monocyte-Derived Cells. *Cell* **2019**, *178*, 1509–1525.e19. [[CrossRef](#)]
136. Kondo, H.; Saito, K.; Grasso, J.P.; Aisen, P. Iron metabolism in the erythrophagocytosing Kupffer cell. *Hepatology* **1988**, *8*, 32–38. [[CrossRef](#)]
137. Stockwell, B.R.; Angeli, J.P.F.; Bayir, H.; Bush, A.; Conrad, M.; Dixon, S.J.; Fulda, S.; Gascón, S.; Hatzios, S.; Kagan, V.E.; et al. Ferroptosis: A Regulated Cell Death Nexus Linking Metabolism, Redox Biology, and Disease. *Cell* **2017**, *171*, 273–285. [[CrossRef](#)]
138. Tassa, C.; Shaw, S.Y.; Weissleder, R. Dextran-Coated Iron Oxide Nanoparticles: A Versatile Platform for Targeted Molecular Imaging, Molecular Diagnostics, and Therapy. *Acc. Chem. Res.* **2011**, *44*, 842–852. [[CrossRef](#)] [[PubMed](#)]
139. Kirschbaum, K.; Sonner, J.K.; Zeller, M.W.; Deumelandt, K.; Bode, J.; Sharma, R.; Krüwel, T.; Fischer, M.; Hoffmann, A.; da Silva, M.C.; et al. In vivo nanoparticle imaging of innate immune cells can serve as a marker of disease severity in a model of multiple sclerosis. *Proc. Natl. Acad. Sci. USA* **2016**, *113*, 13227–13232. [[CrossRef](#)] [[PubMed](#)]
140. Hussain, U.; Zia, K.; Iqbal, R.; Saeed, M.; Ashraf, N. Efficacy of a Novel Food Supplement (Ferfer(R)) Containing Microencapsulated Iron in Liposomal Form in Female Iron Deficiency Anemia. *Cureus* **2019**, *11*, e4603. [[CrossRef](#)]
141. Chow, A.; Huggins, M.; Ahmed, J.; Hashimoto, D.; Lucas, D.; Kunisaki, Y.; Pinho, S.; Leboeuf, M.; Noizat, C.; Van Rooijen, N.; et al. CD169⁺ macrophages provide a niche promoting erythropoiesis under homeostasis and stress. *Nat. Med.* **2013**, *19*, 429–436. [[CrossRef](#)]

142. Ramos, P.; Casu, C.; Gardenghi, S.; Breda, L.; Crielaard, B.J.; Guy, E.; Marongiu, M.F.; Gupta, R.; Levine, R.L.; Abdel-Wahab, O.; et al. Macrophages support pathological erythropoiesis in polycythemia vera and β -thalassemia. *Nat. Med.* **2013**, *19*, 437–445. [[CrossRef](#)] [[PubMed](#)]
143. Liao, C.; Prabhu, K.S.; Paulson, R.F. Monocyte-derived macrophages expand the murine stress erythropoietic niche during the recovery from anemia. *Blood* **2018**, *132*, 2580–2593. [[CrossRef](#)]
144. Chen, Y.; Xiang, J.; Qian, F.; Diwakar, B.T.; Ruan, B.; Hao, S.; Prabhu, K.S.; Paulson, R.F. Epo receptor signaling in macrophages alters the splenic niche to promote erythroid differentiation. *Blood* **2020**, *136*, 235–246. [[CrossRef](#)] [[PubMed](#)]
145. Kidder, K.; Bian, Z.; Shi, L.; Liu, Y. Inflammation Unrestrained by SIRPalpha Induces Secondary Hemophagocytic Lymphohistiocytosis Independent of IFN- γ . *J. Immunol.* **2020**, *205*, 2821–2833. [[CrossRef](#)] [[PubMed](#)]
146. Zoller, E.E.; Lykens, J.E.; Terrell, C.E.; Aliberti, J.; Filipovich, A.H.; Henson, P.M.; Jordan, M.B. Hemophagocytosis causes a consumptive anemia of inflammation. *J. Exp. Med.* **2011**, *208*, 1203–1214. [[CrossRef](#)] [[PubMed](#)]
147. Morimoto, A.; Uchida, K.; Chambers, J.; Sato, K.; Hong, J.; Sanjoba, C.; Matsumoto, Y.; Yamagishi, J.; Goto, Y. Hemophagocytosis induced by *Leishmania donovani* infection is beneficial to parasite survival within macrophages. *PLoS Negl. Trop. Dis.* **2019**, *13*, e0007816. [[CrossRef](#)]
148. Xu, R.; Zhu, D.; Guo, J.; Wang, C. IL-18 promotes erythrophagocytosis and erythrocyte degradation by M1 macrophages in a calcific microenvironment: IL-18 promotes erythrophagocytosis and degradation. *Can. J. Cardiol.* **2021**. online pre-proof. [[CrossRef](#)] [[PubMed](#)]
149. Murray, P.J. Macrophage Polarization. *Annu. Rev. Physiol.* **2017**, *79*, 541–566. [[CrossRef](#)] [[PubMed](#)]
150. Ju, C.; Tacke, F. Hepatic macrophages in homeostasis and liver diseases: From pathogenesis to novel therapeutic strategies. *Cell. Mol. Immunol.* **2016**, *13*, 316–327. [[CrossRef](#)]
151. Kurotaki, D.; Kon, S.; Bae, K.; Ito, K.; Matsui, Y.; Nakayama, Y.; Kanayama, M.; Kimura, C.; Narita, Y.; Nishimura, T.; et al. CSF-1-Dependent Red Pulp Macrophages Regulate CD4 T Cell Responses. *J. Immunol.* **2011**, *186*, 2229–2237. [[CrossRef](#)]
152. Enders, M.; Franken, L.; Philipp, M.-S.; Kessler, N.; Baumgart, A.-K.; Eichler, M.; Wiertz, E.J.H.; Garbi, N.; Kurts, C. Splenic Red Pulp Macrophages Cross-Prime Early Effector CTL That Provide Rapid Defense against Viral Infections. *J. Immunol.* **2019**, *204*, 87–100. [[CrossRef](#)]
153. Hod, E.A.; Zhang, N.; Sokol, S.A.; Wojczyk, B.S.; Francis, R.O.; Ansaldi, D.; Francis, K.P.; Della-Latta, P.; Whittier, S.; Sheth, S.; et al. Transfusion of red blood cells after prolonged storage produces harmful effects that are mediated by iron and inflammation. *Blood* **2010**, *115*, 4284–4292. [[CrossRef](#)]
154. Vinchi, F.; da Silva, M.C.; Ingoglia, G.; Petrillo, S.; Brinkman, N.; Zuercher, A.; Cerwenka, A.; Tolosano, E.; Muckenthaler, M. Hemopexin therapy reverts heme-induced proinflammatory phenotypic switching of macrophages in a mouse model of sickle cell disease. *Blood* **2016**, *127*, 473–486. [[CrossRef](#)] [[PubMed](#)]
155. Olonisakin, T.F.; Suber, T.L.; Gonzalez-Ferrer, S.; Xiong, Z.; Peñaloza, H.F.; van der Geest, R.; Xiong, Y.; Osei-Hwedieh, D.O.; Tejero, J.; Rosengart, M.R.; et al. Stressed erythrophagocytosis induces immunosuppression during sepsis through heme-mediated STAT1 dysregulation. *J. Clin. Investig.* **2021**, *131*. [[CrossRef](#)] [[PubMed](#)]
156. Costa da Silva, M.; Breckwoldt, M.O.; Vinchi, F.; Correia, M.P.; Stojanovic, A.; Thielmann, C.M.; Meister, M.; Muley, T.; Warth, A.; Platten, M.; et al. Iron Induces Anti-tumor Activity in Tumor-Associated Macrophages. *Front. Immunol.* **2017**, *8*, 1479. [[CrossRef](#)] [[PubMed](#)]
157. Alaluf, E.; Vokaer, B.; Detavernier, A.; Azouz, A.; Splittgerber, M.; Carrette, A.; Boon, L.; Libert, F.; Soares, M.P.; Le Moine, A.; et al. Heme oxygenase-1 orchestrates the immunosuppressive program of tumor-associated macrophages. *JCI Insight* **2020**, *5*, e133929. [[CrossRef](#)]
158. Etzerodt, A.; Moulin, M.; Doktor, T.K.; Delfini, M.; Mossadegh-Keller, N.; Bajenoff, M.; Sieweke, M.; Moestrup, S.K.; Auphan-Anezin, N.; Lawrence, T. Tissue-resident macrophages in omentum promote metastatic spread of ovarian cancer. *J. Exp. Med.* **2020**, *217*, e20191869. [[CrossRef](#)] [[PubMed](#)]
159. Etzerodt, A.; Tsalkitzi, K.; Maniecki, M.; Damsky, W.; Delfini, M.; Baudoin, E.; Moulin, M.; Bosenberg, M.; Graversen, J.H.; Auphan-Anezin, N.; et al. Specific targeting of CD163+ TAMs mobilizes inflammatory monocytes and promotes T cell-mediated tumor regression. *J. Exp. Med.* **2019**, *216*, 2394–2411. [[CrossRef](#)] [[PubMed](#)]
160. Etzerodt, A.; Moestrup, S.K. CD163 and Inflammation: Biological, Diagnostic, and Therapeutic Aspects. *Antioxid. Redox Signal.* **2013**, *18*, 2352–2363. [[CrossRef](#)] [[PubMed](#)]

Impaired iron recycling from erythrocytes is an early hallmark of aging

Patryk Slusarczyk^{1†}, Pratik Kumar Mandal^{1†}, Gabriela Zurawska¹, Marta Niklewicz¹, Komal Chouhan¹, Raghunandan Mahadeva¹, Aneta Jończy¹, Matylda Macias¹, Aleksandra Szybinska¹, Magdalena Cybulska-Lubak², Olga Krawczyk², Sylwia Herman³, Michal Mikula², Remigiusz Serwa^{4,5}, Małgorzata Lenartowicz³, Wojciech Pokrzywa¹, Katarzyna Mleczo-Sanecka^{1*}

¹International Institute of Molecular and Cell Biology in Warsaw, Warsaw, Poland; ²Maria Skłodowska-Curie National Research Institute of Oncology, Warsaw, Poland; ³Laboratory of Genetics and Evolution, Institute of Zoology and Biomedical Research, Jagiellonian University, Cracow, Poland; ⁴IMol Polish Academy of Sciences, Warsaw, Poland; ⁵ReMedy International Research Agenda Unit, IMol Polish Academy of Sciences, Warsaw, Poland

Abstract Aging affects iron homeostasis, as evidenced by tissue iron loading and anemia in the elderly. Iron needs in mammals are met primarily by iron recycling from senescent red blood cells (RBCs), a task chiefly accomplished by splenic red pulp macrophages (RPMs) via erythrophagocytosis. Given that RPMs continuously process iron, their cellular functions might be susceptible to age-dependent decline, a possibility that has been unexplored to date. Here, we found that 10- to 11-month-old female mice exhibit iron loading in RPMs, largely attributable to a drop in iron exporter ferroportin, which diminishes their erythrophagocytosis capacity and lysosomal activity. Furthermore, we identified a loss of RPMs during aging, underlain by the combination of proteotoxic stress and iron-dependent cell death resembling ferroptosis. These impairments lead to the retention of senescent hemolytic RBCs in the spleen, and the formation of undegradable iron- and heme-rich extracellular protein aggregates, likely derived from ferroptotic RPMs. We further found that feeding mice an iron-reduced diet alleviates iron accumulation in RPMs, enhances their ability to clear erythrocytes, and reduces damage. Consequently, this diet ameliorates hemolysis of splenic RBCs and reduces the burden of protein aggregates, mildly increasing serum iron availability in aging mice. Taken together, we identified RPM collapse as an early hallmark of aging and demonstrated that dietary iron reduction improves iron turnover efficacy.

*For correspondence: kmsanecka@iimcb.gov.pl

[†]These authors contributed equally to this work

Competing interest: The authors declare that no competing interests exist.

Funding: See page 33

Preprinted: 19 January 2022

Received: 03 April 2022

Accepted: 30 January 2023

Published: 31 January 2023

Reviewing Editor: Yelena Ginzburg, Icahn School of Medicine at Mount Sinai, United States

© Copyright Slusarczyk, Mandal et al. This article is distributed under the terms of the [Creative Commons Attribution License](https://creativecommons.org/licenses/by/4.0/), which permits unrestricted use and redistribution provided that the original author and source are credited.

Editor's evaluation

Slusarczyk et al. present a well written manuscript focused on understanding the mechanisms underlying aging of erythrophagocytic macrophages in the spleen (RPM) and its relationship to iron loading with age. Importantly, the manuscript demonstrates that RPM erythrophagocytic capacity is diminished with age, restored in iron restricted diet fed aged mice. The main conclusion of the manuscript points to accumulation of unavailable insoluble forms of iron as both causing and resulting from RPM failure, likely a consequence of decreased ferroportin expression on RPMs in the spleen.

Introduction

Sufficient iron supplies are critical for the proper functioning of cells and organisms (Cronin et al., 2019; Muckenthaler et al., 2017). At the systemic level, 80% of circulating iron is utilized for hemoglobin synthesis during the daily generation of approximately 200 billion red blood cells (RBCs) (Muckenthaler et al., 2017). The oxygen-carrying capacity of RBCs renders them sensitive to the progressive build-up of reactive oxygen species (ROS) that drive natural RBCs senescence (Bratosin et al., 1998). Due to the prooxidative properties of free heme and iron, high hemoglobin content in physiologically senescent RBCs constitutes a threat to tissues. To reduce the risk of RBC breakdown in the blood vessels and because mammals evolved under limited dietary iron availability, 90% of the body iron needs are met by internal iron recycling from aged RBCs (Ganz, 2012). This task is accomplished predominantly by red pulp macrophages (RPMs) of the spleen, cells that engulf defective RBCs in the process called erythrophagocytosis (EP; Bian et al., 2016; Youssef et al., 2018). Recent findings imply that in parallel to phagocytosis of intact senescent RBCs, which is actively performed by a fraction of RPMs at a given moment (Akilesh et al., 2019; Ma et al., 2021; Youssef et al., 2018) part of the RBC-derived iron is recovered via hemolysis of RBCs within the splenic microenvironment and subsequent hemoglobin uptake (Klei et al., 2020). The latter likely occurs in RPMs, but whether other cell types contribute to this process remains to be determined.

The loss of elasticity due to a build-up of oxidative damage is a key feature of naturally aged RBCs (Arashiki et al., 2013; Bratosin et al., 1998; Ganz, 2012; Higgins, 2015; Lutz, 2012). The unique architecture of the spleen confers a filter for verifying the biomechanical integrity of RBCs, whereby senescent rigid RBCs are retained within the spleen cords (Mebius and Kraal, 2005). Recognition of 'trapped' RBCs by RPMs involves additional mechanisms, such as the binding of exoplasmic phosphatidylserine or opsonizing antibodies, that were proposed to act additively (Gottlieb et al., 2012; Slusarczyk and Mleczko-Sanecka, 2021). Upon engulfment by RPMs, RBCs are degraded in phagolysosomes, and heme is released to the cytoplasm by HRG1 (Klei et al., 2017; Pek et al., 2019). Heme is subsequently catabolized by heme oxygenase 1 (HO-1; encoded by *Hmox1*) to carbon monoxide (CO), biliverdin, and ferrous iron that feeds the labile iron pool (LIP) (Kovtunovych et al., 2010). Iron from the LIP is sequestered by the iron-storing protein ferritin, composed of H and L subunits (Mleczko-Sanecka and Silvestri, 2021). Iron efflux from RPMs occurs via ferroportin (FPN) to replenish the transferrin-bound iron pool in the plasma (Muckenthaler et al., 2017; Zhang et al., 2011). The process of iron release from RPMs is tightly regulated by hepcidin, a liver-derived hormone that mediates FPN degradation and/or occlusion, hence preventing iron release from RPMs (Aschemeyer et al., 2018; Nemeth et al., 2004). Despite the growing body of knowledge, it is still not completely explored how iron balance in RPMs is affected by different pathophysiological conditions and how it may influence their functions.

Similar to erythropoiesis, the rate of RBC clearance is very high, reaching 2–3 million per second in humans (Higgins, 2015), and is considered largely constitutive under physiological conditions. Some reports showed that the intensity of EP can be enhanced by proinflammatory conditions and pathogen components (Bennett et al., 2019; Bian et al., 2016; Delaby et al., 2012). Recent work employing genetic mouse models showed that altered calcium signaling in RPMs due to overactivation or the loss of the PIEZO1 mechanoreceptor controls EP efficiency (Ma et al., 2021). However, it is largely unknown if the capacity for RBC uptake and their degradation within the phagolysosomes are regulated by intrinsic or systemic iron status per se.

Iron dyshomeostasis hallmarks physiological aging. This is exemplified by progressive iron accumulation and iron-dependent oxidative damage in aging organs (Arruda et al., 2013; Cook and Yu, 1998; Sukumaran et al., 2017; Xu et al., 2008). At the same time, limited plasma iron availability is frequent in aged individuals and is a leading cause of a condition referred to as anemia in the elderly (Girelli et al., 2018). RPMs are derived from embryonic progenitor cells (Yona et al., 2013), exhibit low self-renewal capacity (Hashimoto et al., 2013), and are only partially replenished by blood monocytes during aging (Liu et al., 2019). Hence, these specialized cells continuously perform senescent RBCs clearance during their lifespan, thus processing and supplying the majority of the organism's iron requirements. We hypothesized that the exposure to high iron burden might accelerate their aging, affecting body iron indices and RBC homeostasis. Therefore, we aimed to explore the exact relationship between substantial splenic iron deposition during early aging (Altamura et al., 2014) and the iron-recycling functions of RPMs. Here, we found that aging expands iron accumulation in RPMs

and their partial demise in female mice, largely attributable to the downregulation of ferroportin. We propose that the depletion of RPMs depends both on iron-triggered toxicity, resembling ferroptosis, and on the cell death mechanisms involving proteostasis defects. Furthermore, we demonstrate that iron loading impairs the capacity of RPMs to engulf and lyse RBCs. We show that age-related RPM dysfunction affects local RBC balance in the spleen, and RPM decay leads to the formation of iron- and heme-rich extracellular protein aggregates. Finally, we provide evidence that reducing dietary iron during aging 'rejuvenates' RPM functions and fitness, and improves iron homeostasis.

Results

RPMs of aged mice show increased labile iron levels, oxidative stress and diminished iron-recycling functions

To investigate iron-recycling capacity during aging, we used young (2–3 month-old) and aged (10–11 month-old) C57BL/6 J mice fed a diet with standard iron content (200 ppm). The latter age in mice corresponds to approximately 40–45 years in humans when senescent changes begin to occur (Fox *et al.*, 2006). We used female mice which show more pronounced iron deposition in the spleen than males with age progression (Altamura *et al.*, 2014). As expected, aged mice showed tissue iron loading, with the spleen being most affected, followed by the liver and other organs such as muscles and the heart (Figure 1—figure supplement 1A–D). Aging mice exhibited decreased blood hemoglobin values, as previously shown (Peters *et al.*, 2008), and a drop in transferrin saturation, a feature that thus far was observed mostly in elderly humans (Figure 1—figure supplement 1E, F; Girelli *et al.*, 2018). Next, we aimed to verify if aging affects the iron status and essential cellular functions of RPMs. Using intracellular staining and flow cytometric analyses, we uncovered that RPMs [gated as CD11b-dim, F4/80-high, TREML4-high (Haldar *et al.*, 2014) as shown in Figure 1—figure supplement 2] in aged mice exhibited a significant deficiency in H ferritin levels, with unchanged L ferritin protein expression (Figure 1—figure supplement 1G, H; see Figure 1—figure supplement 3A, B for validation of antibodies for intracellular staining). Consistently, using the fluorescent probe Ferro-Orange that interacts specifically with ferrous iron, we detected a significant increase in LIP in aged RPMs (Figure 1—figure supplement 1I) accompanied by marked oxidative stress (Figure 1—figure supplement 1J). We next tested if this increase in labile iron in RPMs would impact the phagocytic activity. Hence, we incubated splenic single-cell suspension with temperature-stressed RBCs fluorescently labeled with PKH67 dye (Klei *et al.*, 2020; Theurl *et al.*, 2016). In parallel, we employed another standard cargo for phagocytosis, zymosan, a yeast cell wall component. Using this *ex vivo* approach, we detected a significant drop in RBC clearance capacity in aged compared to young RPMs (Figure 1—figure supplement 1K). Notably, their capacity for the engulfment of zymosan remained unchanged (Figure 1—figure supplement 1L), thus suggesting a specific defect of EP in aged RPMs. RPMs rely on lysosomal activity to lyse RBC components in phagolysosomes and hence exert their iron-recycling functions. Using a fluorescent probe, we observed decreased lysosomal activity in RPMs isolated from 10- to 11-month-old mice compared to those derived from young control animals (Figure 1—figure supplement 1M). Of note, we also detected diminished mitochondrial activity, a well-established aging marker (Sun *et al.*, 2016), in aged RPMs (Figure 1—figure supplement 1N). Interestingly, peritoneal macrophages of aged mice did not show altered ROS levels or impaired functions of lysosomes and mitochondria (Figure 1—figure supplement 4), suggesting that these age-related changes affect RPMs earlier than other macrophage populations. Altogether, these insights suggest that during aging, RPMs increase LIP and exhibit a reduced capacity for the RBCs engulfment and lysosomal degradation of erythrocyte components.

Iron-reduced diet normalizes body iron parameters during aging, diminishes iron retention in RPMs, and rescues age-related decline in RPMs' iron-recycling capacity

We next set out to explore whether an age-related alteration of systemic iron indices could be prevented. Caloric restriction was previously shown to effectively reduce tissue iron content in older rats (Cook and Yu, 1998; Xu *et al.*, 2008). Analogously, to correct iron dyshomeostasis in aging mice, we reduced dietary iron content from the fifth week of life to a level (25 ppm) that was reported as sufficient to maintain erythropoiesis (Sorbie and Valberg, 1974). This approach reverted the degree

of iron deposition in the spleen and liver (**Figure 1A and B**) and partially alleviated the decreased transferrin saturation characteristic of aged mice fed a standard diet (**Figure 1C**). Notably, the mild drop in blood hemoglobin was not rescued by the iron-reduced (IR) diet (**Figure 1—figure supplement 5A**). Of note, aged mice did not display significant changes in hematocrit, RBCs counts, MCV, MCH, or the intensity of bone marrow erythropoiesis (**Figure 1—figure supplement 5B–F**; see **Figure 1—figure supplement 6** for gating strategy of erythroid progenitors). We observed a small increase in extramedullary erythropoietic activity in the spleen and increased plasma erythropoietin (EPO) levels in aged mice, implying that very mild anemic phenotype and/or decreased transferrin saturation are sensed by the body (**Figure 1—figure supplement 5G, H**). However, these responses were not diminished by the reduced dietary iron content in aged mice. These observations imply that either partial alleviation of plasma iron availability in IR mice is insufficient to correct very mild aging-triggered anemia or other hematopoiesis-related mechanisms may contribute to this phenotype.

Next, we observed that hepcidin mRNA levels were increased in the liver of aged versus young mice, a phenotype that was reverted by feeding them an IR diet (**Figure 1D**). In addition, we did not observe a contribution of inflammatory cues to hepcidin regulation, as the plasma IL-6 levels remained unchanged (**Figure 1E**). We next examined FPN levels in RPMs using an antibody that recognizes the extracellular loop of murine FPN (validated in **Figure 1—figure supplement 7**). As expected from the pattern of hepcidin expression, cell membrane FPN levels in RPMs were decreased in aged mice and this was rescued by feeding them an IR diet (**Figure 1F**). We further characterized RPMs' iron status. We found that despite decreased ferritin H levels in aged mice, regardless of the dietary regimen (**Figure 1G**), accumulation of both labile iron (**Figure 1H**) and total iron (**Figure 1I**) was completely reversed in RPMs of aged mice fed an IR diet as compared to a standard diet. Likewise, we observed alleviation of oxidative stress in aged RPMs in response to a dietary iron restriction (**Figure 1J**).

We next assessed whether altered RPM iron content in aged mice that were maintained on a standard affects their functions. First, we detected a lower representation of RPMs in the spleens of aged mice, a phenotype that was alleviated by limited dietary iron content (**Figure 1K**). We noticed that among 55 genes that were differentially regulated in RNA sequencing (RNA-seq) data between standard and IR diets, 9 genes are involved in proliferation control (**Figure 1—figure supplement 8A**). Consistent with the pattern of their regulation, we found that RPMs derived from aged mice on an IR diet showed mildly increased levels of the proliferation marker Ki-67 (**Figure 1—figure supplement 8B**), a phenomenon that was previously reported to drive RPM niche replenishment after erythrophagocytosis-driven depletion (**Youssef et al., 2018**). Next, by reanalysis of published data from Ms4a3-tdTomato reporter mice (**Liu et al., 2019**) (where macrophages of monocyte origin are fluorescently labeled) we demonstrated that the shortage of RPMs during aging is chiefly driven by the depletion of RPMs of embryonic origin, whereas the low rate of RPM replenishment from monocytes remained constant during aging (**Figure 1—figure supplement 9A**). In line with this, we did not observe any robust change in the splenic population of monocytes or pre-RPMs (**Lu et al., 2020**) in our aged mice (**Figure 1—figure supplement 9B, C**), and we did not detect significant differences in the numbers of granulocytes (**Figure 1—figure supplement 9D**). These data suggest that the drop in RPM representation is not underlain by insufficient recruitment from monocytes or a concurrent increase in granulocyte representation, but involves the demise of embryonically derived cells.

We further assessed if RPM iron status during aging reflects their capacity to engulf and degrade RBCs. To this end, we first performed *in vivo* EP assay via transfusion of PKH67-stained temperature-stressed erythrocytes (**Lu et al., 2020; Theurl et al., 2016**). We observed that aged RPMs were less efficient in sequestering transfused RBCs, an impairment that was partially rescued by feeding mice an IR diet (**Figure 1L**). Similarly to the EP rate, we found that RPMs isolated from aged IR mice restored the lysosomal activity to the levels observed in young mice (**Figure 1M**). These data imply that the diminished capacity of RPMs to engulf and lyse RBCs in phagolysosomes during aging can be ameliorated by limiting dietary iron content. Since earlier studies demonstrated that under conditions of RPM impairment, iron-recycling functions are significantly supported by liver macrophages (**Theurl et al., 2016**), we also measured their EP capacity during aging. Using the transfusion of PKH67-stained RBCs we did not detect significant differences in the percentage of RBC-positive hepatic macrophages in aged mice (**Figure 1N**). However, consistently with the *de novo* recruitment of iron-recycling myeloid cells to the liver upon erythrocytic stress (**Theurl et al., 2016**), we noticed a significant expansion of the KC-like population in aged mice but not in the aged IR group (**Figure 1O**). This

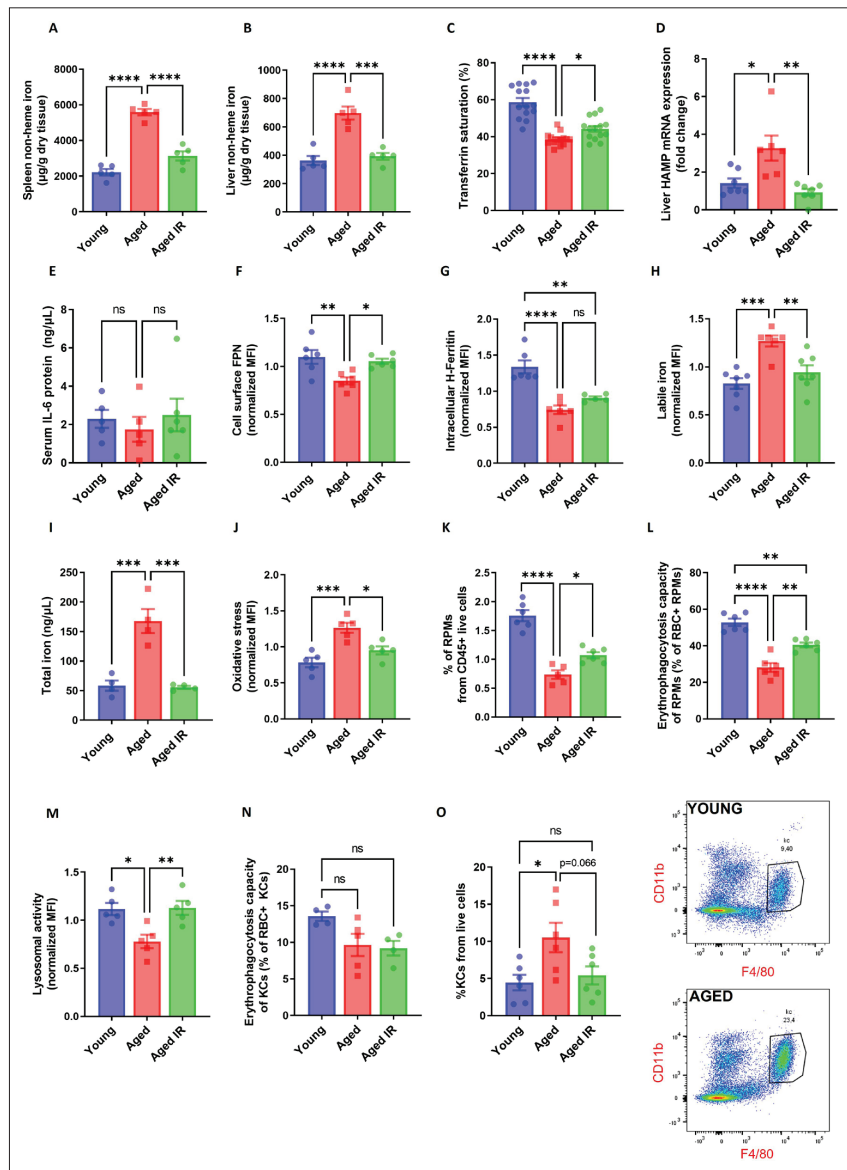


Figure 1. Iron-reduced diet normalizes body iron parameters during aging, diminishes iron retention in RPMs, and prevents oxidative stress. (A) Splenic and (B) liver non-heme iron content was determined in young, aged, and aged IR mice. (C) Plasma transferrin saturation was determined in young, aged, and aged IR mice. (D) Relative mRNA expression of hepcidin (Hamp) in the liver of young, aged, and aged IR mice was determined by qPCR. (E) Serum IL-6 protein levels in young, aged, and aged IR mice were measured by Mouse IL-6 Quantikine ELISA Kit. (F) Expression of ferroportin (FPN) on the cell membrane of young, aged, and aged IR RPMs was assessed by flow cytometry. (G) Intracellular H-Ferritin protein levels in young, aged, and aged IR RPMs were quantified by flow cytometry. (H) Cytosolic ferrous iron (Fe²⁺) levels in young, aged, and aged IR RPMs were measured using FerroOrange with flow cytometry. (I) The total intracellular iron content in young, aged, and aged IR magnetically-sorted RPMs was assessed using the Iron Assay Kit. (J) The cytosolic ROS levels in young, aged, and aged IR RPMs were assessed by determining CellROX Deep Red fluorescence intensity with flow cytometry. (K) The percentage of RPMs from CD45 + live cells present in the spleen of young, aged, and aged IR mice was

Figure 1 continued on next page

Figure 1 continued

assessed by flow cytometry. **(L)** Erythrophagocytosis capacity in young, aged, and aged IR RPMs was determined using flow cytometry by measuring the percentage of RPMs that phagocytosed transfused PKH67-labeled temperature-stressed RBCs. **(M)** Lysosomal activity of young, aged, and aged IR RPMs was determined using Lysosomal Intracellular Activity Assay Kit with flow cytometry. **(N)** Erythrophagocytosis capacity in young, aged, and aged IR Kupffer cells (KCs) was determined using flow cytometry by measuring the percentage of KCs that phagocytosed transfused PKH67-labeled temperature-stressed RBCs. **(O)** Percentages of KCs in total live cells in the livers of young, aged, and aged IR mice and representative flow cytometry plots of KCs. Each dot represents one mouse. Data are represented as mean \pm SEM. Statistical significance among the three groups was determined by One-Way ANOVA test with Tukey's Multiple Comparison test. ns $p > 0.05$, * $p < 0.05$, ** $p < 0.01$, *** $p < 0.001$ and **** $p < 0.0001$.

The online version of this article includes the following source data and figure supplement(s) for figure 1:

Source data 1. Related to *Figure 1A–O*.

Figure supplement 1. RPMs of aged mice show increased labile iron levels, oxidative stress and diminished iron-recycling functions.

Figure supplement 1—source data 1. Related to *Figure 1—figure supplement 1A–N*.

Figure supplement 2. Gating strategy for RPMs.

Figure supplement 3. Validation of the antibodies against H and L ferritin.

Figure supplement 3—source data 1. Related to *Figure 1—figure supplement 3A*.

Figure supplement 4. Peritoneal macrophages in aged mice do not show functional impairments.

Figure supplement 4—source data 1. Related to *Figure 1—figure supplement 4B–D*.

Figure supplement 5. Hematological parameters and erythropoietic activity in aging mice.

Figure supplement 5—source data 1. Related to *Figure 1—figure supplement 5A–H*.

Figure supplement 6. Gating strategy for erythroid progenitor cells in the spleen **(A)** and the bone marrow **(B)**.

Figure supplement 7. Validation of the ferroportin antibody for flow cytometry.

Figure supplement 7—source data 1. Related to *Figure 1—figure supplement 7*.

Figure supplement 8. RPMs derived from aged IR versus aged mice show higher proliferation capacity.

Figure supplement 8—source data 1. Related to *Figure 1—figure supplement 8B*.

Figure supplement 9. RPM depletion in aged mice affects embryonically-derived RPMs and is not a consequence of diminished recruitment from monocytes.

Figure supplement 9—source data 1. Related to *Figure 1—figure supplement 9A–D*.

implies that the liver macrophage may partially compensate for the decreased EP activity in RPMs. In sum, we demonstrate that dietary iron restriction normalizes both systemic and RPM iron levels and reverses the age-related reduction in their numbers and iron-recycling ability.

Aging triggers the retention of senescent RBCs, increased hemolysis, and the formation of non-degradable iron-rich aggregates in the spleen

Having established that dietary iron content in aging modulates RPM representation and EP capacity (*Figure 1L*), we examined parameters related to RBCs' fitness. First, we performed an RBC lifespan assay and found no differences in the rate of RBCs removal from the circulation between young and aged mice (*Figure 2A*, *Figure 2—figure supplement 1* for RBC gating strategy), suggesting intact fitness of circulating RBCs. Likewise, these RBCs did not show increased labile iron or ROS levels (*Figure 2B and C*). However, physiologically aged RBCs are first filtered in the spleen due to the loss of their elasticity, and this step is a prerequisite for their removal via EP (*Slusarczyk and Mleczko-Sanecka, 2021*). In agreement with this model, RBCs isolated from the spleen of young mice showed ROS build-up, a marker of their natural senescence (*Bratosin et al., 1998; Figure 2C*). We thus hypothesized that the reduced numbers and phagocytic capacity of RPMs in aging might impact local rather than systemic RBCs homeostasis. Consistently, splenic RBCs isolated from aged mice showed more pronounced ROS levels than RBCs derived from young mice (*Figure 2D*). In line with the partial mitigation of the defective iron-recycling capacity by restricted dietary iron content (*Figure 1K and L*), we found that mice fed an IR diet exhibited erythrocytic oxidative stress parameters similar to the young

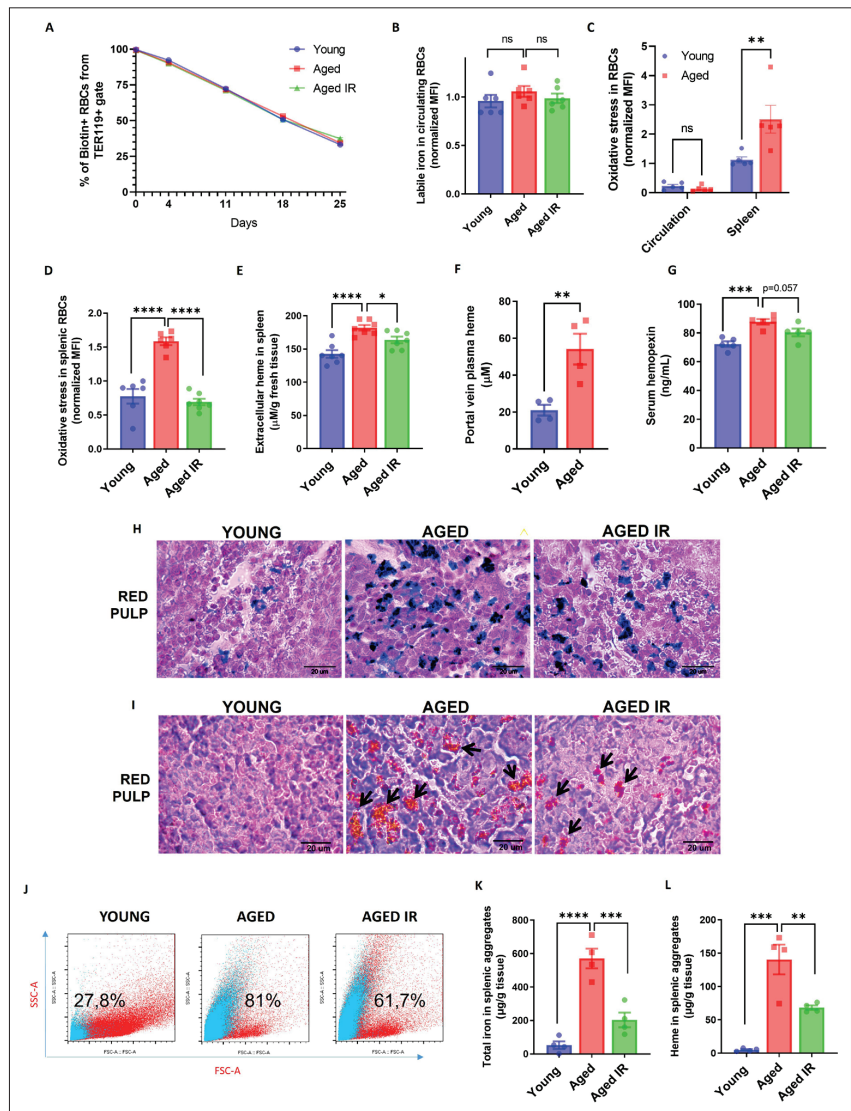


Figure 2. Aging triggers the retention of senescent RBCs, increased hemolysis, and the formation of non-degradable iron-rich aggregates in the spleen. **(A)** The RBC biotinylation lifespan assay was performed on circulating RBCs from young, aged, and aged IR mice. **(B)** Cytosolic ferrous iron (Fe²⁺) levels in RBCs derived from the circulation of young, aged, and aged IR mice were measured using FerroOrange with flow cytometry. **(C–D)** The cytosolic ROS levels in RBCs derived from **(C)** circulation and the spleen of young and aged mice; **(D)** the spleen of young, aged, and aged IR mice. Levels of ROS were estimated by determining CellROX Deep Red fluorescence intensity with flow cytometry. **(E)** Extracellular heme levels were measured in the supernatant obtained after the dissociation of spleens from young, aged, and aged IR mice using the Heme Assay Kit. **(F)** Portal vein plasma heme levels were measured in young, aged, and aged IR mice using Heme Assay Kit. **(G)** Serum hemopexin levels were measured in young, aged, and aged IR mice with Mouse Hemopexin ELISA Kit. **(H)** Perls' Prussian Blue staining of the splenic red pulp in young, aged, and aged IR mice. **(I)** Hematoxylin and eosin staining of the splenic red pulp in young, aged, and aged IR mice. Arrows indicate extracellular dark-colored aggregates. **(J)** Representative flow cytometry plots of magnetically-sorted splenocytes. In blue are events adverse for dead cell staining and cell surface markers CD45, TER119, CD11b, and F4/80. The percentage of these events in total

Figure 2 continued on next page

Figure 2 continued

acquired events is indicated. **(K)** The total iron content in magnetically-sorted, cell-free aggregates derived from spleens of young, aged, and aged IR mice was assessed using the Iron Assay Kit. **(L)** The heme content in magnetically-sorted, cell-free aggregates derived from spleens of young, aged, and aged IR mice was assessed using the Heme Assay Kit. Each dot in the graph **(A)** represents $n=8$. For the other panels, each dot represents one mouse. Data are represented as mean \pm SEM. Welch's unpaired t-test determined statistical significance between the two groups; for the three groups, One-Way ANOVA with Dunnett's or Tukey's Multiple Comparison test was applied. In **(C)** Two-Way ANOVA test was applied. * $p<0.05$, ** $p<0.01$, *** $p<0.001$ and **** $p<0.0001$.

The online version of this article includes the following source data and figure supplement(s) for figure 2:

Source data 1. Related to **Figure 2A–G and K–L**.

Figure supplement 1. Gating strategy for circulating **(A)** and splenic RBCs **(B)**.

Figure supplement 2. FPN levels and iron status in splenic RBCs in aging.

Figure supplement 2—source data 1. Related to **Figure 2—figure supplement 2A–B**.

Figure supplement 3. Post-sorting purity of extracellular aggregates isolated from the aged spleen.

mice (**Figure 2D**). We further corroborated that the differences in ROS levels of splenic RBCs during aging reflect their senescence status, and are not a consequence of diminished FPN or LIP accumulation (**Figure 2—figure supplement 2A** and **B**). In agreement with the notion that a part of senescent RBCs undergoes local hemolysis (Klei et al., 2020), we further detected significantly higher levels of extracellular heme in the aged spleens, likely reflecting a higher burden of defective RBCs that evade efficient EP (**Figure 2E**). Interestingly, we found that the levels of heme in aging spleens were partially rescued by the IR diet. In support of these data, we detected higher levels of heme in plasma obtained from the portal vein (that carries the blood from the spleen to the liver) of aged versus young mice (**Figure 2F**) and higher serum concentrations of heme-scavenging hemopexin (**Figure 2G**). The latter tended to be rescued by the IR diet ($p=0.057$; **Figure 2G**). In conclusion, our data suggest that the reduced iron-recycling capacity of RPMs during aging may promote the retention of senescent RBCs prone to undergo local lysis and that these manifestations may be partially rescued by maintaining mice on an IR diet.

Previous work showed that genetic mouse models hallmarked by RPM depletion display splenic iron accumulation (Haldar et al., 2014; Okreglicka et al., 2021), partially resembling our observation in aged mice. However, the identity of splenic iron deposits in RPM-depleted spleens remains unclear. We thus aimed to characterize iron deposits in the aging spleen. Perls' Prussian blue staining that detects iron deposits showed that aged mice on a standard diet exhibited enhanced iron accumulation in the red pulp, a less pronounced phenotype in mice fed an IR diet (**Figure 2H**). This primarily reflected RPMs' iron status (**Figure 1I**). Intriguingly, eosin and hematoxylin staining visualized deposits in aged spleens that, in contrast to Perls' staining, were completely absent in young controls (**Figure 2I**). They appeared as large and extracellular in the histology sections and seemed smaller and less abundant in mice fed an IR diet (**Figure 2I**). Flow cytometry analyses confirmed that splenic single-cell suspension from aged but not young mice contained superparamagnetic particles, likely rich in iron oxide (Franken et al., 2015), that are characterized by high granularity as indicated by the SSC-A signal (**Figure 2J**). These particles did not show staining indicative of dead cells and failed to express typical splenocyte and erythroid markers (CD45, TER119, CD11b, or F4/80) (**Figure 2J**). With different granularity and size parameters, such particles appeared in mice aged on an IR diet, however, to a lesser extent. To further examine the composition of these aggregates, we established a strategy involving splenocyte separation in the lymphocyte separation medium followed by magnetic sorting, which successfully separated them from iron-rich cells (chiefly RPMs; **Figure 2—figure supplement 3**). We found that these aggregates contained large amounts of total iron (**Figure 2K**) and, interestingly, heme (**Figure 2L**), implying their partial RBC origin. Importantly, both iron and heme content was significantly reduced in mice fed an IR diet. In sum, our data show that aging is associated with local RBC dyshomeostasis in the spleen, and the formation of iron- and heme-rich aggregates, and that both these responses can be alleviated by limiting dietary iron content.

Splenic age-triggered iron deposits are rich in aggregation-prone proteins derived from damaged RPMs

We next sought to explore the origin of the splenic iron aggregates. We imaged spleen sections from young and aged mice with transmission electron microscopy (TEM) to obtain ultrastructural information. We noticed that RPMs in young mice contained only intracellular dark-colored deposits, rich in structures that resemble ferritin (**Figure 3Ai**). Their appearance likely mirrors a form of iron deposits that were in the past referred to as hemosiderin, an intracellular clustered insoluble degradation product of ferritin (**Harrison and Arosio, 1996; Ward et al., 2000**). In older mice, we likewise observed intracellular deposits in morphologically intact cells (**Figure 3Aii**). However, in agreement with histological staining, we detected two other classes of aggregates: those that are still granular and enclosed within the membrane, but present in cells that are morphologically damaged (**Figure 3Aiii**) and those that are large, amorphous, and located extracellularly (**Figure 3Aiv**). Next, we conducted label-free proteomic profiling to determine the composition of magnetically-isolated aging-associated splenic aggregates. We identified over 3770 protein groups, among which 3290 were significantly more abundant in isolates from aged mice compared with the samples derived from young mice (**Figure 3B**). We assume that low-level detection of peptides from the young spleens may represent remnants from intracellular deposits that we observed via TEM and which may be released from RPMs during splenocyte processing. We performed a functional enrichment analysis of the top 387 hits (log₂ fold change >5) with DAVID and ShinyGO bioinformatic tools (**Figure 3B and C**). We first noticed that although the identified proteins were derived from different organelles, one of the top characteristics that they shared was a disordered region in their amino acid sequence, a factor that may increase the risk of protein aggregation (**Uversky, 2009**). Consistently, the top hits were enriched in proteins related to neurodegeneration pathways, amyotrophic lateral sclerosis, Huntington's disease, and heat shock protein binding, linking their origin to proteostasis defects (**Medinas et al., 2017**). These included aggregation-prone huntingtin (HTT), amyloid-beta precursor protein (APP), and ataxin 3 (ATXN3) (**Lieberman et al., 2019; Liu et al., 2018 #251; Figure 3B**). In agreement with the substantial iron load of the aggregates and the fact that iron promotes protein aggregation (**Klang et al., 2014**), we identified 'metal-binding' as another significant functional enrichment. We further observed that the top components of the aggregates included several proteins associated with immunoglobulin-like domains (**Figure 3B and C**), such as antibody chain fragments as well as Fc receptors, proteins associated with complement activation and phagocytosis, thus linking the aggregates to the removal of defective cells, likely senescent RBCs or damaged RPMs. Finally, consistent with our conclusions from EM imaging that cell death likely contributes to the formation of the aggregates (**Figure 3Aiv**), their top components were enriched with apoptosis-related protein (e.g. BID, DFFA, DAXX, and MRCH1; **Figure 3B**) and those linked to the response to stress (**Figure 3B and C**). Supporting the idea that iron-rich protein aggregates emerge primarily from damaged RPMs, and may likely contain some erythrocyte components, we observed an overlap between their protein components and the proteome of RPMs and erythrocytes (**Gautier et al., 2018; Figure 3D**).

To further explore the molecular mechanisms that influence their formation in aged spleens, we performed RNA sequencing of FACS-sorted RPMs from young and aged mice. We identified 570 differentially expressed genes, including 392 up- and 178 down-regulated transcripts (**Figure 3—figure supplement 1A**). RNA-seq data revealed rather an anti-inflammatory transcriptional pattern of aged RPMs, exemplified by the downregulation of genes encoding for MHC class II complexes and the induction of *Il10* (**Figure 3E and Figure 3—figure supplement 1A**). Most importantly, functional enrichment analysis showed that aged RPMs were hallmarked by ER stress, unfolded protein response, and ER-associated degradation (ERAD) (**Figure 3E**), regardless of the diet (**Figure 3—figure supplement 1B**). This observation corroborates the finding that aging-triggered splenic iron-rich protein deposits, enriched in aggregation prone-proteins, may result from proteotoxic stress in aged RPMs. ERAD is a pathway for targeting misfolded ER proteins for cytoplasmic proteasomal degradation (**Qi et al., 2017**). Correspondingly, we identified a significant increase in proteasomal activity in aged RPMs, measured with a dedicated fluorescent probe that undergoes proteasomal cleavage (**Figure 3F**). The IR diet reversed this proteasomal activation (**Figure 3F**). Since misfolded proteins can be also cleared from ER via ER-to-lysosome-associated degradation pathways (**De Leonibus et al., 2019**), and lysosomal activity was diminished in aged RPMs in a diet-dependent fashion, our data imply that proteasomal activity likely compensates for the reduced lysosomal-mediated protein quality

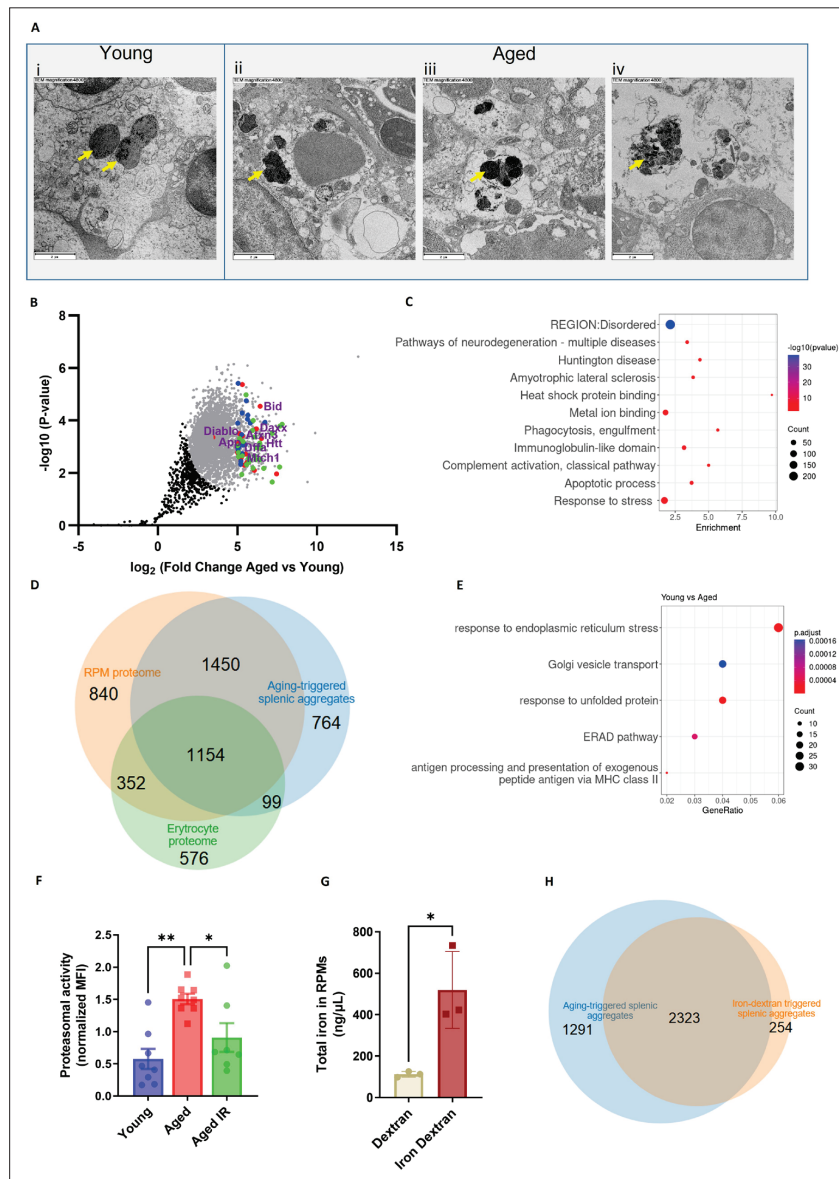


Figure 3. Splenic age-triggered iron deposits are rich in aggregation-prone proteins derived from damaged RPMs. (A) Ultrastructural analyses of the spleen red pulp sections by transmission electron microscopy. Arrows indicate dark-colored dense deposits. (B) Volcano plot illustrating 3290 protein groups (in gray) that are significantly more abundant in magnetically-sorted, cell-free aggregates derived from aged versus young spleen. Based on the functional enrichment analyses, the red color denotes proteins linked with ‘pathways of neurodegeneration’, green - those associated with an ‘apoptotic process’ and blue - those related to the ‘immunoglobulin-like domain’ category. (C) Enriched functional categories among the top 387 protein hits that are more abundant in magnetically-sorted, cell-free aggregates derived from aged versus young spleen. (D) Venn diagram illustrating the number of common proteins identified in RPMs, erythrocytes (human), and aging-triggered splenic aggregates. (E) Enriched functional categories among differentially regulated genes in FACS-sorted RPMs derived from young versus aged mice (identified by RNA-seq). (F) Proteasomal activity was measured in RPMs derived from *Figure 3 continued on next page*

Figure 3 continued

young, aged, and aged IR mice using a fluorescent proteasome activity probe with flow cytometry. (G) The total intracellular iron content in magnetically sorted RPMs derived from spleens of dextran- and iron dextran-injected mice (8 hr post-injection) was assessed using the Iron Assay Kit. (H) Venn diagram illustrating the number of common protein groups identified in aging-triggered and iron dextran-triggered splenic aggregates (log₂ fold change >1.5 versus respective young and dextran-injected controls, respectively; n=2). The dextran-triggered aggregates were isolated 24 hr post-injection. Each dot represents one mouse; in (B) three biological replicates per group were analyzed. Data are represented as mean ± SEM. Welch's unpaired t-test determined statistical significance between the two groups; statistical significance among the three groups was determined by One-Way ANOVA test with Tukey's Multiple Comparison test. *p<0.05, **p<0.01.

The online version of this article includes the following source data and figure supplement(s) for figure 3:

Source data 1. Related to *Figure 3B*.

Source data 2. Related to *Figure 3D*.

Source data 3. Related to *Figure 3F–G*.

Source data 4. Related to *Figure 3H*.

Figure supplement 1. Supplementary data related to RNA-seq analysis of RPMs derived from young, aged, and aged IR mice.

Figure supplement 1—source data 1. Related to *Figure 3—figure supplement 1A*.

Figure supplement 2. Components of lysosomes and ferritins are highly overrepresented in protein aggregates isolated from aged versus aged IR mice.

Figure supplement 2—source data 1. Related to *Figure 3—figure supplement 2A*.

control in RPMs during aging (*Figure 1M*). Finally, assigning a causal relationship between the iron loading of RPMs and their global proteostasis defect, we found that forced iron accumulation in RPMs in response to iron dextran injection in young mice (*Figure 3G*) provoked the formation of iron-rich protein aggregates whose composition largely overlaps with those from aged spleens (*Figure 3H*).

To explore how limited dietary iron content during aging affects the formation of splenic iron-rich deposits, we conducted TMT-based proteomic quantification of their composition. Out of 942 detected protein groups, 50 hits were significantly more abundant in magnetically-isolated aggregates from the aged mice compared to mice fed an IR diet (*Figure 3—figure supplement 2A*). Functional enrichment analysis identified components of lysosomes as by far the most overrepresented hits (*Figure 3—figure supplement 2A* and B), suggesting that alleviation of the lysosomal defects likely contributes to less pronounced aggregates formation in iron-reduced mice. The hits included also both H and L ferritin as being significantly increased in aggregates from aged mice on a standard diet. Of note, we failed to detect ferritin in the aggregates using antibody staining and flow cytometry, thus suggesting that cytoplasmic ferritin deficiency (*Figure 1G*) may result from ferritin aggregation.

Taken together, our data suggest that the splenic heme- and iron-rich deposits are formed of a broad spectrum of aggregation-prone protein debris that most likely originates from RPMs that have been damaged by proteotoxic stress.

RPM dysfunction occurs early in aging and involves ferroportin downregulation

To explore early events that underlie RPM impairments during aging, we monitored in a time-wise manner how the formation of iron-rich aggregates corresponds to the functions of RPMs. We found that RPMs started to show increased LIP levels, and reduced their EP and lysosomal degradation capacity early during age progression (*Figure 4A–C*). Likewise, at 5 months of age, we observed that a larger proportion of splenic RBCs exhibited the senescence marker - increased ROS levels (*Figure 4D*). Interestingly, these changes reflected the accumulation of non-heme iron in the spleen and the appearance of splenic protein aggregates (*Figure 4E and F*). Since these deposits are insoluble, we assumed that their formation limits the bioavailability of iron for further systemic utilization. In support of this possibility, we noticed that the drop in transferrin saturation during aging coincided with RPM failure and the appearance of splenic aggregates (*Figure 4G*). To address the primary events that underlie RPM impairments we investigated mice very early during aging. We observed that ferroportin dropped significantly already in mice aged 4 months, which at least partially was

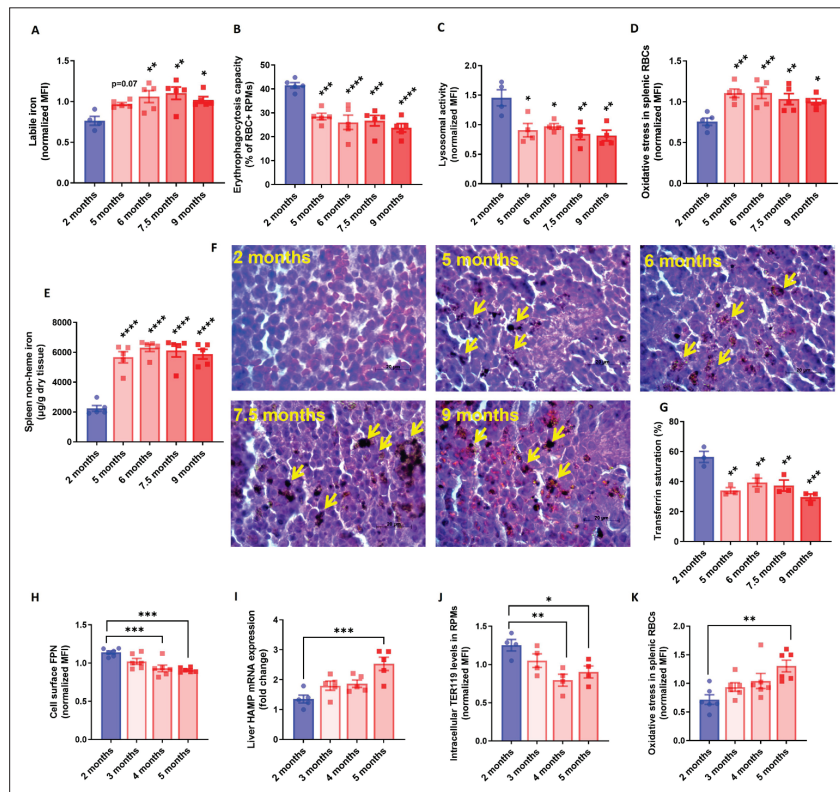


Figure 4. RPM dysfunction develops early in aging and is associated with ferroportin downregulation. (A) Cytosolic ferrous iron (Fe²⁺) content in RPMs derived from mice at the indicated age was measured using FerroOrange with flow cytometry. (B) Erythrophagocytosis capacity of RPMs derived from mice at the indicated age was determined using flow cytometry by measuring the percentage of RPMs that phagocytosed transfused PKH67-labeled temperature-stressed RBCs. (C) Lysosomal activity in RPMs derived from mice at the indicated age was determined using Lysosomal Intracellular Activity Assay Kit by flow cytometry. (D) The cytosolic ROS levels in RBCs derived from the spleens of mice at the indicated age were estimated by determining CellROX Deep Red fluorescence intensity with flow cytometry. (E) Splenic non-heme iron content was determined in mice at the indicated age. (F) Hematoxylin and eosin staining of the splenic red pulp in young, aged, and aged IR mice. Arrows indicate extracellular dark-colored aggregates. (G) Plasma transferrin saturation was determined in mice at the indicated age. (H) Expression of ferroportin (FPN) on the cell membrane of RPMs derived from mice at the indicated age was assessed by flow cytometry. (I) Relative mRNA expression of hepcidin (Hamp) in the liver from mice at the indicated age was determined by qPCR. (J) Erythrophagocytosis capacity of RPMs derived from mice at the indicated age was determined by intracellular staining of the erythrocytic marker TER119 in RPMs and flow cytometry. (K) The cytosolic ROS levels in RBCs derived from the spleens of mice at the indicated age were estimated by determining CellROX Deep Red fluorescence intensity with flow cytometry. Each dot represents one mouse. Data are represented as mean ± SEM. Statistical significance versus young controls (2 months) was determined by One-Way ANOVA test with Dunnett's Multiple Comparison test. *p<0.05, **p<0.01, ***p<0.001 and ****p<0.0001.

The online version of this article includes the following source data for figure 4:

Source data 1. Related to **Figure 4A–E and G–K.**

coupled with increased hepatic hepcidin expression (Figure 4H, I). At the same time point, the cells started to exhibit decreased EP activity [here determined by intracellular staining of the erythrocytic marker TER119 in RPMs Akilesh et al., 2019; Figure 4J], and only afterward, at the age of 5 months, we detected significant retention of senescent, ROS-rich RBCs in the spleen (Figure 4K). In sum, our

data show that iron-triggered dysfunction of RPMs is initiated early during aging, likely due to ferroportin downregulation.

Aging triggers RPM loss via mechanisms that resemble ferroptosis and involve proteotoxicity

Increased iron burden in RPMs was shown previously to drive ferroptotic cell death upon acute transfusion of damaged RBCs (Youssef et al., 2018). Since RPM representation was decreased in aged spleens (Figure 1K) and the TEM imaging revealed damaged iron-loaded RPMs (Figure 3A), we speculated that RPMs may undergo spontaneous ferroptosis during aging. In agreement with this hypothesis, both labile iron (Figure 4A), a factor that promotes ferroptosis, and lipid peroxidation (Figure 5A), a ferroptosis marker (Dixon et al., 2012; Friedmann Angeli et al., 2014) increased in RPMs during aging. Importantly, we observed that feeding mice an IR diet during aging diminished lipid peroxidation to the levels characteristic of young mice (Figure 5B), similar to what we observed for the labile iron build-up (Figure 1H). In line with these findings, we observed that injection of iron dextran in young mice led to robust lipid peroxidation in RPMs (Figure 5C) and their mild depletion ($p=0.056$; Figure 5D) at 8 hr post-injection, before the formation of splenic protein aggregates occurred (Figure 3H).

Earlier studies reported that ferroptotic cells are characterized by reduced mitochondria size and diminished mitochondrial membrane potential but not mitochondrial oxidative stress (Chen et al., 2021; Dixon et al., 2012; Friedmann Angeli et al., 2014; Neitemeier et al., 2017). Consistent with these data, we failed to detect augmented ROS levels in the mitochondria of aged RPMs (Figure 5—figure supplement 1A). Instead, we observed that mitochondria mass (Figure 5E), as well as mitochondrial activity (Figure 5F), decreased in RPMs of aged mice, and both these phenotypes were alleviated by an IR diet. This corresponded to higher ATP levels in FACS-sorted RPMs derived from aged mice fed an IR diet versus a standard diet (Figure 5—figure supplement 1B). Previous ultrastructural studies showed that mitochondria of ferroptotic cells are hallmarked by reduced size and fewer cristae, increased membrane density, and some appear swollen (Chen et al., 2021; Dixon et al., 2012; Friedmann Angeli et al., 2014). Consistently, our TEM imaging showed that in contrast to the RPMs of young mice, those from aged animals exhibited the above mitochondrial defects with some appearing disintegrated (Figure 5G). Mitochondria from mice fed an IR diet were small and dense, but they displayed a lesser degree of swelling and damage.

Since aged RPMs are characterized by proteotoxic stress and iron retention, we investigated how these two factors contribute to their viability. To this end, we employed a cellular model of RPMs [which we termed induced (i)-RPMs] that were generated by exposing bone marrow-derived macrophages to hemin and IL-33, two factors that drive RPM differentiation (Haldar et al., 2014; Lu et al., 2020) and induce RPM-like transcriptional signatures (Lu et al., 2020). We observed that iron loading (with ferric ammonium citrate [FAC]) and blockage of ferroportin by synthetic mini-hepcidin (PR73) (Stefanova et al., 2018) caused protein aggregation in iRPMs and led to their decreased viability but only in cells that were exposed to heat shock, a well-established trigger of proteotoxicity (Figure 5H, I). Interestingly, we observed that although FAC treatment increased lipid peroxidation to a similar extent in intact cells and those exposed to heat shock (Figure 5J), cell viability was only reduced when the iron loading and proteotoxic challenge were combined (Figure 5K). Even more strikingly, the latter synergistic cytotoxic effect was prevented by the ferroptosis blocker Liproxstatin-1 (Friedmann Angeli et al., 2014; Figure 5K). Finally, consistent with the observation that apoptosis markers can be elevated in tissues upon ferroptosis induction (Friedmann Angeli et al., 2014) and proteotoxicity may lead to apoptosis (Brancolini and Iuliano, 2020), we detected DNA fragmentation (via TUNEL assay) in the spleens of aged mice, a phenotype that was less pronounced in mice on an IR diet (Figure 5—figure supplement 2). Taken together, our data suggest that RPM demise during aging is driven by iron-dependent cell death with ferroptosis characteristics coupled with proteostasis collapse.

Iron loading but not oxidative stress undermines the phagocytic activity of aged RPMs in concert with impaired heme metabolism and ER stress

The contribution of iron deposition to age-related deterioration of cellular functions is believed to be primarily mediated by the pro-oxidative properties of labile iron (Xu et al., 2008). We observed

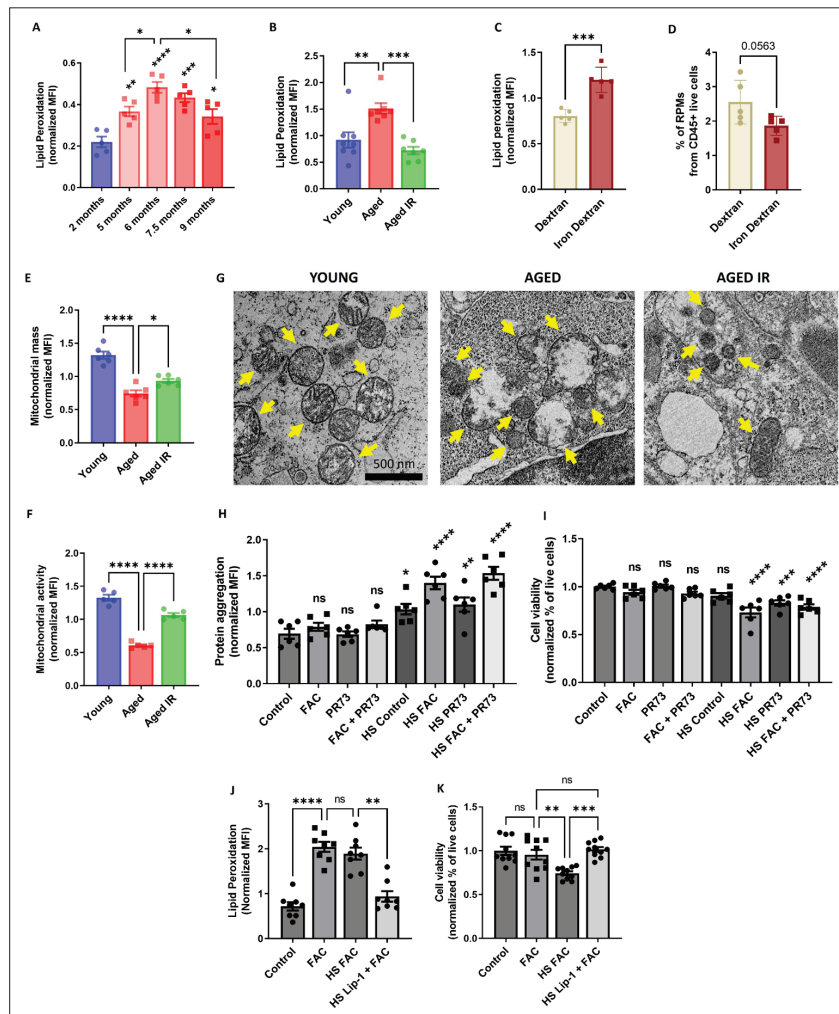


Figure 5. Aging triggers RPM loss via mechanisms that resemble ferroptosis and involve proteotoxicity. **(A)** Lipid peroxidation was determined in RPMs derived from mice at the indicated age using the Lipid Peroxidation Assay Kit with flow cytometry. **(B)** Lipid peroxidation was determined in RPMs derived from young, aged, and aged IR mice using the Lipid Peroxidation Assay Kit with flow cytometry. **(C)** Lipid peroxidation was determined in RPMs derived from dextran- and iron-dextran-injected mice (8 hr post-injection) using the Lipid Peroxidation Assay Kit with flow cytometry. **(D)** The percentage of RPMs from CD45+ live cells present in the spleen of dextran- and iron dextran-injected mice (8 hr post-injection) was assessed by flow cytometry. **(E)** Mitochondrial mass and **(F)** mitochondrial activity were determined in RPMs derived from young, aged, and aged IR mice using MitoTracker Green and TMRE probes, respectively, with flow cytometry. **(G)** Ultrastructural analyses of mitochondrial morphology in spleen red pulp sections obtained from young, aged, and aged IR mice. Yellow arrows indicate mitochondria. **(H)** Protein aggregation and **(I)** cell viability in cultured iRPMs were determined using PROTEOSTAT Aggresome detection kit and a fluorescent Aqua Live/Dead probe, respectively, with flow cytometry. Cells were treated with FAC (150 μ M, 24 hr), PR73 mini-hepcidin (2 μ g/mL, 24 hr), or exposed to heat shock (HS) stress (42 $^{\circ}$ C, 4 hr) as indicated. **(J)** Lipid peroxidation and **(K)** cell viability of cultured iRPMs were determined using the Lipid Peroxidation Assay Kit and fluorescent Aqua Live/Dead probe, respectively, with flow cytometry. Cells were treated with FAC (150 μ M, 24 hr), Liproxstatin-1 (Lip-1; 2 μ M, 25 hr) or exposed to heat shock (HS) stress (42 $^{\circ}$ C, 4 hr) as indicated. Each dot represents one mouse or independent cell-based experiment. Data are represented as mean \pm SEM. Welch's unpaired t-test determined statistical significance between the two groups; statistical significance

Figure 5 continued on next page

Figure 5 continued

among the three or more groups was determined by One-Way ANOVA test with Dunnett's or Tukey's Multiple Comparison test. * $p < 0.05$, ** $p < 0.01$, *** $p < 0.001$ and **** $p < 0.0001$.

The online version of this article includes the following source data and figure supplement(s) for figure 5:

Source data 1. Related to **Figure 5A–F and H–K**.

Figure supplement 1. Mitochondrial oxidative stress and ATP levels in young, aged and aged IR RPMs.

Figure supplement 1—source data 1. Related to **Figure 5—figure supplement 1A–B**.

Figure supplement 2. Apoptotic cell death was detected using In Situ Cell Death Detection Kit in spleen sections of young, aged and aged IR mice spleens.

a clear indication of oxidative stress in aging RPMs (**Figure 1J**) that was rescued by an IR diet. Next, we aimed to verify whether the increased ROS levels solely contribute to RPM decline during aging. To this end, we supplemented aging mice with the antioxidant N-Acetyl-L-cysteine (NAC), which was previously shown to revert aging-related physiological changes (**Berman et al., 2011; Ma et al., 2016**). With this strategy, we successfully reduced oxidative stress in aged RPMs (**Figure 6—figure supplement 1A**). However, we did not observe an improvement in the EP capacity of RPMs isolated from NAC-supplemented mice compared to untreated aged mice (**Figure 6—figure supplement 1B**). Consistently, the retention of senescent RBCs in the spleen (**Figure 6—figure supplement 1C**) and their local hemolysis (**Figure 6—figure supplement 1D**) were not rescued by the NAC administration. Likewise, enhanced RPM lipid peroxidation (**Figure 6—figure supplement 1E**), a ferroptosis marker, the formation of insoluble aggregates (**Figure 6—figure supplement 1F**), and splenic iron overload (**Figure 6—figure supplement 1G**) were equally present in aged mice regardless of the NAC treatment. These data suggest that RPM dysfunction and damage during aging are chiefly driven by RPM iron loading rather than excessive ROS.

Next, we investigated in more detail the causative role of iron loading in suppressing EP. We confirmed that iRPMs significantly decreased the ability for RBC uptake upon iron overload with FAC in a manner that was partially rescued by the iron chelator desferrioxamine (DFO; **Figure 6A and B**). In addition, we observed that iron loading by FAC suppressed lysosomal activity, an important factor for RBC degradation (**Figure 6C**). We also found that mitochondria membrane potential was similarly diminished by FAC and DFO alone, thus uncoupling the phagocytic and lysosomal activity of iRPMs from their mitochondria fitness (**Figure 6D**). Mechanistically, we found that iron loading reduced protein expression levels of the receptors that recognize phosphatidyserine on apoptotic cells MERTK, AXL, and TIM4, and which are highly expressed by RPMs (**Slusarczyk and Mleczko-Sanecka, 2021**), likely contributing to EP (**Figure 6E–G**). Of note, expression levels of another phosphatidyserine receptor STAB2 or the Fc receptor CD16 that as well are present in RPMs (**Slusarczyk and Mleczko-Sanecka, 2021**) were unchanged upon iron/DFO treatment of iRPMs (**Figure 6—figure supplement 2**). Consistent with the important role of calcium signaling in the regulation of EP (**Ma et al., 2021**), we observed that iron accumulation reduced calcium levels in iRPMs (**Figure 6H**). Importantly, the effects of iron excess on the levels of the apoptotic cell receptors and calcium were rescued by DFO.

Interestingly, our RNA-seq data revealed that one of the transcripts that significantly decrease in aged RPMs is *Hmox1* (**Figure 3—figure supplement 1A**), which encodes HO-1. We validated this result using intracellular staining and flow cytometry, and uncovered a marked decrease in HO-1 protein level in RPMs during aging (**Figure 6I and J**; see **Figure 6—figure supplement 3** for antibody validation). Correspondingly, the blockage of HO-1 in iRPMs with zinc protoporphyrin (ZnPP) suppressed the EP intensity (**Figure 6K**) and, to a lesser extent, the capacity for lysosomal degradation (**Figure 6—figure supplement 4A**). Next, we explored why ZnPP, but not hemin alone (**Figure 6—figure supplement 4B**), suppressed EP. We speculated that possibly another co-product of HO-1 enzymatic activity (CO or/and biliverdin), which we expect to be high in hemin-exposed iRPMs, counterbalances the suppressive effect of iron release after EP. Interestingly, we found that the CO donor CORM-A1, but not biliverdin, rescued EP capacity under ZnPP exposure in iRPMs (**Figure 6—figure**

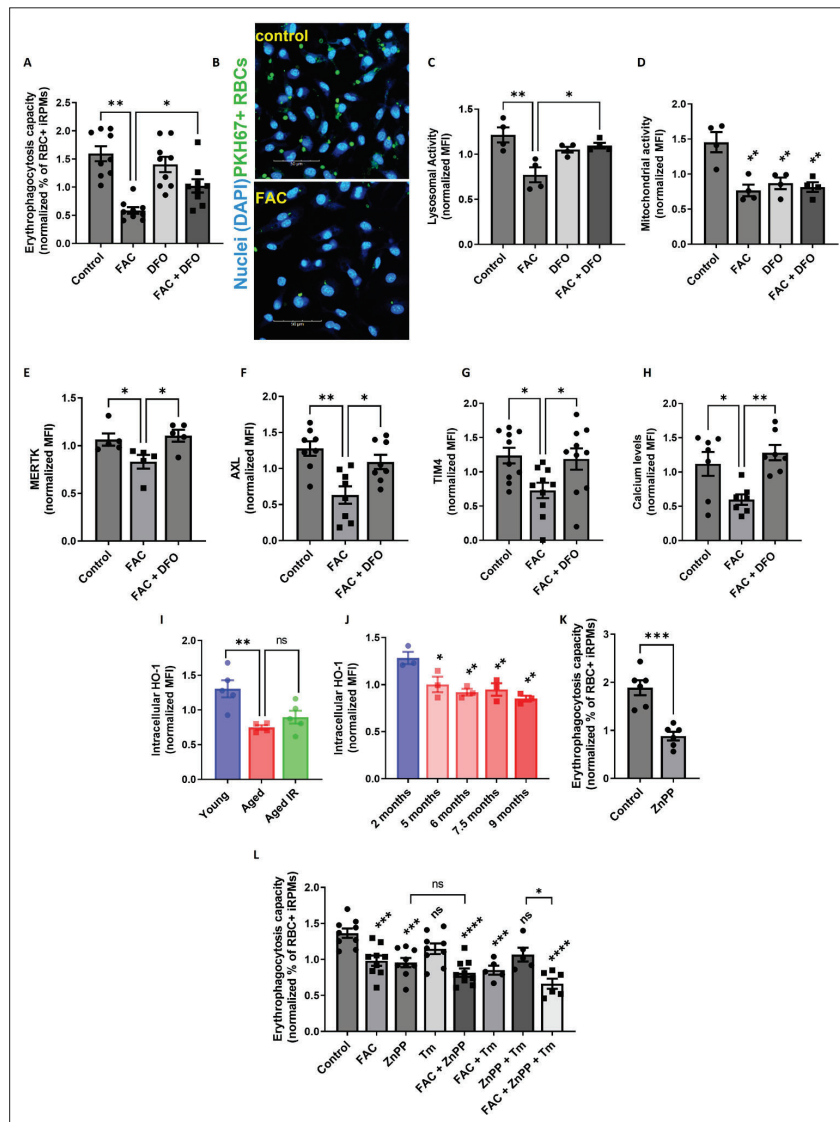


Figure 6. Iron loading undermines the phagocytic activity of iRPMs in concert with impaired heme metabolism and ER stress. **(A)** Normalized erythrophagocytosis capacity of PKH67-labeled temperature-stressed RBCs by cultured iRPMs. Cells were treated with FAC (50 μ M, 24 hr) and DFO (100 μ M, 18 hr) as indicated. **(B)** Representative confocal microscopy images of erythrophagocytosis in FAC-treated iRPMs compared with control cells. **(C)** Lysosomal and **(D)** mitochondrial activity of cultured iRPMs were determined using Lysosomal Intracellular Activity Assay Kit and TMRE probe, respectively, with flow cytometry. Cells were treated with FAC (50 μ M, 24 hr) and DFO (100 μ M, 18 hr) as indicated. **(E)** Cell membrane expression levels of MERTK, **(F)** AXL and **(G)** TIM4 of cultured iRPMs were determined by using fluorescently labeled antibodies and flow cytometry. Cells were treated with FAC (50 μ M, 24 hr) and DFO (100 μ M, 18 hr) as indicated. **(H)** Cytosolic calcium levels of cultured iRPMs were determined using Cal-520 fluorescent probe with flow cytometry. Cells were treated with FAC (50 μ M, 24 hr) and DFO (100 μ M, 18 hr) as indicated. **(I)** Intracellular HO-1 protein levels in RPMs isolated from young, aged, and aged IR mice were measured by flow cytometry. **(J)** Intracellular HO-1 protein levels in RPMs isolated from mice at the indicated age were measured by flow cytometry. **(K)** Normalized erythrophagocytosis capacity of PKH67-labeled temperature-stressed RBCs by cultured iRPMs. Cells were treated with ZnPP (0.5 μ M, 24 hr). **(L)** Normalized

Figure 6 continued on next page

Figure 6 continued

erythrophagocytosis capacity of PKH67-labeled temperature-stressed RBCs by cultured iRPMs. Cells were treated with indicated concentrations of ZnPP (0.5 μ M) and FAC (10 μ M) and with ER stress inducer Tunicamycin (Tm; 2.5 μ M) for 24 hr. Each dot represents one mouse or independent cell-based experiment. Data are represented as mean \pm SEM. Statistical significance among the three or more groups was determined by One-Way ANOVA test with Dunnett's or Tukey's Multiple Comparison test. * p <0.05, ** p <0.01, *** p <0.001 and **** p <0.0001.

The online version of this article includes the following source data and figure supplement(s) for figure 6:

Source data 1. Related to **Figure 6A and C–L**.

Figure supplement 1. Iron loading, but not oxidative stress leads to RPM decline during aging.

Figure supplement 1—source data 1. Related to **Figure 6—figure supplement 1A–E and G**.

Figure supplement 2. The Fc receptor CD16 and the apoptotic cell receptor STAB2 are not regulated by iron-loading.

Figure supplement 2—source data 1. Related to **Figure 6—figure supplement 2A–B**.

Figure supplement 3. Validation of the antibody against HO-1 in flow cytometry.

Figure supplement 3—source data 1. Related to **Figure 6—figure supplement 3**.

Figure supplement 4. The effects of HO-1 inhibition on lysosomal activity and HO-1 co-products on the erythrophagocytosis capacity of iRPMs.

Figure supplement 4—source data 1. Related to **Figure 6—figure supplement 4A–D**.

supplement 4C and D), suggesting that CO acts as a modulator of EP activity in RPMs. Whether deficient CO levels in RPMs *in vivo* contribute to EP suppression would require further investigation. However, in support of this possibility, our RNA-seq data implied that enzymes involved in the pentose phosphate pathway, such as *Tkt*, a transcriptional target of CO-mediated regulation (Bories *et al.*, 2020), are downregulated in aged RPMs (**Figure 3—figure supplement 1A**).

RPMs derived from aging mice show similar HO-1 levels (**Figure 6I**) and the degree of ER stress (**Figure 3—figure supplement 1B**) irrespective of diet and differ primarily in iron status (**Figure 1H, I**). Therefore, we next tested how the combination of ZnPP and the ER stress inducer tunicamycin with a mild FAC exposure (10 μ M) affects EP. Although ER stress alone did not significantly affect EP, we uncovered that FAC treatment elicited an additive effect with combined exposure to ZnPP and tunicamycin, but not with ZnPP alone (**Figure 6L**). Taken together, our data imply that iron content in RPMs represents the key factor that determines their RBC clearance potential, and its excess may exacerbate the suppressive impact of HO-1 loss and ER stress on erythrophagocytosis.

Discussion

RPMs play an essential role in preventing the release of hemoglobin from RBCs and ensuring the turnover of the body an iron pool. To date, impairments of iron recycling were reported in genetically modified mice, hallmarked by the loss of RPMs due to the absence of genes that control their differentiation (Kohyama *et al.*, 2009; Okreglicka *et al.*, 2021). Here, for the first time, we provide evidence that the RPM damage and defective capacity for RBC clearance accompany physiological aging (**Figure 7**).

The present study provides new evidence for the origin and nature of iron deposits in the aging spleen. Recent findings show that aging promotes a global decrease in protein solubility (Sui *et al.*, 2022). The longevity of embryonically-derived RPMs, reaching at least 32 weeks in mice (Hashimoto *et al.*, 2013; Liu *et al.*, 2019), puts pressure on these cells to handle the constant flux of iron, a factor that increases protein insolubility (Klang *et al.*, 2014). This may render RPMs particularly sensitive to the build-up of protein aggregates. Consistently, we found a clear transcriptional signature for unfolded protein response and ER stress in aged RPMs, which may be linked to the constitutive phagocytic activity of this macrophage population (Kim *et al.*, 2018). We propose that unrestricted iron availability from the diet further ameliorates RPM fitness during aging, chiefly via early ferroportin downregulation and intracellular iron accumulation. The latter further decreases protein solubility and

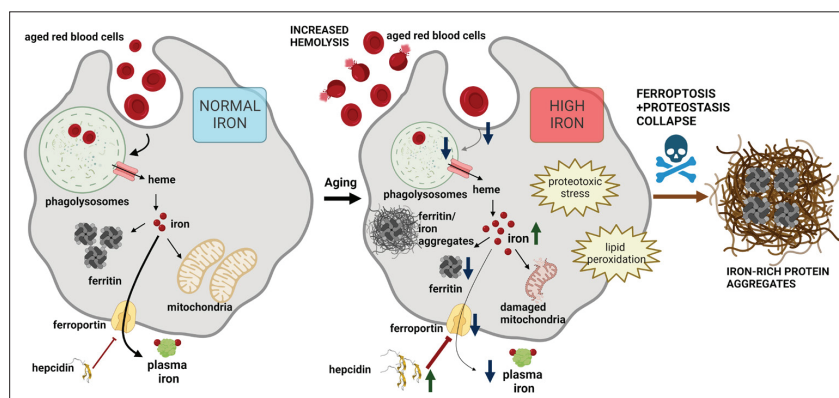


Figure 7. Model of RPM dysfunction and collapse during aging. Iron-dependent functional defects of RPMs are initiated early during aging. Intracellular iron loading of RPMs, in concert with proteostasis defects, precedes the deposition of iron in a form of extracellular protein-rich aggregates, likely emerging from damaged RPMs. The build-up of un-degradable iron-rich deposits, in concert with increased hepcidin levels, and reduced erythrophagocytic and lysosomal activity of the remaining RPMs limit plasma iron availability during aging. A drop in RBC clearance capacity leads to enhanced splenic hemolysis.

inhibits lysosomal activity which is critical for autophagy-mediated protein quality control (*Kaushik and Cuervo, 2015*). Critically, an increase in labile iron ultimately leads to the appearance of toxic lipid peroxides, the oxidation products that drive ferroptosis (*Dixon et al., 2012*). Our results show that only the combination of proteotoxic stress, likely associated *in vivo* with specialized iron-recycling functions of RPMs, with iron loading or ferroportin blockage, is cytotoxic to the cellular model of RPMs. The fact that Liproxstatin-1, a ferroptosis inhibitor (*Friedmann Angeli et al., 2014*), rescues cell viability in this context implies the involvement of ferroptosis, but how mechanistically proteome instability and iron-triggered toxicity synergize remains an open question.

Thus far ferroptotic cell death was mainly described in genetic models, for example with disturbed detoxification of lipid peroxides due to conditional loss of *Gpx4* (*Friedmann Angeli et al., 2014; Matsushita et al., 2015*) or in various pathologies (*Park et al., 2019; Wang et al., 2019; Yan et al., 2021*). Here, we propose that ferroptosis may critically contribute to RPM loss during physiological aging. Notably, the excessive clearance of damaged RBCs in mouse models of blood transfusion, hemolytic anemia, or the anemia of inflammation induced by heat-killed *Brucella abortus* was previously shown to cause transient or sustained RPMs depletion (*Haldar et al., 2014; Theurl et al., 2016; Youssef et al., 2018*). Although the splenic niche may be replenished to some extent via splenic monocyte recruitment and/or resident RPMs proliferation (*Haldar et al., 2014; Youssef et al., 2018*), our data imply that the damage of embryonically derived RPM in these models may lead to the irreversible formation of insoluble iron-rich splenic protein aggregates. Premature clearance of defective RBCs also hallmarks β -thalassemia (*Slusarczyk and Mleczko-Sanecka, 2021*). To the best of our knowledge, RPM loss was not extensively studied in a mouse model of thalassemia. However, interestingly, thalassemic mice display enhanced splenic Perls'-stained deposits that appear to be extracellular and are not amenable to iron chelation therapy (*Sanyal et al., 2020; Vadolas et al., 2021*), possibly resembling those identified by the present study. Of note, genetic disruption of *Hrg1* leads to the formation of heme aggregate hemozoin inside enlarged phagolysosomes (*Pek et al., 2019*). The large size, extracellular localization, and high content of proteins distinguish age-triggered splenic aggregates from hemozoin. However, we cannot exclude the possibility that this polymer-like structure may expand during aging and contribute to the formation of splenic iron deposits.

Our study identified three new factors that affect the intensity of EP, the iron content, the activity of HO-1, and, to less extent, ER stress. Among them, iron accumulation in RPMs, independently of ROS generation, emerged as a major driver of EP suppression during aging, likely via the downregulation of apoptotic cell receptors (Slusarczyk and Mleczko-Sanecka, 2021) and calcium signaling (Ma et al., 2021). The underlying mechanisms for excessive iron deposition in aged RPMs most likely include reduced FPN protein levels and may be further aggravated by the sequestration of ferritin in protein aggregates via the mechanisms that remain to be explored in detail. It is also plausible that, like neurons, aged RPMs show low capacity for heme synthesis (Atamna et al., 2002), which may lead to defective iron utilization in the mitochondria and increased cytoplasmic iron burden. Mitochondrial damage that we identified in aged RPMs may support this possibility. We also demonstrated that iron loading decreases the capacity of RPMs for phagolysosomal RBC degradation. Of note, patients who suffer from lysosomal storage disorder, Gaucher disease, show iron deposits in the splenic macrophages (Clarke et al., 2021; Lefebvre et al., 2018). Iron sequestration in Gaucher macrophages was attributed to the hepcidin-mediated downregulation of ferroportin, or more recently to increased erythrophagocytosis of Gaucher RBCs (Dupuis et al., 2022). Based on our study, it is plausible that defects in proteostasis, due to defective lysosomal-mediated protein quality control, may contribute to aberrant iron management in Gaucher macrophages.

HO-1 is well characterized for its cytoprotective, anti-oxidative, and anti-inflammatory functions, (Gozzelino et al., 2010), and its activity was proposed to prevent cellular senescence (Even et al., 2018; Hedblom et al., 2019; Luo et al., 2018; Suliman et al., 2017). Since RPMs are key cells where HO-1 exerts its enzymatic function (Vijayan et al., 2018), our observation that HO-1 levels decrease in these cells during aging is of high physiological significance. Although aged RPMs show some hallmarks of senescence linked to HO-1 deficiency, such as defective mitochondria or excessive ROS, they do not exhibit proinflammatory gene expression signatures. The suppression of EP by inhibition of HO-1 activity may be mediated by heme overload, as shown previously for general phagocytosis (Martins et al., 2016). However, we provide evidence that another product of HO-1, CO, restores the EP capacity of cells subjected to HO-1 blockage, thus emerging as an inducer of RBC uptake. These findings are in agreement with the previous work, reporting that CO administration protects *Hmox1* knock-out mice from sepsis-induced lethality via stimulation of bacterial phagocytosis (Chung et al., 2008).

Collectively, our study implies that intracellular iron loading of RPMs impairs their EP capacity and synergistically with proteostasis defects leads to their demise. These impairments result in local RBC dyshomeostasis in the spleen, due to the shift from phagocytosis to splenic RBC lysis (Klei et al., 2020), and the formation of extracellular proteinaceous aggregates, rich in iron and heme, emerging from damaged RPMs (Figure 7). We propose that the build-up of un-degradable iron-rich particles, in concert with increased hepcidin levels, and limited iron-recycling activity of the remaining RPMs limit plasma iron availability during aging. Future studies may address whether the consequences of RPM dysfunction for the splenic microenvironment, together with their anti-inflammatory transcriptional profile, contribute to the immunosenescence that accompanies aging (Nikolich-Zugich, 2018). Interestingly, microglia iron overload and ferroptosis were recently identified as critical drivers of neurodegenerative diseases (Kenkhuis et al., 2021; Ryan et al., 2023). In such context, our findings suggest that in addition to various iron chelation approaches (Liu et al., 2018), long-term reduction of dietary iron intake may represent an alternative for neurodegeneration prevention. Finally, our study has some limitations. We characterized in detail RPM dysfunction in female mice on a relatively low-iron C57BL/6 J background. Although we have observed similar phenotypes in Balb/c females, we failed to observe the formation of splenic iron-rich protein aggregates in C57BL/6 J males (data not shown). Having established that the degree of RPM collapse depends on dietary iron and internal hepcidin-ferroportin regulatory circuitry, it remains to be investigated how it is manifested in male mice on iron-rich genetic backgrounds or humans. Lastly, since standard mouse diets contain more-than-sufficient amounts of iron, our study could be also interpreted as the effect of long-term exposure to excessive iron on RPM functions.

Materials and methods

Key resources table

Reagent type (species) or resource	Designation	Source or reference	Identifiers	Additional information
Antibody	Anti-mouse CD45 APC/Cyanine7 (Rat monoclonal)	BioLegend	cat.# 103115	1:200
Antibody	Anti-mouse/human CD45R/B220 Pacific Blue (Rat monoclonal)	BioLegend	cat.# 103230	1:200
Antibody	Anti-mouse F4/80 APC (Rat monoclonal)	BioLegend	cat.# 123115	1:100
Antibody	Anti-mouse F4/80 FITC (Rat monoclonal)	BioLegend	cat.# 123107	1:100
Antibody	Anti-mouse/human CD11b PE/Cyanine7 (Rat monoclonal)	BioLegend	cat.# 101215	1:200
Antibody	Anti-mouse Trem14 PE (Rat monoclonal)	BioLegend	cat.# 143303	1:100
Antibody	Anti-mouse TER-119 Pacifin Blue (Rat monoclonal)	BioLegend	cat.# 116231	1:300
Antibody	Anti-mouse TER-119 FITC (Rat monoclonal)	BioLegend	cat.# 116205	1:300
Antibody	Anti-mouse CD71 APC (Rat monoclonal)	BioLegend	cat.# 113819	1:100
Antibody	Anti-mouse CD71 PE (Rat monoclonal)	BioLegend	cat.# 113807	1:100
Antibody	Anti-mouse TER-119 PE (Rat monoclonal)	BioLegend	cat.# 116207	1:300
Antibody	Anti-mouse CD45 PE/Cyanine7 (Rat monoclonal)	BioLegend	cat.# 147703	1:200
Antibody	Anti-mouse FPN (Rat monoclonal)	Amgen	DOI: 10.1172/JCI127341	1:100
Antibody	Anti-mouse Gr-1 Pacific Blue (Rat monoclonal)	BioLegend	cat.# 108429	1:200
Antibody	Anti-mouse MHCII Pacific Blue (Rat monoclonal)	BioLegend	cat.# 107619	1:200
Antibody	Anti-human/mouse Ferritin Heavy Chain (FTH1) (Rabbit polyclonal)	Cell Signaling Technology	cat.# 3998	1:100
Antibody	Anti-mouse AXL APC (Rat monoclonal)	Invitrogen	cat.# 17-1084-82	1:100
Antibody	Anti-mouse MERTK FITC (Rat monoclonal)	BioLegend	cat.# 151503	1:100
Antibody	Anti-mouse Tim-4 Alexa Fluor 647 (Rat monoclonal)	BioLegend	cat.# 130007	1:100
Antibody	Anti-mouse Stab2 Alexa Fluor 488 (Rabbit polyclonal)	G-Biosciences	cat.# ITN2255	1:100
Antibody	Anti-mouse/human Ferritin Light Chain (FTL) (Rabbit polyclonal)	Abcam	cat.# ab69090	1:100
Antibody	Anti-mouse HO-1 (Rabbit polyclonal)	Enzo Life Sciences	cat.# ADI-OSA-150	1:400

Continued on next page

Continued

Reagent type (species) or resource	Designation	Source or reference	Identifiers	Additional information
Antibody	Anti-mouse Ki-67 Alexa Fluor 488 (Rat monoclonal)	BioLegend	cat.# 652417	1:100
Antibody	Anti-Rabbit IgG (H+L) Alexa Fluor 488 (Donkey polyclonal)	Thermo Fisher Scientific	cat.# A-21206	1:200
Antibody	Anti-Rabbit IgG (H+L) Alexa Fluor 647 (Donkey polyclonal)	ThermoFisher Scientific	cat.# A-31573	1:200
Antibody	Anti-mouse CD116/32 TruStain FcX (Rat monoclonal)	BioLegend	cat.# 101319	1:100
Antibody	Anti-mouse Gr-1 Biotin (Rat monoclonal)	BioLegend	cat.# 108403	1:100
Antibody	Anti-mouse/human CD45R/B220 (Rat monoclonal)	BioLegend	cat.# 103204	1:100
Antibody	Anti-mouse CD3 (Rat monoclonal)	BioLegend	cat.# 100243	1:100
Antibody	Anti-mouse Ly-6C (Rat monoclonal)	BioLegend	cat.# 128003	1:100
Chemical compound, drug	N-Acetyl-L-cysteine (NAC)	Sigma-Aldrich	cat.# A7250	2 g/L in drinking water
Chemical compound, drug	Iron-Dextran Solution	Sigma-Aldrich	cat.# D8517	8 mg
Chemical compound, drug	Hemin	Sigma-Aldrich	cat.# 51280	20 μ M
Chemical compound, drug	Ferric Ammonium Citrate (FAC)	Sigma-Aldrich	cat.# F5879	150, 50 and 10 μ M
chemical compound, drug	CORM-A1	Sigma-Aldrich	cat.# SML0315	50 μ M
Chemical compound, drug	Deferoxamine (DFO)	Sigma-Aldrich	cat.# D9533	100 μ M
Chemical compound, drug	Zinc (II) Protoporphyrin IX (ZnPP)	Sigma-Aldrich	cat.# 691550	5, 1 and 0.5 μ M
Chemical compound, drug	Tunicamycin (Tm)	Sigma-Aldrich	cat.# T7765	2.5 μ M
Chemical compound, drug	Lipoxstatin-1 (Lip-1)	Sigma-Aldrich	cat.# SML1414	2 μ M
Chemical compound, drug	EZ-Link Sulfo-NHS Biotin	Thermo Fisher Scientific	cat.# 21217	1 mg / 100 μ L
Commercial assay, kit	LIVE/DEAD Fixable Aqua	Invitrogen	cat.# L34966	
Commercial assay, kit	LIVE/DEAD Fixable Violet	Invitrogen	cat.# L34964	
Commercial assay, kit	CellROX Deep Red Reagent	Invitrogen	cat.# C10422	
Commercial assay, kit	Lipid Peroxidation Assay Kit	Abcam	cat.# ab243377	
Commercial assay, kit	MitoSOX Red	Invitrogen	cat.# M36008	
Commercial assay, kit	Lysosomal Intracellular Activity Assay Kit	Biovision	cat.# K448	

Continued on next page

Continued

Reagent type (species) or resource	Designation	Source or reference	Identifiers	Additional information
Commercial assay, kit	Me4BodipyFL-Ahx3Leu3VS (Fluorescent Proteasome Activity)	R&D Systems	cat.# I-190	
Commercial assay, kit	tetramethylrhodamine ethyl ester - TMRE (Fluorescent Probe)	Sigma-Aldrich	cat.# 87917	
Commercial assay, kit	MitoTracker Green	Invitrogen	cat.# M7514	
Commercial assay, kit	Cal-520 AM Probe	Abcam	cat.# ab171868	
Commercial assay, kit	FerroOrange	DojinD	cat.# F374	
Commercial assay, kit	PROTEOSTAT Aggresome Detection Kit	Enzo Life Sciences	cat.# ENZ-51035-0025	
Commercial assay, kit	ATP Fluorometric Assay Kit	Sigma-Aldrich	cat.# MAK190	
Commercial assay, kit	Iron Assay Kit	Sigma-Aldrich	cat.# MAK025	
Commercial assay, kit	PKH-67	Sigma-Aldrich	cat.# MIDI67-1KT	
Commercial assay, kit	Heme Assay Kit	Sigma-Aldrich	cat.# MAK316	
Commercial assay, kit	SFBC	Biolabo	cat.# 80008	
Commercial assay, kit	UIBC	Biolabo	cat.# 97408	
Commercial assay, kit	Mouse Erythropoietin/EPO Quantikine ELISA Kit	R&D Systems	cat.# MEP00B	
Commercial assay, kit	IL-6 Quantikine ELISA Kit	R&D Systems	cat.# M600B	
Commercial assay, kit	Mouse Hemopexin ELISA Kit	Abcam	cat.# ab157716	
Commercial assay, kit	Direct-zol RNA Microprep Kit	Zymo Research	cat.# R2062	
Commercial assay, kit	Alexa Fluor 488 Conjugation Kit (Fast) - Lightning-Link	Abcam	cat.# ab236553	
Commercial assay, kit	Alexa Fluor 647 Conjugation Kit (Fast) - Lightning-Link	Abcam	cat.# ab269823	
Commercial assay, kit	RevertAid H Minus Reverse Transcriptase	Thermo Fisher Scientific	cat.# EP0452	
Commercial assay, kit	SG qPCR Master Mix	EURx	cat.# E0401	
Commercial assay, kit	Iron Stain Kit	Sigma-Aldrich	cat.# HT20-1KT	
Commercial assay, kit	Iron Stain Kit	Abcam	cat.# ab150647	
Commercial assay, kit	In Situ Cell Death Detection Kit	Roche	cat.# 11684795910	

Continued on next page

Continued

Reagent type (species) or resource	Designation	Source or reference	Identifiers	Additional information
Other	Standard iron content diet for mice	SAFE	cat.# U8958v0177	Diet for young and aged mice
Other	Reduced iron content diet for mice	SAFE	cat.# U8958v0294	Diet for aged IR mice
Other	Collagenase D	Roche	cat.# 11088882001	Digestion of spleen for sorting
Other	Trizol-LS	Invitrogen	cat.# 10296010	RNA isolation reagent for RNA-seq
Other	Normal Rat Serum	Thermo Fisher Scientific	cat.# 10,710 C	Blocking reagent for flow cytometry
Other	MojoSort Streptavidin Nanobeads	BioLegend	cat.# 480016	Beads for magnetic sorting of RPMs and aggregates
Other	MojoSort Streptavidin Nanobeads	BioLegend	cat.# 480072	Beads for magnetic sorting of RPMs and aggregates
Other	EasyEights EasySep Magnet	STEMCELL	cat.# 18103	Magnet used for magnetic sorting of RPMs and aggregates
Other	LS Separation Column	Milyenyi Biotec	cat.# 130-042-401	Magnet used for magnetic sorting of aggregates
Other	CPDA-1	Sigma-Aldrich	cat.# C4431	Anticoagulant used for blood collection for transfusions
Other	Accutase	BioLegend	cat.# 423201	Reagent used for cells detachment <i>in vitro</i>
Other	Zymosan A BioParticles Alexa Fluor 488	Invitrogen	cat.# Z23373	Cargo for ex vivo phagocytosis
Other	TRIzol Reagent	Invitrogen	cat.# 15596018	RNA isolation reagent
Peptide, recombinant protein	IL-33	BioLegend	cat.# 580506	10 ng/mL
Peptide, recombinant protein	Mini-hepcidin (PR73)	Gift from Elizabeta Nemeth, UCLA, USA	https://doi.org/10.1128/IAI.00253-18	2 µg/mL
Peptide, recombinant protein	Macrophage Colony-Stimulating Factor (M-CSF)	BioLegend	cat.# 576406	20 ng/mL
Sequence-based reagent	HAMP Forward	This paper	Real-time PCR primers	5' ATACCAATGCAGAAGAGAAGG-3'
Sequence-based reagent	HAMP Reverse	This paper	Real-time PCR primers	5'-AACAGATACCACACTGGGAA-3'
Software, algorithm	FlowJo	FlowJo	v10.8.1	
Software, algorithm	CytExpert	Beckman Coulter	v2.4	
Software, algorithm	GraphPad Prism	GraphPad Software	v9	

Mice

Female C57BL/6 J mice were used for all the experiments and were maintained in specific pathogen-free (SPF) conditions at the Experimental Medicine Centre (Bialystok, Poland). Starting with the age of 4 weeks mice were fed a diet with a standard iron content (200 mg/kg, SAFE #U8958v0177; for Young and Aged) or reduced iron content (25 mg/kg; SAFE #U8958v0294; for Aged IR). The diets were from SAFE (Augy, France). Mice were analyzed at 8–10 weeks (Young) and 10–11 months (Aged and Aged IR) of age. For

supplementation with N-Acetyl-L-cysteine (NAC), aging mice (Aged NAC) were supplied with NAC dissolved in drinking water (2 g/L) from 8 weeks of age until 10–11 months of age. Mice were delivered to the local facility at the IIMCB and sacrificed after short acclimatization, or subjected to additional procedures, if applicable. C57BL/6 J for primary cell cultures were maintained in the SPF facility of Mossakowski Medical Research Institute (Warsaw, Poland). All animal experiments and procedures were approved by the local ethical committees in Olsztyn and Warsaw (decisions: WAW2/015/2019; WAW2/149/2019; WAW2/026/2020; WAW2/149/2020).

Iron dextran injections

Mice were injected into the peritoneum (IP injection) with 8 mg of iron dextran (Sigma-Aldrich, D8517) or an equivalent amount of dextran (Sigma-Aldrich, BCBZ5113). Animals were sacrificed for flow cytometric analysis of RPMs or isolation of cell-free iron-rich splenic aggregates (see details below) at the indicated time points. The procedure was approved by the local ethical committee in Warsaw (decision: WAW2/122/2019).

Preparation of single-cell suspension from mouse organs

Bone marrow cells were harvested by flushing the femur and tibia using a 25 G needle and sterile HBSS medium (Gibco, 14025092). Cells were centrifuged at 600 g for 10 min at 4°C. The **spleen** was excised and mashed through a 70 µm strainer (pluriSelect, 43-50070-51). For FACS and magnetic sorting, the spleen was additionally digested in HBSS medium containing 1 mg/ml Collagenase D (Roche, 11088882001) and 50 U/ml DNase I for 30 min at 37°C. After that cells were washed with cold HBSS and centrifuged at 600 g for 10 min at 4°C. The **liver** was extracted and perfused using Liver Perfusion Medium (Gibco, 17701038). Next, the organ was minced and digested in Liver Digest Medium (Gibco, 17703034) for 30 min at 37°C. After that liver was pressed through a 70 µm strainer in the presence of HBSS. Cells were centrifuged at 50 g for 3 min and the pellet was discarded (hepatocytes). The supernatant was centrifuged at 700 g for 15 min at 4°C. Pellet was resuspended in 5 mL of PBS containing 0,5% BSA and 5 mL of 50% Percoll (Cytiva, 17-0891-01) diluted in PBS. The suspension was centrifuged at 700 g for 30 min at 20°C. **Blood** was collected to a heparin-coated tube via heart puncture. Cells were washed with HBSS medium and centrifuged at 400 g for 10 min at 4°C. For **peritoneal cell** isolation, peritoneal cavities were washed with HBSS medium, and the peritoneal fluid was aspirated and filtered through 70 µm strainer, and cells were centrifuged at 600 g for 5 min at 4 °C.

RBCs present in a single-cell suspension were lysed using 1 X RBC Lysis buffer (BioLegend, 420302) for 3 min at 4°C. This step was omitted for analyses of erythroid progenitor cells and RBCs from the spleen or the bone marrow. Next, cells were washed with HBSS and centrifuged at 600 g for 10 min at 4°C. Pellet was prepared for further functional assays and labeling with antibodies.

Generation of iRPMs and treatments

Sterile harvested mononuclear cells obtained from mouse femurs and tibias were cultured at 37°C in 5% CO₂ at 0.5X10⁶/1 mL concentration in RPMI-1640 (Sigma-Aldrich, R2405) supplemented with 10% FBS (Cytiva, SV30160.03), 1 X Penicillin-Streptomycin (Gibco, 15140122), and 20 ng/mL macrophage colony-stimulating factor (M-CSF, BioLegend, 576406). On the 4th and 6th day medium was changed to fresh, supplemented with 20 µM of hemin (Sigma-Aldrich, 51280) and 10 ng/mL of IL-33 (BioLegend, 580506). Assays were performed on the 8th day.

For treatments, ferric ammonium citrate (FAC, Sigma-Aldrich, F5879), CORM-A1 (Sigma-Aldrich, SML0315), deferoxamine (DFO, Sigma-Aldrich, D9533), and mini-hepcidin (PR73, a kind gift from Elizabeth Nemeth, UCLA, USA) (*Stefanova et al., 2018*) were diluted in sterile ddH₂O. Zinc (II) Protoporphyrin IX (ZnPP, Sigma-Aldrich, 691550), tunicamycin (Tm, Sigma-Aldrich, T7765) and Liproxstatin-1 (Lip-1, Sigma-Aldrich, SML1414) were diluted in anhydrous DMSO. Hemin (Sigma-Aldrich, 51280) solution was prepared with 0.15 M NaCl containing 10% NH₄OH. All reagents after dilution were filtered through a 0.22 µm filter and stored at –20°C except ferric ammonium citrate, which was always freshly prepared. The concentration of compounds and duration of treatments are indicated in the descriptions of the figures.

Flow cytometric analysis and cell sorting

Cell suspensions of spleens and livers and iRPMs ($\sim 1 \times 10^7$) were stained with LIVE/DEAD Fixable Aqua/Violet (Invitrogen, L34966/L34964) as per the manufacturer's instructions to identify dead cells. After extensive washing, the cells were incubated with Fc block in a dilution of 1:100 in FACS buffer for 10 min at 4 °C. Cells were then stained with fluorophore-conjugated antibodies, dilution of 1:100 to 1:400, depending on the titration, in FACS buffer for 30 min at 4 °C. Cells were washed thoroughly with FACS buffer and subjected to flow cytometry analysis. For analysis of the *splenic RPM population*, the following surface antibodies were used: CD45 (BioLegend, 30-F11), CD45R/B220 (BioLegend, RA3-6B2), F4/80 (BioLegend, BM8), CD11b (BioLegend, M1/70) and TREML4 (BioLegend, 16E5). TER-119 (BioLegend) and CD71 (BioLegend, RI7217) were included for *erythroid cell* analysis. For analysis of *liver Kupffer cell and iRPM populations*, the following surface antibodies were used: CD45 (BioLegend, 30-F11), F4/80 (BioLegend, BM8) and CD11b (BioLegend, M1/70). *Detection of FPN* was performed with a non-commercial antibody that recognizes the extracellular loop of mouse FPN [rat monoclonal, Amgen, clone 1C7 ([Sangkhae et al., 2019](#)); directly conjugated with Alexa Fluor 488 Labeling Kit (Abcam, ab236553)]. For staining of cell membrane receptors, the following antibodies were used: AXL (Invitrogen), MERTK (BioLegend), Tim4 (BioLegend) and Stab2 (G-Biosciences). For analysis of *circulating and splenic RBCs*, the following surface antibodies were used: CD45 (BioLegend, 30-F11), TER-119 (BioLegend) and CD71 (BioLegend, RI7217). For analysis of *splenic granulocytes*, the following surface antibodies were used: CD45 (BioLegend, 30-F11), CD45R/B220 (BioLegend, RA3-6B2), F4/80 (BioLegend, BM8), CD11b (BioLegend, M1/70) and Gr-1 (BioLegend, RB6-8C5). For analysis of *peritoneal macrophages*, the following surface antibodies were used: CD45 (BioLegend, 30-F11), F4/80 (BioLegend, BM8), MHCII (BioLegend, M5/114.15.2), and CD11b (BioLegend, M1/70). Events were either acquired on Aria II (BD Biosciences) or CytToFLEX (Beckman Coulter) and were analyzed with FlowJo or CytExpert, respectively. For RNA sequencing (RNA-seq) and ATP levels quantification, RPMs were sorted into Trizol-LS (Invitrogen, 10296010) or assay buffer, respectively, using an Aria II cell sorter (BD Biosciences) with an 85 μ m nozzle.

Functional assays and intracellular staining of ferrous iron, proteins and protein aggregates

Intracellular ROS (APC channel) levels were determined by using CellROX Deep Red Reagent (Invitrogen, C10422) fluorescence according to the manufacturer's instructions. **Lipid peroxidation** (FITC vs PE channels) was determined with the Lipid Peroxidation Assay Kit (Abcam, ab243377) according to the manufacturer's instructions. **Mitochondria-associated ROS** (PE channel) levels were measured with MitoSOX Red (Invitrogen, M36008) at 2.5 μ M for 30 min at 37 °C. **Lysosomal activity** (FITC channel) was determined by using Lysosomal Intracellular Activity Assay Kit (Biovision, K448) according to the manufacturer's instructions. **Proteasomal activity** (FITC channel) was determined using Me4BodipyFL-Ahx3Leu3VS fluorescent proteasome activity probe (R&D Systems, I-190) at 2 μ M for 1 hr at 37 °C. **Mitochondria activity** (membrane potential, PE channel) was measured using a tetramethylrhodamine ethyl ester (TMRE) fluorescent probe (Sigma-Aldrich, 87917) at 400 nM for 30 min at 37 °C. **Mitochondrial mass** (FITC/PE channel) was measured by fluorescence levels upon staining with MitoTracker Green (Invitrogen, M7514) at 100 nM for 30 min at 37 °C. **Calcium levels** (FITC channel) were determined by using Cal-520 AM probe (Abcam, ab171868) at 5 μ M for 1 hour at 37 °C.

The content of **intracellular ferrous iron** (PE channel) (Fe^{2+}) was measured using FerroOrange (DojinD, F374) via flow cytometric analysis. Briefly, surface-stained cells were incubated with 1 μ M FerroOrange in HBSS for 30 min at 37 °C, and analyzed directly via flow cytometry without further washing. For **intracellular antibody staining**, surface-stained cells were first fixed with 4% PFA and permeabilized with 0.5% Triton-X in PBS. The cells were then stained with the following primary antibodies for 1 hr at 4 °C: Ferritin Heavy Chain (FTH1, Cell Signaling Technology, 3998), Ferritin Light Chain (FTL, Abcam, ab69090), HO-1 polyclonal antibody (Enzo Life Sciences, ADI-OSA-150) and Ki-67 (BioLegend, 16A8). This was followed by 30 min staining with Alexa Fluor 488 or Alexa Fluor 647 conjugated anti-Rabbit IgG (1:1000 Thermo Fisher Scientific, A-21206). **Protein aggregates (aggregates)** (PE channel) were stained and measured with PROTEOSTAT Aggregosome detection kit (Enzo Life Sciences, ENZ-51035-0025) at concentration 1:2000 for 30 minutes at 37 °C.

The geometric mean fluorescence intensities (MFI) corresponding to the probes/target protein levels were determined by flow cytometry acquired on Aria II (BD Biosciences) or CytoFLEX (Beckman Coulter) and were analyzed with FlowJo or CytExpert, respectively. For the probes that have emissions in PE, TREML4 was excluded, and RPMs were gated as F4/80-high CD11b-dim. For quantifications, MFI of the adequate fluorescence minus one (FMO) controls were subtracted from samples MFI, and data were further normalized.

ATP levels

Cellular ATP levels in FACS-sorted RPMs (10000 cells/sample) were determined using ATP Fluorometric Assay Kit (Sigma-Aldrich, MAK190), as per the manufacturer's instructions.

Magnetic sorting of RPMs and isolation of extracellular iron-containing aggregates

60×10^6 of mouse splenocytes were incubated for 15 min at 4 ° C in PBS containing 5% Normal Rat Serum (Thermo Fisher Scientific, 10,710 C) and anti-CD16/32 (BioLegend, 101320) antibody in 5 mL round bottom tube. Afterward, cells were labeled with anti-F4/80 (APC, BioLegend, 123116), anti-Ly-6G/Ly-6C (Gr-1) (Biotin, BioLegend, 108403), anti-CD3 (Biotin, BioLegend, 100243), anti-mouse Ly-6C (Biotin, BioLegend, 128003) and anti-B220 (Biotin, BioLegend, 103204) for 20 min in 4 ° C in dark. Next, cells were washed with cold PBS containing 2 mM EDTA, 0.5% BSA (hereafter referred to as 'sorting buffer'), and centrifuged at 600 g for 10 min. Pellet was resuspended in 400 μ L of sorting buffer containing 50 μ L of MojoSort Streptavidin Nanobeads (BioLegend, 480016) and kept in cold and dark for 15 min. After incubation, an additional 400 μ L was added to cells, and the tube was placed on EasyEight's EasySep Magnet (STEMCELL, 18103) for 7 min. After that supernatant was transferred to a fresh 5 mL tube and centrifuged at 600 g for 10 min. Pellet was resuspended in 100 μ L of sorting buffer and 10 μ L of MojoSort Mouse anti-APC Nanobeads (BioLegend, 480072) was added. The suspension was gently pipetted and incubated for 15 min at 4 ° C in the dark. Afterward, the tube was placed on a magnet for 7 min. Next, the supernatant was saved for analysis, and beads with attached F4/80 + cells were washed with sorting buffer and counted under a light microscope with a Neubauer chamber. Cells were pelleted and frozen in liquid nitrogen for further analysis.

For isolation of extracellular iron-containing aggregates, splenocytes were resuspended in HBSS and then carefully layered over Lymphosep (3:1) in a FACS tube, creating a sharp spleen cell suspension-Lymphosep interphase. Leukocytes were sorted out from the supernatant after density centrifugation at 400 g at 20 ° C for 25 min. The pellet comprising mostly RBCs, granulocytes, and extracellular iron-containing aggregates was then washed again with HBSS to remove Lymphosep. The cell pellet was re-suspended in a sorting buffer and then passed through a magnetized LS separation column (Miltenyi Biotec). The iron-containing superparamagnetic cells/aggregates were eluted from the demagnetized column, washed, and re-suspended in a sorting buffer. To achieve a pure yield of extracellular iron-containing aggregates and remove any trace contaminations from superparamagnetic RPMs or other leukocytes, cells expressing F4/80, B220, Gr-1, CD3, and Ly-6C were sorted out using MojoSort magnetic cell separation system as previously described. The remaining material comprising mostly aggregates was washed thoroughly and either pelleted and frozen in liquid nitrogen for further analysis (mass spectrometry and iron/heme measurements) or stained with fluorophore-conjugated antibodies for purity verification with flow cytometry.

Proteomic analyses of splenic aggregates using label-free quantification (LFQ)

Sample preparation

Magnetically-isolated aggregates were dissolved in neat trifluoroacetic acid. Protein solutions were neutralized with 10 volumes of 2 M Tris base, supplemented with TCEP (8 mM) and chloroacetamide (32 mM), heated to 95 ° C for 5 min, diluted with water 1:5, and subjected to overnight enzymatic digestion (0.5 μ g, Sequencing Grade Modified Trypsin, Promega) at 37 ° C. Tryptic peptides were then incubated with Chelex 100 resin (25 mg) for 1 hr at RT, desalted with the use of AttractSPE Disks Bio C18 (Affinisep), and concentrated using a SpeedVac concentrator. Prior to LC-MS measurement, the samples were resuspended in 0.1% TFA, 2% acetonitrile in water.

LC-MS/MS analysis

Chromatographic separation was performed on an Easy-Spray Acclaim PepMap column 50 cm long \times 75 μ m inner diameter (Thermo Fisher Scientific) at 45 °C by applying a 90 min acetonitrile gradients in 0.1% aqueous formic acid at a flow rate of 300 nL/min. An UltiMate 3000 nano-LC system was coupled to a Q Exactive HF-X mass spectrometer via an easy-spray source (all Thermo Fisher Scientific). The Q Exactive HF-X was operated in data-dependent mode with survey scans acquired at a resolution of 120,000 at m/z 200. Up to 12 of the most abundant isotope patterns with charges 2–5 from the survey scan were selected with an isolation window of 1.3 m/z and fragmented by higher-energy collision dissociation (HCD) with normalized collision energies of 27, while the dynamic exclusion was set to 30 s. The maximum ion injection times for the survey scan and the MS/MS scans (acquired with a resolution of 15,000 at m/z 200) were 45 and 96ms, respectively. The ion target value for MS was set to 3e6 and for MS/MS to 1e5, and the minimum AGC target was set to 1e3.

Data processing

The data were processed with MaxQuant v. 1.6.17.0 or v. 2.0.3.0 (Cox and Mann, 2008), and the peptides were identified from the MS/MS spectra searched against the reference mouse proteome UP000000589 (<https://www.uniprot.org/>) using the build-in Andromeda search engine. Raw files corresponding to three replicate samples obtained from Ag isolates and three replicate samples obtained from Y isolates were processed together. Raw files corresponding to two replicate samples corresponding to isolates obtained from control animals (dextran-injected, Dex) and two replicate samples corresponding to isolates obtained from animals subjected to intraperitoneal iron dextran injection (Fe-Dex) were processed together. Cysteine carbamidomethylation was set as a fixed modification and methionine oxidation, glutamine/asparagine deamidation, and protein N-terminal acetylation were set as variable modifications. For in silico digests of the reference proteome, cleavages of arginine or lysine followed by any amino acid were allowed (trypsin/P), and up to two missed cleavages were allowed. LFQ min. ratio count was set to 1. The FDR was set to 0.01 for peptides, proteins and sites. Match between runs was enabled. Other parameters were used as pre-set in the software. Unique and razor peptides were used for quantification enabling protein grouping (razor peptides are the peptides uniquely assigned to protein groups and not to individual proteins). Data were further analyzed using Perseus version 1.6.10.0 (Tyanova et al., 2016) and Microsoft Office Excel 2016.

Data processing and bioinformatics

Intensity values for protein groups were loaded into Perseus v. 1.6.10.0. Standard filtering steps were applied to clean up the dataset: reverse (matched to decoy database), only identified by site, and potential contaminants (from a list of commonly occurring contaminants included in MaxQuant) protein groups were removed. Reporter intensity values were normalized to the tissue weight the aggregates were isolated from and then Log₂ transformed. Protein groups with valid values in less than 2 Ag (Ag vs Y dataset) or less than 2 Fe-Dex (Fe-Dex vs Dex dataset) samples were removed. For protein groups with less than 2 valid values in Y or Dex, missing values were imputed from a normal distribution (random numbers from the following range were used: downshift = 1.8StdDev, width = 0.4StdDev). For the Ag vs Y dataset, which contained three biological replicate samples per condition, one-sided Student T-testing (permutation-based FDR = 0.001, S₀=1) was performed to return 3290 protein groups with levels statistically significantly greater in Ag samples compared to Y samples. For the Fe-Dex vs Dex dataset, which contained two biological replicate samples per condition, a significance cut-off of Log₂ fold change Fe-Dex vs Dex >1.5 was applied to return 2577 protein groups with levels significantly greater in Fe-Dex samples compared to Dex samples. For direct comparisons of these two datasets an analogous significance cut-off (Log₂ fold change Ag vs Y >1.5) was applied also to the Ag vs Y dataset to return 3614 protein groups with levels significantly greater in Ag samples compared to Y samples. Annotation enrichment analysis was performed using DAVID (<https://david.ncifcrf.gov/>) and ShinyGO (<http://bioinformatics.sdstate.edu/go/>), using FDR = 0,05 as a threshold.

Proteomic analyses of splenic aggregates using Tandem Mass Tag (TMT) labeling

Sample preparation

Magnetically isolated aggregates were dissolved in neat trifluoroacetic acid. Protein solutions were neutralized with 10 volumes of 2 M Tris base, supplemented with TCEP (8 mM) and chloroacetamide (32 mM), heated to 95° for 5 min, diluted with water 1:5, and subjected to overnight enzymatic digestion (0.5 µg, Sequencing Grade Modified Trypsin, Promega) at 37 °C. Tryptic peptides were then incubated with Chelex 100 resin (25 mg) for 1 hr at RT, desalted with the use of AttractSPE Disks Bio C18 (Affinisep), TMT-labeled on the solid support (*Myers et al., 2019*), compiled into a single TMT sample and concentrated using a SpeedVac concentrator. Prior to LC-MS measurement, the samples were resuspended in 0.1% TFA, 2% acetonitrile in water.

LC-MS/MS analysis

Chromatographic separation was performed on an Easy-Spray Acclaim PepMap column 50 cm long ×75 µm inner diameter (Thermo Fisher Scientific) at 45 °C by applying a 120 min acetonitrile gradients in 0.1% aqueous formic acid at a flow rate of 300 nl/min. An UltiMate 3000 nano-LC system was coupled to a Q Exactive HF-X mass spectrometer via an easy-spray source (all Thermo Fisher Scientific). Three samples injections were performed. The Q Exactive HF-X was operated in data-dependent mode with survey scans acquired at a resolution of 60,000 at m/z 200. Up to 15 of the most abundant isotope patterns with charges 2–5 from the survey scan were selected with an isolation window of 0.7 m/z and fragmented by higher-energy collision dissociation (HCD) with normalized collision energies of 32, while the dynamic exclusion was set to 35 s. The maximum ion injection times for the survey scan and the MS/MS scans (acquired with a resolution of 45,000 at m/z 200) were 50 and 96ms, respectively. The ion target value for MS was set to 3e6 and for MS/MS to 1e5, and the minimum AGC target was set to 1e3.

Data processing

The data were processed with MaxQuant v. 1.6.17.0 (*Cox and Mann, 2008*), and the peptides were identified from the MS/MS spectra searched against the reference mouse proteome UP000000589 (<https://www.uniprot.org/>) using the build-in Andromeda search engine. Raw files corresponding to 3 replicate injections of the combined TMT sample were processed together as a single experiment/single fraction. Cysteine carbamidomethylation was set as a fixed modification and methionine oxidation, glutamine/asparagine deamidation, and protein N-terminal acetylation were set as variable modifications. For in silico digests of the reference proteome, cleavages of arginine or lysine followed by any amino acid were allowed (trypsin/P), and up to two missed cleavages were allowed. Reporter ion MS2 quantification was performed with the min. reporter PIF was set to 0.75. The FDR was set to 0.01 for peptides, proteins and sites. Match between runs was enabled and second peptides function was disabled. Other parameters were used as pre-set in the software. Unique and razor peptides were used for quantification enabling protein grouping (razor peptides are the peptides uniquely assigned to protein groups and not to individual proteins). Data were further analyzed using Perseus version 1.6.10.0 (*Tyanova et al., 2016*) and Microsoft Office Excel 2016.

Data processing and bioinformatics

Reporter intensity corrected values for protein groups were loaded into Perseus v. 1.6.10.0. Standard filtering steps were applied to clean up the dataset: reverse (matched to decoy database), only identified by site, and potential contaminants (from a list of commonly occurring contaminants included in MaxQuant) protein groups were removed. Reporter intensity values were Log2 transformed and normalized by median subtraction within TMT channels. 942 Protein groups with the complete set of valid values were kept. Student T-testing (permutation-based FDR = 0.05, S0=0.1) was performed on the dataset to return 70 protein groups, which levels were statistically significantly changed in Ag vs IR samples. Annotation enrichment analysis was performed using DAVID (<https://david.ncifcrf.gov/>) and ShinyGO (<http://bioinformatics.sdstate.edu/go/>), using FDR = 0,05 as a threshold.

Identification of proteins in RPMs

Sample preparation

Magnetically isolated RPMs were isolated from spleens of two female 8-weeks-old C57BL/6 J. Cells were lysed in RIPA buffer. Proteins were precipitated with chloroform/methanol, protein pellet washed with methanol, and then reconstituted in 100 mM HEPES pH 8.0 containing 10 mM TCEP and 10 mM chloroacetamide. Proteins were subjected to overnight enzymatic digestion (Sequencing Grade Modified Trypsin, Promega) at 37 °C. Tryptic peptides were acidified with trifluoroacetic acid (final conc. 1%), desalted with the use of AttractSPE Disks Bio C18 (Affinisep), and concentrated using a SpeedVac concentrator. Prior to LC-MS measurement, the samples were resuspended in 0.1% TFA, 2% acetonitrile in water.

LC-MS/MS analysis

Chromatographic separation was performed on an Easy-Spray Acclaim PepMap column 50 cm long \times 75 μ m inner diameter (Thermo Fisher Scientific) at 55 °C by applying a 90 min (protein aggregates) or a 180 min (RPM extract) acetonitrile gradients in 0.1% aqueous formic acid at a flow rate of 300 nl/min. An UltiMate 3000 nano-LC system was coupled to a Q Exactive HF-X mass spectrometer via an easy-spray source (all Thermo Fisher Scientific). The Q Exactive HF-X was operated in data-dependent mode with survey scans acquired at a resolution of 120,000 at m/z 200. Up to 12 of the most abundant isotope patterns with charges 2–5 from the survey scan were selected with an isolation window of 1.3 m/z and fragmented by higher energy collision dissociation (HCD) with normalized collision energies of 27, while the dynamic exclusion was set to 30 s. The maximum ion injection times for the survey scan and the MS/MS scans (acquired with a resolution of 15,000 at m/z 200) were 45 and 96ms, respectively. The ion target value for MS was set to $3e6$ and for MS/MS to $1e5$, and the minimum AGC target was set to $1e3$.

Data processing

The data were processed with MaxQuant 2.1.3.0, and the peptides were identified from the MS/MS spectra searched against Uniprot Mouse Reference Proteome (UP000000589) using the built-in Andromeda search engine. Cysteine carbamidomethylation was set as a fixed modification and methionine oxidation, glutamine/asparagine deamination, as well as protein N-terminal acetylation were set as variable modifications. For *in silico* digests of the reference proteome, cleavages of arginine or lysine followed by any amino acid were allowed (trypsin/P), and up to two missed cleavages were allowed. The FDR was set to 0.01 for peptides, proteins and sites. Match between runs was enabled. Other parameters were used as pre-set in the software. Proteins were identified and intrasample quantified using iBAQ algorithm available in MaxQuant.

Measurement of cellular iron levels

Determination of cellular total iron levels in magnetically-sorted RPMs and splenic protein aggregates was carried out using the Iron Assay Kit (Sigma-Aldrich, MAK025) according to the manufacturer's instructions, and as shown previously (Folgueras *et al.*, 2018). For the measurement of total iron in RPMs and splenic aggregates volumes of buffers and reagents were decreased proportionally. Absorbance at 593 nm was measured with Nanodrop ND-1000 Spectrophotometer (Thermo Fisher Scientific). For RPMs, iron concentrations (ng/ μ L) were calculated from the standard curve and normalized to the number of cells in each sample. For the aggregates, iron amounts (μ g/g fresh tissue) were calculated from the standard curve and normalized to the weight of fresh tissue.

In vivo RBC lifespan

EZ-Link Sulfo-NHS Biotin (Thermo Fisher Scientific, 21217) was dissolved in sterile PBS to a final concentration of 1 mg per 100 μ L and filtered through a 0.1 μ m filter (Millipore, SLVV033RS). A day before the first blood collection, 100 μ L of the sterile solution was injected intravenously into mice. On days 0, 4, 11, 18, and 25 approximately 10 μ L of whole blood was collected from the tail vein with heparinized capillary to a tube containing HBSS. RBCs were centrifuged at 400 g for 5 min at 4 °C. Each sample was resuspended in 250 μ L of HBSS containing 5% normal rat serum (Thermo Fisher Scientific). Then 2 μ L of fluorescently labeled anti-TER-119 and streptavidin was added to the

suspension. Fluorescent streptavidin was omitted for FMO samples in each group. After incubation at 4°C for 30 min, samples were centrifuged and resuspended with HBSS. The percentage of biotinylated erythrocytes was determined by flow cytometry.

Preparation of stressed erythrocytes for erythrophagocytosis assays

Preparation and staining of stressed RBCs (sRBCs) were performed as described before (Theurl et al., 2016), with some modifications. *Preparation of RBCs:* Mice were sacrificed and whole blood was aseptically collected via cardiac puncture to CPDA-1 solution (Sigma-Aldrich, C4431). The final concentration of CPDA-1 was 10%. Whole blood obtained from mice was pooled and then centrifuged at 400 g for 15 min at 4°C. Plasma was collected and filtered through a 0.1 µm filter and stored at 4°C. RBCs were resuspended in HBSS and leukoreduced using Lymphosep (Biowest, L0560-500). Cells were washed with HBSS and then heated for 30 min at 48°C while continuously shaking, generating sRBC. *Staining of sRBCs:* 1×10^{10} RBC were resuspended in 1 ml diluent C, mixed with 1 ml diluent C containing 4 µM PKH-67 (Sigma-Aldrich, MIDI67-1KT) and incubated in dark for 5 min in 37°C, the reaction was stopped by adding 10 mL HBSS containing 2% FCS and 0.5% BSA. Staining was followed by two washing steps with HBSS. For *in vitro* and *ex vivo* erythrophagocytosis assay cells were resuspended in RPMI-1640 and counted.

For *in vivo* approach, RBCs were resuspended to 50% hematocrit in previously collected and filtered plasma.

In vitro erythrophagocytosis

Stained and counted sRBCs were added to iRPMs on 12-well plates in 10-fold excess for 1.5 h in 37 °C, 5% CO₂ on the 8th day after seeding. After that cells were extensively washed with cold PBS to discard not engulfed sRBCs. Next, cells were detached with Accutase (BioLegend, 423201), transferred to a round bottom tube, washed with HBSS, and centrifuged at 600 g for 5 min. Cells were labeled with antibodies and analyzed by flow cytometry.

In vivo erythrophagocytosis

Mice were injected into the tail vein with 100 µL of RBCs resuspended in plasma to 50% hematocrit. Mice were maintained for 1.5 hr in cages with constant access to water and food. After that time animals were sacrificed for organ isolation.

Ex vivo phagocytosis and erythrophagocytosis

10×10^6 splenocytes were resuspended in a 5 mL round bottom tube in 200 µL of warm complete RPMI-1640. Fluorescent sRBCs or fluorescent Zymosan A particles (Invitrogen, Z23373) were added to cells at ratio 10:1 (sRBCs/Zymosan: Cells) for 1.5 hr at 37°C, 5% CO₂. Afterward, cells were centrifuged at 600 g for 5 min. Excess of sRBCs was lysed using 1 X RBCs lysis buffer, cells were washed with HBSS and centrifuged. Next, cells were labeled with fluorescent antibodies and analyzed by flow cytometry.

Heme content analysis

For the *extracellular splenic heme content*, the whole spleen was weighted, quickly dissected, and gently mashed through a 100 µm strainer in the presence of 3 mL HBSS. After that suspension was centrifuged at 400 g for 10 min at 4 °C. A splenocyte pellet was used for other purposes and the supernatant was transferred to a 1,5 mL tube and centrifuged at 1000 g for 10 min at 4 °C to remove the rest of the cells and membranes. *Splenic aggregates* for heme measurements were isolated as previously described and were resuspended directly in Heme Reagent from Heme Assay Kit (Sigma-Aldrich, MAK316). *Blood from the portal vein* was collected to the heparin-coated tube, centrifuged at 400 g for 10 min at 4 °C and plasma was transferred to the 1,5 mL tube. Heme concentrations were measured using Heme Assay Kit (Sigma-Aldrich, MAK316) according to manufacturer instructions. Absorbance was measured at 400 nm. The amount of heme was calculated against Heme Calibrator and additionally normalized to the initial weight of fresh spleens (for splenic extracellular heme content and splenic aggregates).

Transferrin saturation and tissue iron measurements

Serum iron and unsaturated iron-binding capacity were measured with SFBC (Biolabo, 80008) and UIBC (Biolabo, 97408) kits according to manufacturer protocols. Transferrin saturation was calculated

using the formula $SFBC/(SFBC + UIBC) \times 100$. For measurement of tissue non-heme iron content, the bathophenanthroline method was applied and calculations were made against tissue dry weight, as described previously (Torrance and Bothwell, 1968).

Erythropoietin (EPO), IL-6 and hemopexin (HPX) measurement with ELISA

The plasma levels of erythropoietin, IL-6 and hemopexin were measured by Mouse Erythropoietin/EPO Quantikine ELISA Kit (R&D Systems, MEP00B), IL-6 Quantikine ELISA Kit (R&D Systems, M6000B) and Mouse Hemopexin ELISA Kit (Abcam, ab157716) according to the manufacturer's instructions. The optical density was measured on a microplate reader at a wavelength of 450 nm with wavelength correction set to 570 nm.

RNA isolation

RNA from sorted cells was isolated from TRIzol LS Reagent (Invitrogen, 10296028) using Direct-zol RNA Microprep Kit (Zymo Research, R2062) according to the manufacturer's instructions. RNA from tissues was isolated from TRIzol Reagent (Invitrogen, 15596018) following the guidelines of the manufacturer protocol.

Reverse transcription and qRT-PCR

cDNA was synthesized with RevertAid H Minus Reverse Transcriptase (Thermo Fisher Scientific, EP0452) according to manufacturer guidelines. Real-time PCR was performed by using SG qPCR Master Mix (EURx, E0401) and HAMP gene primers (Forward 5'-ATACCAATGCAGAAGAGAAGG-3', Reverse 5'-AACAGATACCACTGGGAA-3') as described in manufacturer protocol. qRT-PCR was run on LightCycler 96 System (Roche).

Histological and histochemical analysis

Following fixation in 10% formalin for 24 h, spleens were stored in 70% ethanol before further preparation. The tissue was embedded in paraffin and 7 μ m cross-sections were cut with a microtome (Reichert-Jung, Germany). The sections were stained with hematoxylin and eosin. Slides were examined by light microscopy (Olympus, type CH2). Non-heme iron staining of spleen samples was analyzed using Iron Stain Kit (Sigma-Aldrich, HT20-1KT). Sections were prepared as described above. After mounting on glass slides, sections were deparaffinized, incubated with a working solution containing Perls' Prussian Blue for 30 min, counterstained with pararosaniline solution for 2 min, and analyzed under standard light microscopy (Olympus CH2).

Detection of apoptotic cell death

Spleens were dissected, fixed in 4% paraformaldehyde (Sigma-Aldrich) in phosphate-buffered saline (PBS) (Sigma-Aldrich) at 4 °C for 24 hr and then washed two times for 30 min in PBS, soaked in 12.5% sucrose (Bioshop) for 1.5 hr and in 25% sucrose (Bioshop) for not less than 24 hr. All incubations were performed at 4 °C. Next, tissues were washed in PBS, embedded in Tissue-Tek compound, frozen in liquid nitrogen and sectioned into 20 μ m slices using a cryostat (Shandon, UK). Apoptotic cell death was detected using In Situ Cell Death Detection Kit (Roche, 11684795910) according to the manual instruction with small modifications. The sections were washed in PBS for 10 min and permeabilized in 0.1% Triton X-100 in 0.1% sodium citrate (Sigma-Aldrich) for 30 min at room temperature. Then the sections were washed 3 times with PBS and incubated with PBS for 30 min. After it, sections were incubated with 50 μ l of solution of Enzyme Solution (Blue) and Label Solution (Purple) (mix in a 1: 9 ratio) from the kit at 37 °C for 2 hr. Finally, the sections were washed three times for 5 min in PBS at RT and mounted using Vectashield with 49,6-diamidino-2-phenylindole (DAPI; Vector Labs). Slides were analyzed with a Zeiss LSM 510 Meta confocal microscope (Carl Zeiss, Jena, Germany) using the 60 x objective.

Transmission electron microscopy (TEM) of the spleen

Fresh samples of the spleen, about 3 square mm, were fixed in 2.5% glutaraldehyde for 24 hr at 4 °C, then washed in PBS and postfixed with 1% osmium tetroxide for 1 hr. After washing with water they were incubated with 1% aqueous uranyl acetate for 12 hr at 4 °C. Next, samples were dehydrated

at room temperature with increasing concentrations of ethanol, infiltrated with epoxy resin (Sigma-Aldrich, 45-359-1EA-F) and subjected for polymerization for 48 hr at 60 °C. Polymerized resin blocks were trimmed with a tissue processor (Leica EM TP), cut with an ultramicrotome (EM UC7, Leica) for ultrathin sections (65 nm thick), and collected on nickel grids, mesh 200 (Agar Scientific, G2200N). Specimen grids were examined with a transmission electron microscope Tecnai T12 BioTwin (FEI, Hillsboro, OR, USA) equipped with a 16 megapixel TemCam-F416 (R) camera (TVIPS GmbH) at in-house Microscopy and Cytometry Facility.

Transcriptome analysis by RNA-seq

To prepare libraries from FACS-sorted RPMs (at least 100,000 cells/sample), we used the previously described Smart-seq2 protocol (Picelli et al., 2013), suitable for low-input total mRNA sequencing. The quality of RNA and material during the preparation of libraries was checked by Bioanalyzer. The samples were sequenced on NextSeq500 (Illumina) with 75 bp single-end reads, with ~50 million reads/sample. RNAseq was performed at GeneCore at EMBL (Heidelberg, Germany). The quality of the reads was assessed with FastQC software [https://www.bioinformatics.babraham.ac.uk/projects/fastqc/]. Reads were mapped to the *Mus musculus* genome assembly GRCm38(mm10) with HISAT2 software (RRID:SCR_015530; version 2.2.1) [http://daehwankimlab.github.io/hisat2/] on default parameters. Then, the mapped reads were counted into Ensembl annotation intervals using HTSeq-count software [https://www.ncbi.nlm.nih.gov/labs/pmc/articles/PMC4287950/]. Differentially expressed genes were estimated using DESeq2 software [https://www.ncbi.nlm.nih.gov/labs/pmc/articles/PMC4302049/] with default parameters. Genes with p-adjusted <0.05 were regarded as differentially expressed and included in further analysis. Functional analysis was conducted using ClusterProfiler [https://doi.org/10.1016/j.xinn.2021.100141].

Statistical analysis

Female mice of the same age were randomly attributed to experimental groups (diets or NAC administration). Mouse-derived samples were collected randomly within groups and often assessed/measured randomly, and groups were harvested in a different order in individual experiments. The investigators were not blinded during experiments and assessments. Sample size (typically 4–7 mice/group or independent biological cell-based experiments) was determined based on power analysis, prior experience of performing similar experiments, and previously published papers in the field of RPM biology (Akilesh et al., 2019; Lu et al., 2020; Ma et al., 2021; Okreglicka et al., 2021). Statistical analysis was performed with GraphPad Prism (GraphPad software, Version 9). Data are represented as mean ± SEM, unless otherwise specified. ROUT method was applied (in rare cases) to identify and remove outliers. For all experiments, $\alpha=0.05$. When two groups were compared two-tailed unpaired Welch's t-test was applied, whereas for multiple comparisons, the One-Way Analysis of Variance (ANOVA) test was performed. For ANOVA, Dunnett's Multiple Comparison test was used for experiments comparing multiple experimental groups to a single control, while post-hoc Tukey's test was used to compare multiple experimental groups. The number of mice/samples per group or the number of independent cell-based experiments are shown in the figures or indicated in figure legends. Results were considered as significant for $p<0.05$ (* - $p<0.05$, ** - $p<0.01$, *** - $p<0.001$, ****- $p<0.0001$).

Acknowledgements

We thank the GeneCore team (EMBL, Heidelberg) for performing RNA sequencing. We thank Tara Arvedson (Amgen Inc.Inc, USA) for the anti-ferroportin antibody, Elizabeta Nemeth (UCLA, USA) for PR73, and Ewelina Szymańska (IIMCB, Warsaw) for Liproxstatin-1. Many thanks to Agnieszka Popielska and Anna Kosson, and the staff of the Experimental Medicine Centre (Białystok, Poland) and Mossakowski Medical Research Institute (Warsaw, Poland) for their technical support. We thank Dr. Dorota Stadnik for the preparation and measurement of the proteomic samples and Dawid Hatala for his assistance in histological analyses. We acknowledge the help of Raffaella Gozzellino in the initial phase of project conceptualization as well as the advice from Malgorzata Piechota (IIMCB, Warsaw) on heat shock application in cell culture. We thank Eryk Szymanski for his help in the bioinformatic analysis of the proteomics data and the generation of Venn diagrams. We are grateful to Florent Ginhoux and Zhaoyuan Liu [Singapore Immunology Network (SIgN)] for sharing their raw experimental data and

assisting in their re-analysis. The model figure was prepared using <https://biorender.com/>. Proteomic measurements were performed at the Proteomics Core Facility, IMoI Polish Academy of Sciences utilizing the equipment funded by the 'Regenerative Mechanisms for Health' project MAB/2017/2 within the International Research Agendas program of the Foundation for Polish Science, co-financed by the European Union under the European Regional Development Fund. WP and KMS acknowledge internal IIMCB funding for inter-lab projects. WP acknowledges funding from Norwegian Financial Mechanism 2014–2021 and operated by the Polish National Science Center under the project contract no UMO-2019/34 /H/NZ3/00691. KMS acknowledges funding from the National Science Centre Sonata Bis grant (UMO-2020/38/E/NZ4/00511).

Additional information

Funding

Funder	Grant reference number	Author
National Science Centre	Sonata Bis grant (UMO-2020/38/E/NZ4/00511)	Raghunandan Mahadeva Komal Chouhan Marta Niklewicz
Norwegian Financial Mechanism 2014-2021/ Polish National Science Centre	UMO-2019/34/H/ NZ3/00691	Wojciech Pokrzywa
Foundation for Polish Science	International Research Agendas program MAB/2017/2	Remigiusz Serwa

The funders had no role in study design, data collection and interpretation, or the decision to submit the work for publication.

Author contributions

Patryk Slusarczyk, Pratik Kumar Mandal, Conceptualization, Formal analysis, Investigation, Visualization, Methodology, Writing – original draft; Gabriela Zurawska, Matylda Macias, Formal analysis, Investigation, Visualization, Methodology; Marta Niklewicz, Komal Chouhan, Magdalena Cybulska-Lubak, Sylwia Herman, Investigation; Raghunandan Mahadeva, Aneta Jończy, Investigation, Visualization; Aleksandra Szybinska, Formal analysis, Investigation, Methodology; Olga Krawczyk, Formal analysis, Visualization, Methodology; Michal Mikula, Formal analysis, Validation; Remigiusz Serwa, Formal analysis, Funding acquisition, Validation, Visualization, Methodology; Małgorzata Lenartowicz, Formal analysis, Validation, Investigation, Visualization, Methodology; Wojciech Pokrzywa, Conceptualization, Resources, Formal analysis, Supervision, Funding acquisition, Validation, Investigation, Visualization, Methodology, Project administration, Writing – review and editing; Katarzyna Mleczko-Sanecka, Conceptualization, Resources, Formal analysis, Supervision, Funding acquisition, Validation, Investigation, Visualization, Methodology, Writing – original draft, Project administration, Writing – review and editing

Author ORCIDs

Patryk Slusarczyk <http://orcid.org/0000-0003-2383-3630>
 Pratik Kumar Mandal <http://orcid.org/0000-0002-1566-5641>
 Gabriela Zurawska <http://orcid.org/0000-0003-1465-8957>
 Marta Niklewicz <http://orcid.org/0000-0002-3407-795X>
 Komal Chouhan <http://orcid.org/0000-0003-4769-8787>
 Raghunandan Mahadeva <http://orcid.org/0000-0001-5865-6430>
 Aneta Jończy <http://orcid.org/0000-0002-4333-6853>
 Magdalena Cybulska-Lubak <http://orcid.org/0000-0002-1029-3156>
 Sylwia Herman <http://orcid.org/0000-0001-9750-0746>
 Michal Mikula <http://orcid.org/0000-0003-3447-7328>
 Remigiusz Serwa <http://orcid.org/0000-0002-4684-3754>
 Małgorzata Lenartowicz <http://orcid.org/0000-0003-4714-0783>

Wojciech Pokrzywa  <http://orcid.org/0000-0002-5110-4462>
 Katarzyna Mleczko-Sanecka  <http://orcid.org/0000-0001-9095-9597>

Ethics

All animal experiments and procedures were approved by the local ethical committees for animal care and use in Olsztyn and Warsaw (II LKE) (decisions: WAW2/015/2019; WAW2/149/2019; WAW2/026/2020; WAW2/149/2020; WAW2/122/2019).

Decision letter and Author response

Decision letter <https://doi.org/10.7554/eLife.79196.sa1>

Author response <https://doi.org/10.7554/eLife.79196.sa2>

Additional files

Supplementary files

- MDAR checklist

Data availability

RNA sequencing data are deposited in the GEO repository (under accession no: GSE199879). Mass spectrometry proteomics data were deposited to the ProteomeXchange Consortium via the PRIDE partner repository with the dataset identifiers: PXD032900 and PXD038660. All other numerical data used to generate the figures are provided as Source data files.

The following datasets were generated:

Author(s)	Year	Dataset title	Dataset URL	Database and Identifier
Slusarczyk P, Mandal PK, Zurawska G, Niklewicz M, Chouhan K, Macias M, Szybinska A, Cybulska M, Krawczyk O, Herman S, Mikula M, Lenartowicz M, Pokrzywa W, Mleczko-Sanecka K	2022	Impaired iron recycling from erythrocytes is an early hallmark of aging	https://www.ncbi.nlm.nih.gov/geo/query/acc.cgi?acc=GSE199879	NCBI Gene Expression Omnibus, GSE199879
Slusarczyk P, Mandal PK, Zurawska G, Niklewicz M, Chouhan K, Macias M, Szybinska A, Cybulska M, Krawczyk O, Herman S, Mikula M, Lenartowicz M, Pokrzywa W, Mleczko-Sanecka K	2022	Impaired iron recycling from erythrocytes is an early hallmark of aging	http://proteomecentral.proteomexchange.org/cgi/GetDataset?ID=PXD032900	ProteomeXchange, PXD032900
Slusarczyk P, Mandal PK, Zurawska G, Niklewicz M, Chouhan K, Mahadeva R, Jonczy A, Macias M, Szybinska A, Cybulska M, Krawczyk O, Herman S, Mikula M, Lenartowicz M, Pokrzywa W, Mleczko-Sanecka K	2022	Aging-triggered iron-rich insoluble protein aggregates in the spleen originate chiefly from red pulp macrophages	http://proteomecentral.proteomexchange.org/cgi/GetDataset?ID=PXD038660	ProteomeXchange, PXD038660

References

Akilesh HM, Buechler MB, Duggan JM, Hahn WO, Matta B, Sun X, Gessay G, Whalen E, Mason M, Presnell SR, Elkon KB, Lacy-Hulbert A, Barnes BJ, Pepper M, Hamerman JA. 2019. Chronic TLR7 and TLR9 signaling drives

- anemia via differentiation of specialized hemophagocytes. *Science* **363**:eaa05213. DOI: <https://doi.org/10.1126/science.aao5213>, PMID: 30630901
- Altamura S**, Kessler R, Gröne H-J, Gretz N, Hentze MW, Galy B, Muckenthaler MU. 2014. Resistance of ferroportin to hepcidin binding causes exocrine pancreatic failure and fatal iron overload. *Cell Metabolism* **20**:359–367. DOI: <https://doi.org/10.1016/j.cmet.2014.07.007>, PMID: 25100063
- Arashiki N**, Kimata N, Manno S, Mohandas N, Takakuwa Y. 2013. Membrane peroxidation and methemoglobin formation are both necessary for band 3 clustering: mechanistic insights into human erythrocyte senescence. *Biochemistry* **52**:5760–5769. DOI: <https://doi.org/10.1021/bi400405p>, PMID: 23889086
- Arruda LF**, Arruda SF, Campos NA, de Valencia FF, Siqueira Em. 2013. Dietary iron concentration may influence aging process by altering oxidative stress in tissues of adult rats. *PLOS ONE* **8**:e61058. DOI: <https://doi.org/10.1371/journal.pone.0061058>, PMID: 23593390
- Aschemeyer S**, Qiao B, Stefanova D, Valore EV, Sek AC, Ruwe TA, Vieth KR, Jung G, Casu C, Rivella S, Jormakka M, Mackenzie B, Ganz T, Nemeth E. 2018. Structure-Function analysis of ferroportin defines the binding site and an alternative mechanism of action of hepcidin. *Blood* **131**:899–910. DOI: <https://doi.org/10.1182/blood-2017-05-786590>, PMID: 29237594
- Atamna H**, Killilea DW, Killilea AN, Ames BN. 2002. Heme deficiency may be a factor in the mitochondrial and neuronal decay of aging. *PNAS* **99**:14807–14812. DOI: <https://doi.org/10.1073/pnas.192585799>, PMID: 12417755
- Bennett LF**, Liao C, Quickel MD, Yeoh BS, Vijay-Kumar M, Hankey-Giblin P, Prabhu KS, Paulson RF. 2019. Inflammation induces stress erythropoiesis through heme-dependent activation of SPI-C. *Science Signaling* **12**:598. DOI: <https://doi.org/10.1126/scisignal.aap7336>, PMID: 31506384
- Berman AE**, Chan WY, Brennan AM, Reyes RC, Adler BL, Suh SW, Kauppinen TM, Edling Y, Swanson RA. 2011. N-Acetylcysteine prevents loss of dopaminergic neurons in the EAAC1-/- mouse. *Annals of Neurology* **69**:509–520. DOI: <https://doi.org/10.1002/ana.22162>, PMID: 21446024
- Bian Z**, Shi L, Guo YL, Lv Z, Tang C, Niu S, Tremblay A, Venkataramani M, Culpepper C, Li L, Zhou Z, Mansour A, Zhang Y, Gewirtz A, Kidder K, Zen K, Liu Y. 2016. Cd47-sirpα interaction and IL-10 constrain inflammation-induced macrophage phagocytosis of healthy self-cells. *PNAS* **113**:E5434–E5443. DOI: <https://doi.org/10.1073/pnas.1521069113>, PMID: 27578867
- Bories GFP**, Yeudall S, Serbulea V, Fox TE, Isakson BE, Leitinger N. 2020. Macrophage metabolic adaptation to heme detoxification involves co-dependent activation of the pentose phosphate pathway. *Blood* **136**:1535–1548. DOI: <https://doi.org/10.1182/blood.2020004964>, PMID: 32556090
- Brancolini C**, Luliano L. 2020. Proteotoxic stress and cell death in cancer cells. *Cancers* **12**:2385. DOI: <https://doi.org/10.3390/cancers12092385>, PMID: 32842524
- Bratosin D**, Mazurier J, Tissier JP, Estaquier J, Huart JJ, Ameisen JC, Aminoff D, Montreuil J. 1998. Cellular and molecular mechanisms of senescent erythrocyte phagocytosis by macrophages: A review. *Biochimie* **80**:173–195. DOI: [https://doi.org/10.1016/s0300-9084\(98\)80024-2](https://doi.org/10.1016/s0300-9084(98)80024-2), PMID: 9587675
- Chen X**, Comish PB, Tang D, Kang R. 2021. Characteristics and biomarkers of ferroptosis. *Frontiers in Cell and Developmental Biology* **9**:637162. DOI: <https://doi.org/10.3389/fcell.2021.637162>, PMID: 33553189
- Chung SW**, Liu X, Macias AA, Baron RM, Perrella MA. 2008. Heme oxygenase-1-derived carbon monoxide enhances the host defense response to microbial sepsis in mice. *The Journal of Clinical Investigation* **118**:239–247. DOI: <https://doi.org/10.1172/JCI32730>, PMID: 18060048
- Clarke J**, Kayatekin C, Viel C, Shihabuddin L, Sardi SP. 2021. Murine models of lysosomal storage diseases exhibit differences in brain protein aggregation and neuroinflammation. *Biomedicine* **9**:446. DOI: <https://doi.org/10.3390/biomedicine9050446>, PMID: 33919140
- Cook CI**, Yu BP. 1998. Iron accumulation in aging: modulation by dietary restriction. *Mechanisms of Ageing and Development* **102**:1–13. DOI: [https://doi.org/10.1016/s0047-6374\(98\)00005-0](https://doi.org/10.1016/s0047-6374(98)00005-0), PMID: 9663787
- Cox J**, Mann M. 2008. MaxQuant enables high peptide identification rates, individualized p.p.b.-range mass accuracies and proteome-wide protein quantification. *Nature Biotechnology* **26**:1367–1372. DOI: <https://doi.org/10.1038/nbt.1511>, PMID: 19029910
- Cronin SJF**, Woolf CJ, Weiss G, Penninger JM. 2019. The role of iron regulation in immunometabolism and immune-related disease. *Frontiers in Molecular Biosciences* **6**:116. DOI: <https://doi.org/10.3389/fmolb.2019.00116>, PMID: 31824960
- Delaby C**, Rondeau C, Pouzet C, Willemetz A, Pilard N, Desjardins M, Canonne-Hergaux F. 2012. Subcellular localization of iron and heme metabolism related proteins at early stages of erythrophagocytosis. *PLOS ONE* **7**:e42199. DOI: <https://doi.org/10.1371/journal.pone.0042199>, PMID: 22860081
- De Leonibus C**, Cinque L, Settembre C. 2019. Emerging lysosomal pathways for quality control at the endoplasmic reticulum. *FEBS Letters* **593**:2319–2329. DOI: <https://doi.org/10.1002/1873-3468.13571>, PMID: 31388984
- Dixon SJ**, Lemberg KM, Lamprecht MR, Skouta R, Zaitsev EM, Gleason CE, Patel DN, Bauer AJ, Cantley AM, Yang WS, Morrison B, Stockwell BR. 2012. Ferroptosis: an iron-dependent form of nonapoptotic cell death. *Cell* **149**:1060–1072. DOI: <https://doi.org/10.1016/j.cell.2012.03.042>, PMID: 22632970
- Dupuis L**, Chauvet M, Bourdelier E, Dussiot M, Belmatoug N, Le Van Kim C, Chêne A, Franco M. 2022. Phagocytosis of erythrocytes from gaucher patients induces phenotypic modifications in macrophages, driving them toward gaucher cells. *International Journal of Molecular Sciences* **23**:14. DOI: <https://doi.org/10.3390/ijms23147640>, PMID: 35886988
- Even B**, Fayad-Kobeissi S, Gagliolo JM, Motterlini R, Boczkowski J, Foresti R, Dagouassat M. 2018. Heme oxygenase-1 induction attenuates senescence in chronic obstructive pulmonary disease lung fibroblasts by

- protecting against mitochondria dysfunction. *Aging Cell* **17**:e12837. DOI: <https://doi.org/10.1111/accel.12837>, PMID: 30341816
- Folgueras AR**, Freitas-Rodríguez S, Ramsay AJ, Garabaya C, Rodríguez F, Velasco G, López-Otín C. 2018. Matriptase-2 deficiency protects from obesity by modulating iron homeostasis. *Nature Communications* **9**:1350. DOI: <https://doi.org/10.1038/s41467-018-03853-1>, PMID: 29636509
- Fox JBS**, Davisson M, Newcomer C. 2006. The Mouse in Biomedical Research. Elsevier.
- Franken L**, Klein M, Spasova M, Elskova A, Wiedwald U, Welz M, Knolle P, Farle M, Limmer A, Kurts C. 2015. Splenic red pulp macrophages are intrinsically superparamagnetic and contaminate magnetic cell isolates. *Scientific Reports* **5**:12940. DOI: <https://doi.org/10.1038/srep12940>, PMID: 26260698
- Friedmann Angeli JP**, Schneider M, Proneth B, Tyurina YY, Tyurin VA, Hammond VJ, Herbach N, Aichler M, Walch A, Eggenhofer E, Basavarajappa D, Rådmark O, Kobayashi S, Seibt T, Beck H, Neff F, Esposito I, Wanke R, Förster H, Yefremova O, et al. 2014. Inactivation of the ferroptosis regulator GPX4 triggers acute renal failure in mice. *Nature Cell Biology* **16**:1180–1191. DOI: <https://doi.org/10.1038/ncb3064>, PMID: 25402683
- Ganz T**. 2012. Macrophages and systemic iron homeostasis. *Journal of Innate Immunity* **4**:446–453. DOI: <https://doi.org/10.1159/000336423>, PMID: 22441209
- Gautier E-F**, Leduc M, Cochet S, Bailly K, Lacombe C, Mohandas N, Guillonnet F, El Nemer W, Mayeux P. 2018. Absolute proteome quantification of highly purified populations of circulating reticulocytes and mature erythrocytes. *Blood Advances* **2**:2646–2657. DOI: <https://doi.org/10.1182/bloodadvances.2018023515>, PMID: 30327373
- Girelli D**, Marchi G, Camaschella C. 2018. Anemia in the elderly. *HemaSphere* **2**:e40. DOI: <https://doi.org/10.1097/HS9.000000000000040>, PMID: 31723768
- Gottlieb Y**, Topaz O, Cohen LA, Yakov LD, Haber T, Morgenstern A, Weiss A, Chait Berman K, Fibach E, Meyron-Holtz EG. 2012. Physiologically aged red blood cells undergo erythrophagocytosis in vivo but not in vitro. *Haematologica* **97**:994–1002. DOI: <https://doi.org/10.3324/haematol.2011.057620>, PMID: 22331264
- Gozzelino R**, Jeney V, Soares MP. 2010. Mechanisms of cell protection by heme oxygenase-1. *Annual Review of Pharmacology and Toxicology* **50**:323–354. DOI: <https://doi.org/10.1146/annurev.pharmtox.010909.105600>, PMID: 20055707
- Haldar M**, Kohyama M, So AY-L, Kc W, Wu X, Briseño CG, Satpathy AT, Kretzer NM, Arase H, Rajasekaran NS, Wang L, Egawa T, Igarashi K, Baltimore D, Murphy TL, Murphy KM. 2014. Heme-Mediated SPI-C induction promotes monocyte differentiation into iron-recycling macrophages. *Cell* **156**:1223–1234. DOI: <https://doi.org/10.1016/j.cell.2014.01.069>, PMID: 24630724
- Harrison PM**, Arosio P. 1996. The ferritins: molecular properties, iron storage function and cellular regulation. *Biochimica et Biophysica Acta* **1275**:161–203. DOI: [https://doi.org/10.1016/0005-2728\(96\)00022-9](https://doi.org/10.1016/0005-2728(96)00022-9), PMID: 8695634
- Hashimoto D**, Chow A, Noizat C, Teo P, Beasley MB, Leboeuf M, Becker CD, See P, Price J, Lucas D, Greter M, Mortha A, Boyer SW, Forsberg EC, Tanaka M, van Rooijen N, García-Sastre A, Stanley ER, Ginhoux F, Frenette PS, et al. 2013. Tissue-Resident macrophages self-maintain locally throughout adult life with minimal contribution from circulating monocytes. *Immunity* **38**:792–804. DOI: <https://doi.org/10.1016/j.immuni.2013.04.004>, PMID: 23601688
- Hedblom A**, Hejazi SM, Canesin G, Choudhury R, Hanafy KA, Cszimadia E, Persson JL, Wegiel B. 2019. Heme detoxification by heme oxygenase-1 reinstates proliferative and immune balances upon genotoxic tissue injury. *Cell Death & Disease* **10**:72. DOI: <https://doi.org/10.1038/s41419-019-1342-6>, PMID: 30683864
- Higgins JM**. 2015. Red blood cell population dynamics. *Clinics in Laboratory Medicine* **35**:43–57. DOI: <https://doi.org/10.1016/j.cll.2014.10.002>, PMID: 25676371
- Kaushik S**, Cuervo AM. 2015. Proteostasis and aging. *Nature Medicine* **21**:1406–1415. DOI: <https://doi.org/10.1038/nm.4001>, PMID: 26646497
- Kautz L**, Meynard D, Monnier A, Darnaud V, Bouvet R, Wang R-H, Deng C, Vaulont S, Mosser J, Coppin H, Roth M-P. 2008. Iron regulates phosphorylation of Smad1/5/8 and gene expression of BMP6, Smad7, Id1, and atoh8 in the mouse liver. *Blood* **112**:1503–1509. DOI: <https://doi.org/10.1182/blood-2008-03-143354>, PMID: 18539898
- Kenkhuis B**, Somarakis A, de Haan L, Dzyubachyk O, IJsselsteijn ME, de Miranda N, Lelieveldt BPF, Dijkstra J, van Roon-Mom WMC, Höllt T, van der Weerd L. 2021. Iron loading is a prominent feature of activated microglia in alzheimer's disease patients. *Acta Neuropathologica Communications* **9**:27. DOI: <https://doi.org/10.1186/s40478-021-01126-5>, PMID: 33597025
- Kim SH**, Cho SN, Lim YJ, Choi JA, Lee J, Go D, Song CH. 2018. Phagocytosis influences the intracellular survival of mycobacterium smegmatis via the endoplasmic reticulum stress response. *Cell & Bioscience* **8**:52. DOI: <https://doi.org/10.1186/s13578-018-0250-2>, PMID: 30288253
- Klang IM**, Schilling B, Sorensen DJ, Sahu AK, Kapahi P, Andersen JK, Swoboda P, Killilea DW, Gibson BW, Lithgow GJ. 2014. Iron promotes protein insolubility and aging in *C. elegans*. *Aging* **6**:975–991. DOI: <https://doi.org/10.18632/aging.100689>, PMID: 25554795
- Klei TRL**, Meinderts SM, van den Berg TK, van Bruggen R. 2017. From the cradle to the grave: the role of macrophages in erythropoiesis and erythrophagocytosis. *Frontiers in Immunology* **8**:73. DOI: <https://doi.org/10.3389/fimmu.2017.00073>, PMID: 28210260
- Klei TRL**, Dalimot J, Nota B, Veldthuis M, Mul FPJ, Rademakers T, Hoogenboezem M, Nagelkerke SQ, van IJcken WFJ, Oole E, Svendsen P, Moestrup SK, van Alphen FPJ, Meijer AB, Kuijpers TW, van Zwieten R,

- van Bruggen R. 2020. Hemolysis in the spleen drives erythrocyte turnover. *Blood* **136**:1579–1589. DOI: <https://doi.org/10.1182/blood.202005351>, PMID: 32777816
- Kohyama M, Ise W, Edelson BT, Wilker PR, Hildner K, Mejia C, Murphy KM. 2009. Role for spi-C in the development of red pulp macrophages and splenic iron homeostasis. *Nature* **457**:318–321. DOI: <https://doi.org/10.1038/nature07472>
- Kovtunovych G, Eckhaus MA, Ghosh MC, Ollivierre-Wilson H, Rouault TA. 2010. Dysfunction of the heme recycling system in heme oxygenase 1-deficient mice: effects on macrophage viability and tissue iron distribution. *Blood* **116**:6054–6062. DOI: <https://doi.org/10.1182/blood-2010-03-272138>, PMID: 20844238
- Lefebvre T, Reihani N, Daher R, de Villemeur TB, Belmatoug N, Rose C, Colin-Aronovicz Y, Puy H, Le Van Kim C, Franco M, Karim Z. 2018. Involvement of hepcidin in iron metabolism dysregulation in gaucher disease. *Haematologica* **103**:587–596. DOI: <https://doi.org/10.3324/haematol.2017.177816>, PMID: 29305416
- Lieberman AP, Shakkottai VG, Albin RL. 2019. Polyglutamine repeats in neurodegenerative diseases. *Annual Review of Pathology* **14**:1–27. DOI: <https://doi.org/10.1146/annurev-pathmechdis-012418-012857>, PMID: 30089230
- Liu JL, Fan YG, Yang ZS, Wang ZY, Guo C. 2018. Iron and alzheimer's disease: from pathogenesis to therapeutic implications. *Frontiers in Neuroscience* **12**:632. DOI: <https://doi.org/10.3389/fnins.2018.00632>, PMID: 30250423
- Liu Z, Gu Y, Chakarov S, Bleriot C, Kwok I, Chen X, Shin A, Huang W, Dress RJ, Dutertre C-A, Schlitzer A, Chen J, Ng LG, Wang H, Liu Z, Su B, Ginhoux F. 2019. Fate mapping via ms4a3-expression history traces monocyte-derived cells. *Cell* **178**:1509–1525. DOI: <https://doi.org/10.1016/j.cell.2019.08.009>, PMID: 31491389
- Lu Y, Basatemur G, Scott IC, Chiarugi D, Clement M, Harrison J, Jugdaohsingh R, Yu X, Newland SA, Jolin HE, Li X, Chen X, Szymanska M, Haraldsen G, Palmer G, Fallon PG, Cohen ES, McKenzie ANJ, Mallat Z. 2020. Interleukin-33 signaling controls the development of iron-recycling macrophages. *Immunity* **52**:782–793. DOI: <https://doi.org/10.1016/j.immuni.2020.03.006>, PMID: 32272082
- Luo W, Wang Y, Yang H, Dai C, Hong H, Li J, Liu Z, Guo Z, Chen X, He P, Li Z, Li F, Jiang J, Liu P, Li Z. 2018. Heme oxygenase-1 ameliorates oxidative stress-induced endothelial senescence via regulating endothelial nitric oxide synthase activation and coupling. *Aging* **10**:1722–1744. DOI: <https://doi.org/10.18632/aging.101506>, PMID: 30048241
- Lutz HU. 2012. Naturally occurring antibodies (nabs). Lutz HU (Ed). *Advances in Experimental Medicine and Biology*. Springer. p. 0065–2598. DOI: <https://doi.org/10.1007/978-1-4614-3461-0>
- Ma Y, Gao M, Liu D. 2016. N-Acetylcysteine protects mice from high fat diet-induced metabolic disorders. *Pharmaceutical Research* **33**:2033–2042. DOI: <https://doi.org/10.1007/s11095-016-1941-1>, PMID: 27161488
- Ma S, Dubin AE, Zhang Y, Mousavi SAR, Wang Y, Coombs AM, Loud M, Andolfo I, Patapoutian A. 2021. A role of Piezo1 in iron metabolism in mice and humans. *Cell* **184**:969–982. DOI: <https://doi.org/10.1016/j.cell.2021.01.024>, PMID: 33571427
- Martins R, Maier J, Gorki A-D, Huber KVM, Sharif O, Starkl P, Saluzzo S, Quattrone F, Gawish R, Lakovits K, Aichinger MC, Radic-Sarikas B, Lardeau C-H, Hladik A, Korosec A, Brown M, Vaahoteri K, Duggan M, Kerjaschki D, Esterbauer H, et al. 2016. Heme drives hemolysis-induced susceptibility to infection via disruption of phagocyte functions. *Nature Immunology* **17**:1361–1372. DOI: <https://doi.org/10.1038/ni.3590>, PMID: 27798618
- Matsushita M, Freigang S, Schneider C, Conrad M, Bornkamm GW, Kopf M. 2015. T cell lipid peroxidation induces ferroptosis and prevents immunity to infection. *The Journal of Experimental Medicine* **212**:555–568. DOI: <https://doi.org/10.1084/jem.20140857>, PMID: 25824823
- Mebius RE, Kraal G. 2005. Structure and function of the spleen. *Nature Reviews. Immunology* **5**:606–616. DOI: <https://doi.org/10.1038/nri1669>, PMID: 16056254
- Medinas DB, Valenzuela V, Hetz C. 2017. Proteostasis disturbance in amyotrophic lateral sclerosis. *Human Molecular Genetics* **26**:R91–R104. DOI: <https://doi.org/10.1093/hmg/ddx274>, PMID: 28977445
- Mleczko-Sanecka K, Silvestri L. 2021. Cell-Type-Specific insights into iron regulatory processes. *American Journal of Hematology* **96**:110–127. DOI: <https://doi.org/10.1002/ajh.26001>, PMID: 32945012
- Muckenthaler MU, Rivella S, Hentze MW, Galy B. 2017. A red carpet for iron metabolism. *Cell* **168**:344–361. DOI: <https://doi.org/10.1016/j.cell.2016.12.034>, PMID: 28129536
- Myers SA, Rhoads A, Cocco AR, Peckner R, Haber AL, Schweitzer LD, Krug K, Mani DR, Clauser KR, Rozenblatt-Rosen O, Hacohen N, Regev A, Carr SA. 2019. Streamlined protocol for deep proteomic profiling of FAC-sorted cells and its application to freshly isolated murine immune cells. *Molecular & Cellular Proteomics* **18**:995–1009. DOI: <https://doi.org/10.1074/mcp.RA118.001259>, PMID: 30792265
- Neitemeier S, Jelinek A, Laino V, Hoffmann L, Eisenbach I, Eying R, Ganjam GK, Dolga AM, Oppermann S, Culmsee C. 2017. Bid links ferroptosis to mitochondrial cell death pathways. *Redox Biology* **12**:558–570. DOI: <https://doi.org/10.1016/j.redox.2017.03.007>, PMID: 28384611
- Nemeth E, Tuttle MS, Powelson J, Vaughn MB, Donovan A, Ward DM, Ganz T, Kaplan J. 2004. Hepcidin regulates cellular iron efflux by binding to ferroportin and inducing its internalization. *Science* **306**:2090–2093. DOI: <https://doi.org/10.1126/science.1104742>, PMID: 15514116
- Nikolich-Zugich J. 2018. The twilight of immunity: emerging concepts in aging of the immune system. *Nature Immunology* **19**:10–19. DOI: <https://doi.org/10.1038/s41590-017-0006-x>, PMID: 29242543
- Okreglicka K, Iten I, Pohlmeier L, Onder L, Feng Q, Kurrer M, Ludewig B, Nielsen P, Schneider C, Kopf M. 2021. Pparγ is essential for the development of bone marrow erythroblastic island macrophages and splenic red pulp macrophages. *The Journal of Experimental Medicine* **218**:e20191314. DOI: <https://doi.org/10.1084/jem.20191314>, PMID: 33765133

- Pagani A**, Nai A, Corna G, Bosurgi L, Rovere-Querini P, Camaschella C, Silvestri L. 2011. Low hepcidin accounts for the proinflammatory status associated with iron deficiency. *Blood* **118**:736–746. DOI: <https://doi.org/10.1182/blood-2011-02-337212>, PMID: 21628413
- Park TJ**, Park JH, Lee GS, Lee JY, Shin JH, Kim MW, Kim YS, Kim JY, Oh KJ, Han BS, Kim WK, Ahn Y, Moon JH, Song J, Bae KH, Kim DH, Lee EW, Lee SC. 2019. Quantitative proteomic analyses reveal that GPX4 downregulation during myocardial infarction contributes to ferroptosis in cardiomyocytes. *Cell Death & Disease* **10**:835. DOI: <https://doi.org/10.1038/s41419-019-2061-8>, PMID: 31685805
- Pek RH**, Yuan X, Rietzschel N, Zhang J, Jackson L, Nishibori E, Ribeiro A, Simmons W, Jagadeesh J, Sugimoto H, Alam MZ, Garrett L, Haldar M, Ralle M, Phillips JD, Bodine DM, Hamza I. 2019. Hemozoin produced by mammals confers heme tolerance. *eLife* **8**:e49503. DOI: <https://doi.org/10.7554/eLife.49503>, PMID: 31571584
- Peters LL**, Tsaih S, Yuan R. 2008. Modeling anemia of aging in inbred mouse strains. *Blood* **112**:3444. DOI: <https://doi.org/10.1182/blood.V112.11.3444.3444>
- Picelli S**, Björklund ÅK, Faridani OR, Sagasser S, Winberg G, Sandberg R. 2013. Smart-seq2 for sensitive full-length transcriptome profiling in single cells. *Nature Methods* **10**:1096–1098. DOI: <https://doi.org/10.1038/nmeth.2639>, PMID: 24056875
- Qi L**, Tsai B, Arvan P. 2017. New insights into the physiological role of endoplasmic reticulum-associated degradation. *Trends in Cell Biology* **27**:430–440. DOI: <https://doi.org/10.1016/j.tcb.2016.12.002>, PMID: 28131647
- Ryan SK**, Zelic M, Han Y, Teeple E, Chen L, Sadeghi M, Shankara S, Guo L, Li C, Pontarelli F, Jensen EH, Comer AL, Kumar D, Zhang M, Gans J, Zhang B, Proto JD, Saleh J, Dodge JC, Savova V, et al. 2023. Microglia ferroptosis is regulated by SEC24B and contributes to neurodegeneration. *Nature Neuroscience* **26**:12–26. DOI: <https://doi.org/10.1038/s41593-022-01221-3>, PMID: 36536241
- Sangkhae V**, Fisher AL, Wong S, Koenig MD, Tussing-Humphreys L, Chu A, Lelić M, Ganz T, Nemeth E. 2019. Effects of maternal iron status on placental and fetal iron homeostasis. *The Journal of Clinical Investigation* **130**:625–640. DOI: <https://doi.org/10.1172/JCI127341>, PMID: 31661462
- Sanyear C**, Butthep P, Eamsaard W, Fucharoen S, Svasti S, Masaratana P. 2020. Iron homeostasis in a mouse model of thalassemia intermedia is altered between adolescence and adulthood. *PeerJ* **8**:e8802. DOI: <https://doi.org/10.7717/peerj.8802>, PMID: 32219031
- Slusarczyk P**, Mleczko-Sanecka K. 2021. The multiple facets of iron recycling. *Genes* **12**:1364. DOI: <https://doi.org/10.3390/genes12091364>, PMID: 34573346
- Sorbie J**, Valberg LS. 1974. Iron balance in the mouse. *Laboratory Animal Science* **24**:900–904. PMID: 4374593.
- Stefanova D**, Raychev A, Deville J, Humphries R, Campeau S, Ruchala P, Nemeth E, Ganz T, Bulut Y. 2018. Hepcidin protects against lethal *Escherichia coli* sepsis in mice inoculated with isolates from septic patients. *Infection and Immunity* **86**:e00253-18. DOI: <https://doi.org/10.1128/IAI.00253-18>, PMID: 29735522
- Sui X**, Prado MA, Paulo JA, Gygi SP, Finley D, Morimoto RI. 2022. Global Proteome Metastability Response in Isogenic Animals to Missense Mutations and Polyglutamine Expansions in Aging. *bioRxiv*. DOI: <https://doi.org/10.1101/2022.09.28.509812>
- Sukumaran A**, Chang J, Han M, Mintri S, Khaw BA, Kim J. 2017. Iron overload exacerbates age-associated cardiac hypertrophy in a mouse model of hemochromatosis. *Scientific Reports* **7**:5756. DOI: <https://doi.org/10.1038/s41598-017-05810-2>, PMID: 28720890
- Suliman HB**, Keenan JE, Piantadosi CA. 2017. Mitochondrial quality-control dysregulation in conditional HO-1^{-/-} mice. *JCI Insight* **2**:e89676. DOI: <https://doi.org/10.1172/jci.insight.89676>, PMID: 28194437
- Sun N**, Youle RJ, Finkel T. 2016. The mitochondrial basis of aging. *Molecular Cell* **61**:654–666. DOI: <https://doi.org/10.1016/j.molcel.2016.01.028>, PMID: 26942670
- Theurl I**, Hilgendorf I, Nairz M, Tymoszek P, Haschka D, Asshoff M, He S, Gerhardt LMS, Holderried TAW, Seifert M, Sopper S, Fenn AM, Anzai A, Rattik S, McAlpine C, Theurl M, Wieghofer P, Iwamoto Y, Weber GF, Harder NK, et al. 2016. On-Demand erythrocyte disposal and iron recycling requires transient macrophages in the liver. *Nature Medicine* **22**:945–951. DOI: <https://doi.org/10.1038/nm.4146>, PMID: 27428900
- Torrance JD**, Bothwell TH. 1968. A simple technique for measuring storage iron concentrations in formalinised liver samples. *The South African Journal of Medical Sciences* **33**:9–11. PMID: 5676884.
- Tyanova S**, Temu T, Sinitcyn P, Carlson A, Hein MY, Geiger T, Mann M, Cox J. 2016. The perseus computational platform for comprehensive analysis of (prote) omics data. *Nature Methods* **13**:731–740. DOI: <https://doi.org/10.1038/nmeth.3901>, PMID: 27348712
- Uversky VN**. 2009. Intrinsic disorder in proteins associated with neurodegenerative diseases. *Frontiers in Bioscience* **14**:5188–5238. DOI: <https://doi.org/10.2741/3594>, PMID: 19482612
- Vadolos J**, Ng GZ, Kysenius K, Crouch PJ, Dames S, Eisermann M, Nualkaew T, Vilcassim S, Schaeper U, Grigoriadis G. 2021. SLN124, a galnac-sirna targeting transmembrane serine protease δ , in combination with deferiprone therapy reduces ineffective erythropoiesis and hepatic iron-overload in a mouse model of β -thalassaemia. *British Journal of Haematology* **194**:200–210. DOI: <https://doi.org/10.1111/bjh.17428>, PMID: 33942901
- Vijayan V**, Wagener F, Immenschuh S. 2018. The macrophage heme-heme oxygenase-1 system and its role in inflammation. *Biochemical Pharmacology* **153**:159–167. DOI: <https://doi.org/10.1016/j.bcp.2018.02.010>, PMID: 29452096
- Wang W**, Green M, Choi JE, Gijón M, Kennedy PD, Johnson JK, Liao P, Lang X, Kryczek I, Sell A, Xia H, Zhou J, Li G, Li J, Li W, Wei S, Vatan L, Zhang H, Szeliga W, Gu W, et al. 2019. CD8⁺ T cells regulate tumour ferroptosis during cancer immunotherapy. *Nature* **569**:270–274. DOI: <https://doi.org/10.1038/s41586-019-1170-y>

- Ward RJ**, Legssyer R, Henry C, Crichton RR. 2000. Does the haemosiderin iron core determine its potential for chelation and the development of iron-induced tissue damage? *Journal of Inorganic Biochemistry* **79**:311–317. DOI: [https://doi.org/10.1016/s0162-0134\(99\)00237-8](https://doi.org/10.1016/s0162-0134(99)00237-8), PMID: 10830882
- Xu J**, Knutson MD, Carter CS, Leeuwenburgh C. 2008. Iron accumulation with age, oxidative stress and functional decline. *PLOS ONE* **3**:e2865. DOI: <https://doi.org/10.1371/journal.pone.0002865>, PMID: 18682742
- Yan HF**, Zou T, Tuo QZ, Xu S, Li H, Belaidi AA, Lei P. 2021. Ferroptosis: mechanisms and links with diseases. *Signal Transduction and Targeted Therapy* **6**:49. DOI: <https://doi.org/10.1038/s41392-020-00428-9>, PMID: 33536413
- Yona S**, Kim K-W, Wolf Y, Mildner A, Varol D, Breker M, Strauss-Ayali D, Viukov S, Guilliams M, Misharin A, Hume DA, Perlman H, Malissen B, Zelzer E, Jung S. 2013. Fate mapping reveals origins and dynamics of monocytes and tissue macrophages under homeostasis. *Immunity* **38**:79–91. DOI: <https://doi.org/10.1016/j.immuni.2012.12.001>, PMID: 23273845
- Youssef LA**, Rebbaa A, Pampou S, Weisberg SP, Stockwell BR, Hod EA, Spitalnik SL. 2018. Increased erythrophagocytosis induces ferroptosis in red pulp macrophages in a mouse model of transfusion. *Blood* **131**:2581–2593. DOI: <https://doi.org/10.1182/blood-2017-12-822619>, PMID: 29666112
- Zhang Z**, Zhang F, An P, Guo X, Shen Y, Tao Y, Wu Q, Zhang Y, Yu Y, Ning B, Nie G, Knutson MD, Anderson GJ, Wang F. 2011. Ferroportin1 deficiency in mouse macrophages impairs iron homeostasis and inflammatory responses. *Blood* **118**:1912–1922. DOI: <https://doi.org/10.1182/blood-2011-01-330324>, PMID: 21705499

7. Podsumowanie i wnioski

W ramach publikacji stanowiących niniejszą rozprawę doktorską dostarczono po raz pierwszy dowodów na to, że fizjologicznemu starzeniu towarzyszy uszkodzenie makrofagów czerwonej miazgi śledziony oraz upośledzenie zdolności usuwania starych czerwonych krwinek. Głównym czynnikiem prowadzącym do uszkodzenia RPMs jest wewnątrzkomórkowa akumulacja żelaza wraz z defektami proteostatycznymi. Deplecja komórek RPMs i ich upośledzona zdolność do erytrofagocytozy skutkują lokalną dyshomeostazą erytrocytów w śledzionie, u podstaw której leży zmiana balansu pomiędzy fagocytozą a lizą erytrocytów w stronę lizy. Dodatkowo, uszkodzenia RPMs powodują powstawanie złogów białkowych bogatych w hem i żelazo, będących wynikiem nagromadzenia się nieulegających degradacji proteolitycznej cząsteczek. Retencja żelaza w formie złogów białkowych, wraz z zwiększoną ekspresją hepcydyny i ograniczoną aktywnością fagocytarną pozostałych RPM, ograniczają dostępność żelaza w osoczu podczas starzenia się.

Wnioski szczegółowe:

- RPMs wyizolowane ze starszych myszy wykazują zwiększony poziomy labilnego żelaza, zwiększony stres oksydacyjny oraz upośledzoną funkcję recyklingu żelaza,
- dieta o obniżonej zawartości żelaza normalizuje parametry żelaza w organizmie podczas starzenia się, zmniejsza retencję żelaza w RPMs i normalizuje zdolność RPMs do recyklingu żelaza,
- starzenie się powoduje retencje starzejących się erytrocytów w śledzionie oraz ich zwiększoną hemolizę,
- starzenie się skutkuje utratą RPMs spowodowaną ferroptozą i proteotoksycnością,
- uszkodzone komórki RPMs tworzenie się nierozpuszczalnych agregatów białkowych bogatych w żelazo i hem w śledzionie,
- dysfunkcja RPMs pojawia się na wczesnym etapie starzenia się i związana jest z obniżonym poziomem ferroportyny,
- główną przyczyną zmniejszonej aktywności fagocytarnej RPMs oraz upośledzonym metabolizmem hemu i stresem retikulum endoplazmatycznego jest przeładowanie żelazem.

8. Bibliografia

1. Gardi C, Arezzini B, Fortino V, Comporti M. Effect of free iron on collagen synthesis, cell proliferation and MMP-2 expression in rat hepatic stellate cells. *Biochem Pharmacol.* 1 październik 2002; 64(7):1139–45.
2. Kim J, Wessling-Resnick M. Iron and mechanisms of emotional behavior. *J Nutr Biochem.* 1 listopad 2014; 25(11):1101–7.
3. Santiago González DA, Cheli VT, Wan R, Paez PM. Iron Metabolism in the Peripheral Nervous System: The Role of DMT1, Ferritin, and Transferrin Receptor in Schwann Cell Maturation and Myelination. *Journal of Neuroscience.* 11 grudzień 2019; 39(50):9940–53.
4. Paul BT, Manz DH, Torti FM, Torti S v. Mitochondria and Iron: current questions. <http://dx.doi.org/101080/1747408620161268047>. 2 styczeń 2016; 10(1):65–79.
5. Johnson EE, Wessling-Resnick M. Iron metabolism and the innate immune response to infection. *Microbes Infect.* 1 marzec 2012; 14(3):207–16.
6. Tian Y, Tian Y, Yuan Z, Zeng Y, Wang S, Fan X, i in. Iron Metabolism in Aging and Age-Related Diseases. *Int J Mol Sci.* 1 kwiecień 2022; 23(7).
7. Rivella S, Crielard BJ. Disorders of Iron Metabolism: Iron Deficiency and Iron Overload and Anemia of Chronic Diseases. *Pathobiology of Human Disease: A Dynamic Encyclopedia of Disease Mechanisms.* 1 styczeń 2014; 1471–87.
8. Coffey R, Ganz T. Iron homeostasis: An anthropocentric perspective. *Journal of Biological Chemistry.* 4 sierpień 2017; 292(31):12727–34.
9. Mleczko-Sanecka K, Silvestri L. Cell-type-specific insights into iron regulatory processes. *Am J Hematol.* 1 styczeń 2021; 96(1):110–27.
10. McKie AT, Barrow D, Latunde-Dada GO, Rolfs A, Sager G, Mudaly E, i in. An iron-regulated ferric reductase associated with the absorption of dietary iron. *Science.* 2 marzec 200; 291(5509):1755–9.
11. Gunshin H, Mackenzie B, Berger U v., Gunshin Y, Romero MF, Boron WF, i in. Cloning and characterization of a mammalian proton-coupled metal-ion transporter. *Nature.* 1997; 388(6641):482–8.
12. Donovan A, Brownlie A, Zhou Y, Shepard J, Pratt SJ, Moynihan J, i in. Positional cloning of zebrafish ferroportin1 identifies a conserved vertebrate iron exporter. *Nature.* 17 luty 2000; 403(6771):776–81.

13. McKie AT, Marciani P, Rolfs A, Brennan K, Wehr K, Barrow D, i in. A novel duodenal iron-regulated transporter, IREG1, implicated in the basolateral transfer of iron to the circulation. *Mol Cell*. 2000; 5(2):299–309.
14. Vulpe CD, Kuo YM, Murphy TL, Cowley L, Askwith C, Libina N, i in. Hephhaestin, a ceruloplasmin homologue implicated in intestinal iron transport, is defective in the sla mouse. *Nat Genet*. luty 1999; 21(2):195–9.
15. Oates PS, West AR. Heme in intestinal epithelial cell turnover, differentiation, detoxification, inflammation, carcinogenesis, absorption and motility. *World J Gastroenterol*. 21 lipiec 2006; 12(27):4281–95.
16. Shayeghi M, Latunde-Dada GO, Oakhill JS, Laftah AH, Takeuchi K, Halliday N, i in. Identification of an Intestinal Heme Transporter. *Cell*. 9 wrzesień 2005;122(5):789–801.
17. Antileo E, Garri C, Tapia V, Muñoz JP, Chiong M, Nualart F, i in. Endocytic pathway of exogenous iron-loaded ferritin in intestinal epithelial (Caco-2) cells. *Am J Physiol Gastrointest Liver Physiol*. 2013; 304(7).
18. Orkin S, Nathan D, Ginsburg D, Look A, Fisher D. Nathan and Oski's hematology of infancy and childhood E-Book. 2008
19. Klei TRL, Dalimot J, Nota B, Veldthuis M, Mul FPJ, Rademakers T, i in. Hemolysis in the spleen drives erythrocyte turnover. *Blood*. 1 październik 2020; 136(14):1579–89.
20. Theurl I, Hilgendorf I, Nairz M, Tymoszek P, Haschka D, Asshoff M, i in. On-demand erythrocyte disposal and iron recycling requires transient macrophages in the liver. *Nat Med*. 1 sierpień 2016; 22(8):945.
21. Marro S, Chiabrando D, Messana E, Stolte J, Turco E, Tolosano E, i in. Heme controls ferroportin1 (FPN1) transcription involving Bach1, Nrf2 and a MARE/ARE sequence motif at position –7007 of the FPN1 promoter. *Haematologica*. 2010; 95(8):1261.
22. Delaby C, Rondeau C, Pouzet C, Willemetz A, Pilard N, Desjardins M, i in. Subcellular Localization of Iron and Heme Metabolism Related Proteins at Early Stages of Erythrophagocytosis. *PLoS One*. 30 lipiec 2012; 7(7).
23. White C, Yuan X, Schmidt PJ, Bresciani E, Samuel TK, Campagna D, i in. HRG1 is essential for heme transport from the phagolysosome of macrophages during erythrophagocytosis. *Cell Metab*. 5 luty 2013;17(2):261–70.

24. Slusarczyk P, Mleczko-Sanecka K. The Multiple Facets of Iron Recycling. *Genes* (Basel). 2021; 12(9).
25. Beaumont C, Delaby C. Recycling iron in normal and pathological states. *Semin Hematol.* październik 2009; 46(4):328–38.
26. Kovtunovych G, Ghosh MC, Ollivierre W, Weitzel RP, Eckhaus MA, Tisdale JF, i in. Wild-type macrophages reverse disease in heme oxygenase 1-deficient mice. *Blood.* 8 sierpień 2014; 124(9):1522.
27. Kovtunovych G, Eckhaus MA, Ghosh MC, Ollivierre-Wilson H, Rouault TA. Dysfunction of the heme recycling system in heme oxygenase 1-deficient mice: effects on macrophage viability and tissue iron distribution. *Blood.* 12 grudzień 2010; 116(26):6054.
28. Rossi E. Hepcidin--the iron regulatory hormone. *The Clinical biochemist Reviews / Australian Association of Clinical Biochemists.* 2005;26(3):47–9.
29. Ganz T, Nemeth E. Iron Sequestration and Anemia of Inflammation. *Semin Hematol.* październik 2009;46(4):387–93.
30. Yu PB, Hong CC, Sachidanandan C, Babitt JL, Deng DY, Hoyng SA, i in. Dorsomorphin inhibits BMP signals required for embryogenesis and iron metabolism. *Nature Chemical Biology* 2008 4:1. 18 listopad 2007; 4(1):33–41.
31. Pagani A, Nai A, Silvestri L, Camaschella C. Hepcidin and Anemia: A Tight Relationship. *Front Physiol.* 9 październik 2019;10:1294.
32. de Domenico I, Ward DMV, Langelier C, Vaughn MB, Nemeth E, Sundquist WI, i in. The molecular mechanism of hepcidin-mediated ferroportin down-regulation. *Mol Biol Cell.* 2 lipiec 2007; 18(7):2569–78.
33. Wang CY, Babitt JL. Hepcidin regulation in the anemia of inflammation. *Curr Opin Hematol.* 2016; 23(3):189–97.
34. McCranor BJ, Langdon JM, Prince OD, Femnou LK, Berger AE, Cheadle C, i in. Investigation of the role of interleukin-6 and hepcidin antimicrobial peptide in the development of anemia with age. *Haematologica.* 1 październik 2013; 98(10):1633–40.
35. Muckenthaler MU, Rivella S, Hentze MW, Galy B. A Red Carpet for Iron Metabolism. *Cell.* 26 styczeń 2017;168(3):344–61.
36. Muckenthaler MU, Rivella S, Hentze MW, Galy B. A Red Carpet for Iron Metabolism. *Cell.* 26 styczeń 2017; 168(3):344–61.

37. Stoorvogel W, Strous GJ, Geuze HJ, Oorschot V, Schwartz AL. Late endosomes derive from early endosomes by maturation. *Cell*. 3 maj 1991; 65(3):417–27.
38. Killisch I, Steinlein P, ... KRJ of C, 1992 undefined. Characterization of early and late endocytic compartments of the transferrin cycle. Transferrin receptor antibody blocks erythroid differentiation by trapping the receptor. *journals.biologists.com*.
39. Chen C, Garcia-Santos D, Ishikawa Y, Seguin A, Li L, Fegan KH, i in. Snx3 Regulates Recycling of the Transferrin Receptor and Iron Assimilation. *Cell Metab*. 5 marzec 2013; 17(3):343–52.
40. Sobh A, Loguinov A, Zhou J, Jenkitkasemwong S, Zeidan R, el Ahmadie N, i in. Genetic screens reveal CCDC115 as a modulator of erythroid iron and heme trafficking. *Am J Hematol*. 1 wrzesień 2020; 95(9):1085–98.
41. Sheftel A, Stehling O, Lill R. Iron-sulfur proteins in health and disease. *Trends Endocrinol Metab*. maj 2010; 21(5):302–14.
42. Cronin SJF, Woolf CJ, Weiss G, Penninger JM. The Role of Iron Regulation in Immunometabolism and Immune-Related Disease. *Front Mol Biosci*. 22 listopad 2019; 6.
43. Philpott CC, Ryu MS, Frey A, Patel S. Cytosolic iron chaperones: Proteins delivering iron cofactors in the cytosol of mammalian cells. *J Biol Chem*. 4 sierpień 2017; 292(31):12764–71.
44. Xu J, Knutson MD, Carter CS, Leeuwenburgh C. Iron Accumulation with Age, Oxidative Stress and Functional Decline. *PLoS One*. 6 sierpień 2008; 3(8):e2865.
45. Sukumaran A, Chang J, Han M, Mintri S, Khaw BA, Kim J. Iron overload exacerbates age-associated cardiac hypertrophy in a mouse model of hemochromatosis. *Scientific Reports* 2017 7:1. 18 lipiec 2017; 7(1):1–10.
46. Cook CI, Yu BP. Iron accumulation in aging: modulation by dietary restriction. *Mech Ageing Dev*. 1 maj 1998;102(1):1–13.
47. Arruda LF, Arruda SF, Campos NA, de Valencia FF, Siqueira EM de A. Dietary Iron Concentration May Influence Aging Process by Altering Oxidative Stress in Tissues of Adult Rats. *PLoS One*. 12 kwiecień 2013; 8(4):e61058.
48. Weiss G, Ganz T, Goodnough LT. Review Series IRON METABOLISM AND ITS DISORDERS Anemia of inflammation. 2019.
49. Busti F, Campostrini N, Martinelli N, Girelli D. Iron deficiency in the elderly population, revisited in the hepcidin era. *Front Pharmacol*. 2014; 5 APR.

50. Arruda LF, Arruda SF, Campos NA, de Valencia FF, Siqueira EM de A. Dietary Iron Concentration May Influence Aging Process by Altering Oxidative Stress in Tissues of Adult Rats. *PLoS One*. 12 kwiecień 2013; 8(4).
51. FINCH CA, HEGSTED M, KINNEY TD, THOMAS ED, RATH CE, HASKINS D, i in. IRON METABOLISM: The Pathophysiology of Iron Storage. *Blood*. 1 listopad 1950; 5(11):983–1008.
52. Cankurtaran M, Yavuz BB, Halil M, Ulger Z, Haznedaroglu IC, Ariogul S. Increased ferritin levels could reflect ongoing aging-associated inflammation and may obscure underlying iron deficiency in the geriatric population. *Eur Geriatr Med*. październik 2012; 3(5):277–80.
53. Cohen LA, Gutierrez L, Weiss A, Leichtmann-Bardoogo Y, Zhang DL, Crooks DR, i in. Serum ferritin is derived primarily from macrophages through a nonclassical secretory pathway. *Blood*. 2 wrzesień; 116(9):1574–84.
54. Casale G, Bonora C, Migliavacca A, Zurita IE, de Nicola P. Serum ferritin and ageing. *Age Ageing*. 1981;10(2):119–22.
55. Liu B, Sun Y, Xu G, Snetselaar LG, Ludewig G, Wallace RB, i in. Association between Body Iron Status and Leukocyte Telomere Length, a Biomarker of Biological Aging, in a Nationally Representative Sample of US Adults. *J Acad Nutr Diet*. 1 kwiecień 2019; 119(4):617–25.
56. Ashraf A, Clark M, So PW. The aging of iron man. *Front Aging Neurosci*. 12 marzec 2018; 10(MAR).
57. Yu Z, Persson HL, Eaton JW, Brunk UT. Intralysosomal iron: a major determinant of oxidant-induced cell death. *Free Radic Biol Med*. 15 maj 2003;34(10):1243–52.
58. Masaldan S, Clatworthy SAS, Gamell C, Meggyesy PM, Rigopoulos AT, Haupt S, i in. Iron accumulation in senescent cells is coupled with impaired ferritinophagy and inhibition of ferroptosis. *Redox Biol*. 1 kwiecień 2018; 14:100–15.
59. Yan H fa, Zou T, Tuo Q zhang, Xu S, Li H, Belaidi AA, i in. Ferroptosis: mechanisms and links with diseases. *Signal Transduction and Targeted Therapy* 2021 6:1. 3 luty 2021; 6(1):1–16.
60. Cozzi A, Orellana DI, Santambrogio P, Rubio A, Cancellieri C, Giannelli S, i in. Stem Cell Modeling of Neuroferritinopathy Reveals Iron as a Determinant of Senescence and Ferroptosis during Neuronal Aging. *Stem Cell Reports*. 12 listopad 2019; 13(5):832–46.

61. do Van B, Gouel F, Jonneaux A, Timmerman K, Gelé P, Pétrault M, i in. Ferroptosis, a newly characterized form of cell death in Parkinson's disease that is regulated by PKC. *Neurobiol Dis.* 1 październik 2016; 94:169–78.
62. Guiney SJ, Adlard PA, Bush AI, Finkelstein DI, Ayton S. Ferroptosis and cell death mechanisms in Parkinson's disease. *Neurochem Int.* 1 marzec 2017;104:34-48.
63. Kenny EM, Fidan E, Yang Q, Anthonymuthu TS, New LA, Meyer EA, i in. Ferroptosis Contributes to Neuronal Death and Functional Outcome after Traumatic Brain Injury*. *Crit Care Med.* 1 marzec 2019; 47(3):410–8.
64. Morris G, Berk M, Carvalho AF, Maes M, Walker AJ, Puri BK. Why should neuroscientists worry about iron? The emerging role of ferroptosis in the pathophysiology of neuroprogressive diseases. *Behavioural Brain Research.* 2 kwiecień 2018; 341:154–75.

9. Opinia komisji bioetycznej

Doświadczenia z wykorzystaniem zwierząt w publikacji „**Impaired iron recycling from erythrocytes is an early hallmark of aging**” zostały wykonane za zgodą komisji bioetycznej zasiadającej w Warszawie oraz Olsztynie.

Numery opinii komisji bioetycznej:

- WAW2/015/2019
- WAW2/122/2019
- WAW2/149/2019
- WAW2/026/2020
- WAW2/149/2020

10. Oświadczenia współautorów publikacji

Warszawa, 12.04.2023

Mgr inż. Patryk Ślusarczyk
Studium Medycyny Molekularnej
Warszawski Uniwersytet Medyczny
ul. Żwirki i Wigury 61
02-091 Warszawa

OŚWIADCZENIE

Jako autor pracy pt. „**The Multiple Facets of Iron Recycling**” oświadczam, iż mój własny wkład w przedstawienie pracy w formie publikacji stanowi konceptualizacja, wizualizacja oraz przygotowanie pierwotnej wersji manuskryptu wraz z jego ostateczną wersją.

Ślusarczyk Patryk

Warszawa, 12.04.2023

Dr Katarzyna Mleczko-Sanecka
Laboratorium Homeostazy Żelaza
Międzynarodowy Instytut Biologii Molekularnej i Komórkowej
ul. Księcia Trojdena 4
02-109 Warszawa

OŚWIADCZENIE

Jako współautorka pracy pt. „**The Multiple Facets of Iron Recycling**” oświadczam, iż mój własny wkład w przedstawienie pracy w formie publikacji stanowi konceptualizacja, wizualizacja oraz przygotowanie pierwotnej wersji manuskryptu wraz z jego ostateczną wersją. Dodatkowo oświadczam, że mgr inż. Patryk Michał Ślusarczyk jest pierwszym autorem pracy i wyrażam zgodę na wykorzystanie jej jako części rozprawy doktorskiej.



Warszawa, 14.03.2023

Mgr inż. Patryk Ślusarczyk
Studium Medycyny Molekularnej
Warszawski Uniwersytet Medyczny
ul. Żwirki i Wigury 61
02-091 Warszawa

OŚWIADCZENIE

Jako autor pracy pt. „**Impaired iron recycling from erythrocytes is an early hallmark of aging**” oświadczam, iż mój własny wkład merytoryczny w przygotowanie publikacji stanowi konceptualizacja, metodologia badań, wykonanie badań, analiza danych, wizualizacja oraz przygotowanie pierwotnej wersji manuskryptu wraz z jego ostateczną wersją.

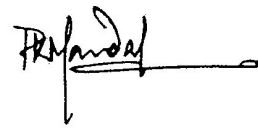
Ślusarczyk Patryk

Warsaw, 16.03.2023

MSc Pratik Kumar Mandal
Laboratory of Iron Homeostasis
International Institute of Molecular and Cell Biology
Trojdena 4 Street
02-109 Warsaw

STATEMENT

As a co-author of the article titled "**Impaired iron recycling from erythrocytes is an early hallmark of aging**" I declare that my own substantive contribution to the preparation of the article includes conceptualization, formal analysis, investigation, visualization, methodology and writing of the manuscript. Additionally, I declare that MSc BEng Patryk Michał Ślusarczyk is the article's first author, and I consent to its use as part of a doctoral dissertation.

A handwritten signature in black ink, appearing to read 'Pratik Mandal', with a horizontal line extending to the right from the end of the signature.

Warszawa, 16.03.2023

Mgr Gabriela Żurawska
Laboratorium Homeostazy Żelaza
Międzynarodowy Instytut Biologii Molekularnej i Komórkowej
ul. Księcia Trojdena 4
02-109 Warszawa

OŚWIADCZENIE

Jako współautorka pracy pt. „**Impaired iron recycling from erythrocytes is an early hallmark of aging**” oświadczam, iż mój własny wkład merytoryczny w przygotowanie publikacji stanowi analiza, wykonanie badań, wizualizacja oraz metodologia dotycząca analizy komórek wątroby przy użyciu cytometrii przepływowej. Dodatkowo oświadczam, że mgr inż. Patryk Michał Ślusarczyk jest pierwszym autorem pracy i wyrażam zgodę na wykorzystanie jej jako części rozprawy doktorskiej.



Warszawa, 16.03.2023

Mgr Marta Niklewicz
Laboratorium Homeostazy Żelaza
Międzynarodowy Instytut Biologii Molekularnej i Komórkowej
ul. Księcia Trojdena 4
02-109 Warszawa

OŚWIADCZENIE

Jako współautorka pracy pt. „**Impaired iron recycling from erythrocytes is an early hallmark of aging**” oświadczam, iż mój własny wkład merytoryczny w przygotowanie publikacji stanowi wykonanie badań związanych z pomiarem zawartości żelaza w tkankach. Dodatkowo oświadczam, że mgr inż. Patryk Michał Ślusarczyk jest pierwszym autorem pracy i wyrażam zgodę na wykorzystanie jej jako części rozprawy doktorskiej.

Niklewicz

Warsaw, 16.03.2023

MSc Komal Chouhan
Laboratory of Iron Homeostasis
International Institute of Molecular and Cell Biology
Trojdena 4 Street
02-109 Warsaw

STATEMENT

As a co-author of the article titled "**Impaired iron recycling from erythrocytes is an early hallmark of aging**" I declare that my own substantive contribution to the preparation of the article includes investigation. Additionally, I declare that MSc BEng Patryk Michał Ślusarczyk is the article's first author, and I consent to its use as part of a doctoral dissertation.

Komal

Warsaw, 16.03.2023

MSc Raghunandan Mahadeva
Laboratory of Iron Homeostasis
International Institute of Molecular and Cell Biology
Trojdena 4 Street
02-109 Warsaw

STATEMENT

As a co-author of the article titled "**Impaired iron recycling from erythrocytes is an early hallmark of aging**" I declare that my own substantive contribution to the preparation of the article includes investigation and visualization of antibody validation for flow cytometry. Additionally, I declare that MSc BEng Patryk Michał Ślusarczyk is the article's first author, and I consent to its use as part of a doctoral dissertation.



Warszawa, 16.03.2023

Dr Aneta Jończy
Laboratorium Homeostazy Żelaza
Międzynarodowy Instytut Biologii Molekularnej i Komórkowej
ul. Księcia Trojdena 4
02-109 Warszawa

OŚWIADCZENIE

Jako współautorka pracy pt. „**Impaired iron recycling from erythrocytes is an early hallmark of aging**” oświadczam, iż mój własny wkład merytoryczny w przygotowanie publikacji stanowi wykonanie badań oraz wizualizacja badań histologicznych wątroby. Dodatkowo oświadczam, że mgr inż. Patryk Michał Ślusarczyk jest pierwszym autorem pracy i wyrażam zgodę na wykorzystanie jej jako części rozprawy doktorskiej.



Warszawa, 12.04.2023

Dr Matylda Macias
Pracownia Mikroskopii i Cytometrii
Międzynarodowy Instytut Biologii Molekularnej i Komórkowej
ul. Księcia Trojdena 4
02-109 Warszawa

OŚWIADCZENIE

Jako współautorka pracy pt. „**Impaired iron recycling from erythrocytes is an early hallmark of aging**” oświadczam, iż mój własny wkład merytoryczny w przygotowanie publikacji stanowi analiza, wizualizacja, metodologia oraz wykonanie badań z wykorzystaniem mikroskopii elektronowej. Dodatkowo oświadczam, że mgr inż. Patryk Michał Ślusarczyk jest pierwszym autorem pracy i wyrażam zgodę na wykorzystanie jej jako części rozprawy doktorskiej.



Warszawa, 16.03.2023

Mgr Aleksandra Szybińska
Pracownia Mikroskopii i Cytometrii
Międzynarodowy Instytut Biologii Molekularnej i Komórkowej
ul. Księcia Trojdena 4
02-109 Warszawa

OŚWIADCZENIE

Jako współautor pracy pt. „**Impaired iron recycling from erythrocytes is an early hallmark of aging**” oświadczam, iż mój własny wkład merytoryczny w przygotowanie publikacji stanowi analiza oraz wykonanie badań z wykorzystaniem mikroskopii elektronowej. Dodatkowo oświadczam, że mgr inż. Patryk Michał Ślusarczyk jest pierwszym autorem pracy i wyrażam zgodę na wykorzystanie jej jako części rozprawy doktorskiej.

A. Szybińska

Warszawa, 23.03.2023

Dr Magdalena Cybulska-Lubak

Pracownia Onkologii Eksperymentalnej i Badań Przedklinicznych

Narodowy Instytut Onkologii - Państwowy Instytut Badawczy im. Marii Skłodowskiej-Curie

ul. Wilhelma Konrada Roentgena 5

02-781 Warszawa

OŚWIADCZENIE

Jako współautor pracy pt. „**Impaired iron recycling from erythrocytes is an early hallmark of aging**” oświadczam, iż mój własny wkład merytoryczny w przygotowanie publikacji stanowi wykonanie iniekcji sztucznie postarzonych czerwonych krwinek do myszy. Dodatkowo oświadczam, że mgr inż. Patryk Michał Ślusarczyk jest pierwszym autorem pracy i wyrażam zgodę na wykorzystanie jej jako części rozprawy doktorskiej.



Warszawa, 05.04.2022

Olga Krawczyk

Pracownia Badań Wielkoskalowych Zakładu Genetyki

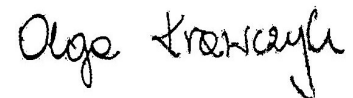
Narodowy Instytut Onkologii - Państwowy Instytut Badawczy im. Marii Skłodowskiej-Curie

ul. Wilhelma Konrada Roentgena 5

02-781 Warszawa

OŚWIADCZENIE

Jako współautorka pracy pt. „**Impaired iron recycling from erythrocytes is an early hallmark of aging**” oświadczam, iż mój własny wkład merytoryczny w przygotowanie publikacji stanowi analiza, wizualizacja oraz metodologia dotycząca sekwencjonowania RNA. Dodatkowo oświadczam, że mgr inż. Patryk Michał Ślusarczyk jest pierwszym autorem pracy i wyrażam zgodę na wykorzystanie jej jako części rozprawy doktorskiej.

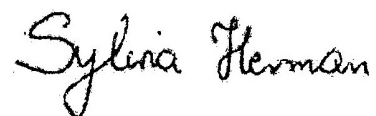


Kraków, 27.03.2023

Mgr Sylwia Herman
Instytut Zoologii i Badań Biomedycznych
Uniwersytet Jagielloński
ul. Gronostajowa 9
30-387 Kraków

OŚWIADCZENIE

Jako współautorka pracy pt. „**Impaired iron recycling from erythrocytes is an early hallmark of aging**” oświadczam, iż mój własny wkład merytoryczny w przygotowanie publikacji stanowi wykonanie badań histologicznych. Dodatkowo oświadczam, że mgr inż. Patryk Michał Ślusarczyk jest pierwszym autorem pracy i wyrażam zgodę na wykorzystanie jej jako części rozprawy doktorskiej.



Warszawa, 22.03.2023

Prof. dr hab. n. med. Michał Miukła

Pracownia Badań Wielkoskalowych Zakładu Genetyki

Narodowy Instytut Onkologii - Państwowy Instytut Badawczy im. Marii Skłodowskiej-Curie
ul. Wilhelma Konrada Roentgena 5

02-781 Warszawa

OŚWIADCZENIE

Jako współautor pracy pt. „**Impaired iron recycling from erythrocytes is an early hallmark of aging**” oświadczam, iż mój własny wkład merytoryczny w przygotowanie publikacji stanowi analiza sekwencjonowania RNA. Dodatkowo oświadczam, że mgr inż. Patryk Michał Ślusarczyk jest pierwszym autorem pracy i wyrażam zgodę na wykorzystanie jej jako części rozprawy doktorskiej.



Signed by /
Podpisano przez:

Michał Marek
Mikula

Date / Data:
2023-03-22 15:00

Warszawa, 23.03.2023

Dr inż. Remigiusz Serwa

Laboratorium Specjalistyczne Proteomiki

Międzynarodowy Instytut Mechanizmów i Maszyn Molekularnych Polskiej Akademii Nauk

ul. Marcina Flisa 6

02-247 Warszawa

OŚWIADCZENIE

Jako współautor pracy pt. „**Impaired iron recycling from erythrocytes is an early hallmark of aging**” oświadczam, iż mój własny wkład merytoryczny w przygotowanie publikacji stanowi analiza, oraz wizualizacja danych proteomicznych. Dodatkowo oświadczam, że mgr inż. Patryk Michał Ślusarczyk jest pierwszym autorem pracy i wyrażam zgodę na wykorzystanie jej jako części rozprawy doktorskiej.

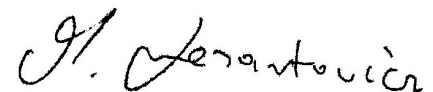


Kraków, 23.03.2023

Prof. UJ dr hab. Małgorzata Lenartowicz
Instytut Zoologii i Badań Biomedycznych
Uniwersytet Jagielloński
ul. Gronostajowa 9
30-387 Kraków

OŚWIADCZENIE

Jako współautorka pracy pt. „**Impaired iron recycling from erythrocytes is an early hallmark of aging**” oświadczam, iż mój własny wkład merytoryczny w przygotowanie publikacji stanowi analiza, wykonanie badań, wizualizacja oraz metodologia dotycząca badań histologicznych. Dodatkowo oświadczam, że mgr inż. Patryk Michał Ślusarczyk jest pierwszym autorem pracy i wyrażam zgodę na wykorzystanie jej jako części rozprawy doktorskiej.



Warszawa, 16.03.2023

Dr hab. Wojciech Pokrzywa
Laboratorium Metabolizmu Białek
Międzynarodowy Instytut Biologii Molekularnej i Komórkowej
ul. Księcia Trojdena 4
02-109 Warszawa

OŚWIADCZENIE

Jako współautor pracy pt. „**Impaired iron recycling from erythrocytes is an early hallmark of aging**” oświadczam, iż mój własny wkład merytoryczny w przygotowanie publikacji stanowi konceptualizacja, analiza, pozyskanie finansowania, wykonanie badań, wizualizacja, metodologia, administracja projektu, pisanie manuskryptu oraz jego edycja. Dodatkowo oświadczam, że mgr inż. Patryk Michał Ślusarczyk jest pierwszym autorem pracy i wyrażam zgodę na wykorzystanie jej jako części rozprawy doktorskiej.



Warszawa, 12.04.2023

Dr Katarzyna Mleczko-Sanecka
Laboratorium Homeostazy Żelaza
Międzynarodowy Instytut Biologii Molekularnej i Komórkowej
ul. Księcia Trojdena 4
02-109 Warszawa

OŚWIADCZENIE

Jako współautorka pracy pt. „**Impaired iron recycling from erythrocytes is an early hallmark of aging**” oświadczam, iż mój własny wkład merytoryczny w przygotowanie publikacji stanowi konceptualizacja, analiza, pozyskanie finansowania, wykonanie badań, wizualizacja, metodologia, administracja projektu, pisanie manuskryptu oraz jego edycja. Dodatkowo oświadczam, że mgr inż. Patryk Michał Ślusarczyk jest pierwszym autorem pracy i wyrażam zgodę na wykorzystanie jej jako części rozprawy doktorskiej.

